39th NOAA Climate Diagnostics and Prediction Workshop
Special Issue


St. Louis, MO

Climate Prediction S&T Digest

February 2015

NWS Science & Technology Infusion Climate Bulletin Supplement

Inside this issue:

1. Hydroclimate monitoring, prediction and variability.
2. Extreme events: Prediction, attribution and assessment.
3. North American multi model ensemble.
4. Subseasonal to interannual predictability.
5. Intraseasonal predictability.
6. Monsoon predictability
7. Climate service development and challenges

NOAA's National Weather Service

Office of Science and Technology
1325 East West Highway
Silver Spring, MD 20910

Climate Prediction Center
5830 University Research Court
College Park, MD 20740

Although the skill of current operational climate prediction is limited and the research on the topic presents many challenges, there are promises of improvement on the horizon. To accelerate advancement in climate services, an effective mechanism of S&T infusion from research to operation for application is much needed. This bulletin has been established to clarify science-related problems and relevant issues identified in operation, helping our partners in the research community to understand which R&D activities are needed to "shoot arrows at the target".

Science and Technology Infusion Climate Bulletin
http://www.nws.noaa.gov/ost/climate/STIP/index.htm

National Weather Service
National Oceanic and Atmospheric Administration
U.S. Department of Commerce

PREFACE

It is with great pleasure that the Climate Prediction Center and the Office of Science and Technology offer you this synthesis of the 39th Climate Diagnostics and Prediction Workshop (CDPW). The CDPW remains a must attend workshop for the climate monitoring and prediction community. As is clearly evident in this digest, considerable progress is being made both in our ability to monitor and predict climate. The purpose of this digest is to ensure that climate research advances are shared with the broader community and also transitioned into operations. This is especially important as NOAA works to enhance climate services both across the agency and with external partners. We hope you find this digest to be useful and stimulating. And please drop me a note if you have suggestions to improve the digest.

I would like to thank Dr. Jiayu Zhou of the Office of Science and Technology (NWS), for developing the digest concept and seeing it through to completion. This partnership between OST and CPC is an essential element of NOAA climate services.

David DeWitt

Director, Climate Prediction Center
National Centers for Environmental Prediction
NOAA's National Weather Service

CONTENTS

OVERVIEW

NOAA's 39th Climate Diagnostics and Prediction Workshop was held in St. Louis, Missouri during 20-23 October 2014. The workshop addressed the status and prospects for advancing climate prediction, monitoring, and diagnostics, and focused on five major themes:

1. Prediction, monitoring, and variability of the hydroclimate with an emphasis on the Midwest during the growing season;
2. The prediction, attribution, and assessment of extreme events;
3. Sub-seasonal to interannual predictability;
4. Latest developments in models, tools, and techniques in relation to improving climate prediction;
5. Developing applications to improve climate services.

The workshop was hosted by St. Louis University (SLU) and co-hosted by the Climate Prediction Center (CPC) of the National Centers for Environmental Prediction (NCEP). The American Meteorological Society (AMS) is a cooperating sponsor.

The workshop featured daytime oral presentations, invited speakers and a poster session event. This Digest is a collection of extended summaries of the presentations contributed by participants. The workshop is continuing to grow and expected to provide a stimulus for further improvements in climate monitoring, diagnostics, prediction, applications and services.

1. HYDROCLIMATE MONITORING, PREDICTION AND VARIABILITY

Science and Technology Infusion Climate Bulletin
NOAA's National Weather Service
39th NOAA Annual Climate Diagnostics and Prediction Workshop
St. Louis, MO, 20-23 October 2014

Mechanism Behind the Spring to Summer Drought Memory and Its Potential for Improving the Predictability of Summer Drought over the US Great Plains

Rong Fu[1], Bing Pu[1], Robert Dickinson[1], and Nelun Fernando[1, 2]

[1] *Jackson School of Geosciences, The University of Texas at Austin*

[2] *Texas Water Development Board, Austin, TX*

1. Introduction

Droughts in the US cause severe economic loss ($210B during 1980-2011 adjusted to 2011 dollars), making them one of the costliest of natural disasters (Smith and Katz, 2013). "Worst droughts on record" now occur frequently, such as the 2011 Tex-Mex drought, the 2012 US Great Plains drought and the 2014 California drought, enhancing the urgency for societal drought preparedness. Current climate models could not predict these droughts and have provided no more prediction skill than the persistence of rainfall anomalies (Quan *et al.*, 2012; Hoerling *et al.*, 2014), especially over the Great Plains, the "bread basket" of the US.

Strong (Severe to exceptional) summer droughts are a result of persistent rainfall deficits. Some droughts are initiated by La Niñas, and some are intensified by the sea surface temperature anomalies (SSTA) over the tropical Atlantic and Indian Ocean (*e.g.*,Trenberth *et al.*, 1988; Lau and Peng, 1990; Cayan *et al.*, 1999; Hoerling and Kumar, 2003; McCabe *et al.*, 2004; Schubert *et al.*, 2004; Hu and Feng, 2007; Mo *et al.*, 2009; Kushnir *et al.*, 2010; Nigam *et al.*, 2011). However, other strong droughts, such as those in 1988 and 2012, were intensified in absence of SSTA. The latter persists from spring to summer, leading to extreme droughts without clear forcing from SSTA (*e.g.*, Namias, 1982, 1991; Hoerling *et al.*, 2013; Seager *et al.*, 2014; Wang *et al.*, 2014). Although land surface feedbacks can contribute to the drought memory (*e.g.*,Carson and Sangster, 1981; Rind, 1982; Karl, 1983; Mintz, 1984; Oglesby and Erickson, 1989; Oglesby, 1991; Dirmeyer,

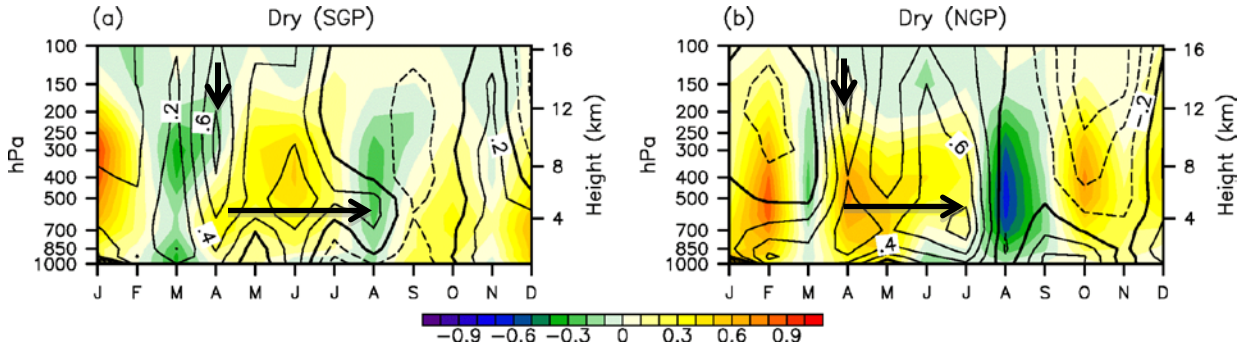

Fig. 1 Seasonal evolutions of the vertical atmospheric dynamic structure (color shades are vertical velocity anomalies, contours stream function anomalies normalized by their standard deviation) suggesting that summer droughts begin with a bartropic-like strong anomalous anticyclonic circulation in April (indicated by solid contours and the vertical arrow). This anticyclonic circulation anomaly persists in the low-middle troposphere (indicated by horizontal arrow), along with mid-tropospheric subsidence (yellow shades), from spring to summer. The seasonal and vertical distributions of the normalized streamfunction anomalies (approximately and equivalent to geopotential height anomalies) and those of anomalies of vertical velocity (unit: Pa/s) are obtained from the composite for all the severe-to-extreme droughts based on NCEP reanalysis during the period of 1979-2012 for the SGP (left) and NGP (right), respectively.

Correspondence to: Rong Fu, Jackson School of Geosciences, The University of Texas at Austin;
Email: rongfu@jsg.utexas.edu

1994; Hong and Kalnay, 2000; Schubert *et al.*, 2004; Myoung and Nielsen-Gammon, 2010), such effects cannot sustain drought for much more than one month in climate models' prediction.

Our analysis suggests that 8 out of 13 severe-to-exceptional summer droughts were developed from spring droughts during the period of 1948-2012 over the US southern Great Plains (SGP). Only 2 spring droughts were not followed by summer droughts. Thus, it is important to understand the mechanisms behind such a spring to summer drought memory and its potential for improving summer drought predictability.

2. What could cause the spring to summer drought memory?

Namias (1982, 1991) and Oglesby (1991) showed that the anomalous anticyclonic circulation or soil moisture in late spring are phase locked with the mean atmospheric circulation transition from the lower to middle troposphere westerly or cyclonic flow in spring to the anticyclonic circulation in summer. In doing so, the anomalous circulation appears to strengthen the summer anticyclonic circulation during the rest of the summer, leading to strong summer droughts. To explore the potential sources for this persistent anomalous anticyclonic circulation, we analyze the composite streamfunction anomalies normalized by their standard deviation at each height (NSFA) for all the years with strong summer droughts during the period of 1979-2012 (Figure 1). Over both the SGP and northern Great Plains (NGP), the summer anticyclonic NSFA in the middle and lower troposphere appears to directly stem from a strong deep tropospheric anticyclonic NSFA in spring following a drier winter that is then maintained in the lower and middle troposphere.

The dominant cause for such persistent anticyclonic anomalies in the middle and lower troposphere is explored in Fig. 2, which shows a comparison between the auto-correlation of the pentad 500hPa geopotential height (Z'_{500hPa}) with the lead-lag correlation between Z'_{500hPa} and soil moisture. The pentad Z'_{500hPa} is more significantly correlated with underlying soil moisture anomalies about 15-30 days earlier than with itself, evidencing that the persistent anomalous anticyclonic vorticity during the summer is caused by land surface feedbacks.

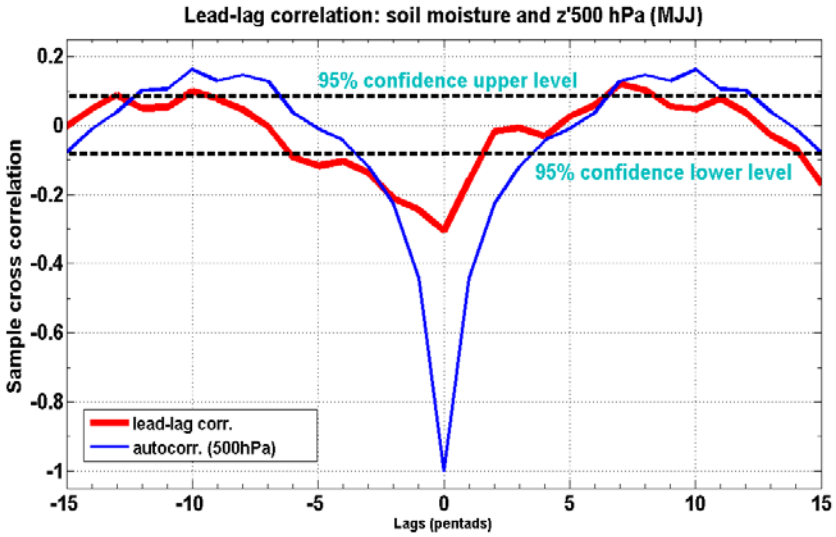

Fig. 2 The correlation coefficients between soil moisture anomalies (red curve) and the 15-30 days lagging (negative 3-5 pentads) 500 hPa geopotential height anomalies (Z'_{500hPa}) are stronger than the auto-correlation of Z'_{500hPa} of the same phase (blue curve) during May-July for the period of 1979-2012. Soil moisture is derived from NLDAS-Noah model.

In summer an extensive ridge occurs in the mid-troposphere centered over the eastern Great Plains. Hydrostatically, this ridge requires relatively cold air. Since dynamic processes are weak, the ridge is largely a consequence of relative diabatic cooling compared to the east coast with its stronger rainfall and clouds, and to the western US with elevated surface heating and deeper turbulent heat transport. This relative cooling results from relative dryness of the continental air at middle troposphere suppressing the diabatic heating from precipitation and the radiative heating from middle to high clouds, with a dynamic response of sinking motion. Thus, *we hypothesize that the persistent anticyclonic vorticity in summer is mainly a response to the sinking motions needed to balance a radiative and latent cooling spatial anomaly in the troposphere from decreases of clouds and precipitation.*

Without thermodynamic feedbacks, the adiabatic warming induced by subsidence would damp the anticyclonic anomalies associated with drought. However, the decreases of clouds, rainfall and water vapor

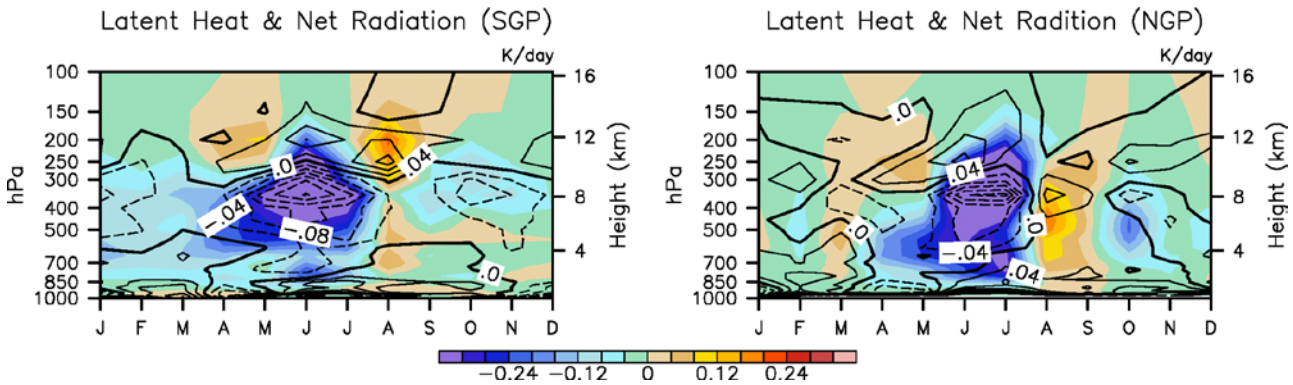

Fig. 3 Seasonal evolutions show strong reduction of latent heating (color shades, K/day) and radaitive heating (contours, K/day) due to decreased clouds and rainfall during April to July. Such anomalous diabatic cooling, initiated by land surface drying, are responsible to the sustained subsidence shown in Figure 1. The seasonal and vertical distributions of the latent and radiative heating anomalies are obtained from the composite for all the severe-to-extreme droughts based on MERRA reanalysis during the period of 1979-2012 for the SGP (left) and NGP (right), respectively.

induce anomalous diabatic cooling in the mid-troposphere to balance the adiabatic warming, thus maintain the subsidence and anticyclonic circulation (Fig. 3). The latter further suppresses convection and associated clouds, and also enhances anticyclonic circulation through friction induced divergence in the PBL and weaker northward vorticity advection. *Thus, decreases of clouds, water vapor and precipitation induced by droughts can maintain and enhance the anticyclonic circulation through anomalous diabatic cooling in the mid-troposphere and friction induced divergence in the PBL. These thermodynamic feedbacks play a critical role in sustaining spring to summer drought memory*.

Figure 4 illustrates the key processes and feedback pathways for the initiation and development of the summer drought, based on the above observational evidence and discussion. *Although SSTA and/or interannual atmospheric variability can be critical for initiating the drought anomalies in winter and spring, the positive feedbacks between land surface and atmosphere, especially through cloud/water vapor and radiative feedbacks, precipitation feedback and PBL friction induced vorticity feedback are important for re-enforcing the anticyclonic circulation anomalies and surface dryness.*

3. Could the spring-to-summer drought memory improve the summer drought predictability over the US Great Plains?

Based on the results shown in Section 2, we have identified three important pre-conditions for spring to summer drought memory over the US Great Plains. These conditions are the geopotential height anomalies at 500 hPa, the difference between temperature at 700 hPa and surface dewpoint, and percentile soil moisture anomalies. We have also developed a combined Multivariate Empirical Orthogonal Function (EOF) and a Canonical Correlation

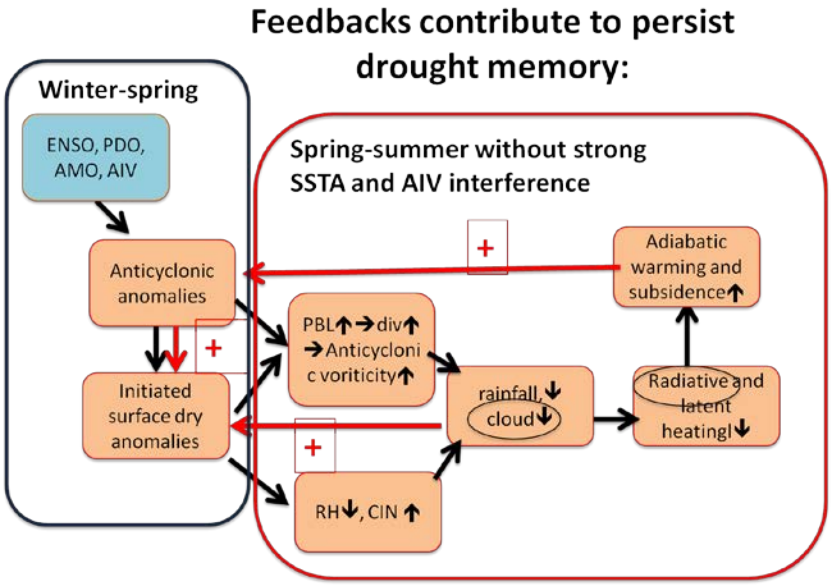

Fig. 4 Observed key processes important for drought initiation, development and intensification over the US Great Plains.

Analysis (CCA) [1] statistical prediction model to explore whether these pre-conditions provide an improved drought predictability and its potential for a summer drought early warning over the US Great Plains.

Figure 5 compares the prediction skills of this statistical drought prediction with 3-months lead time to those of the ensemble prediction of the National Mulit-model Ensemble Prediction (NMME). The overall higher prediction skills than those of the dynamic models suggest that the spring-to-summer drought memory could provide improved drought prediction over the US Great Plains. We have provided our drought early warning to the Texas Water Development Broad (TWDB) in April 2014 for its brief to the State Drought Preparedness Council. TWDB has formally introduced our drought early warning system to its stake holder (http://www.twdb.texas.gov/newsmedia/press_releases/2015/02/drought.asp).

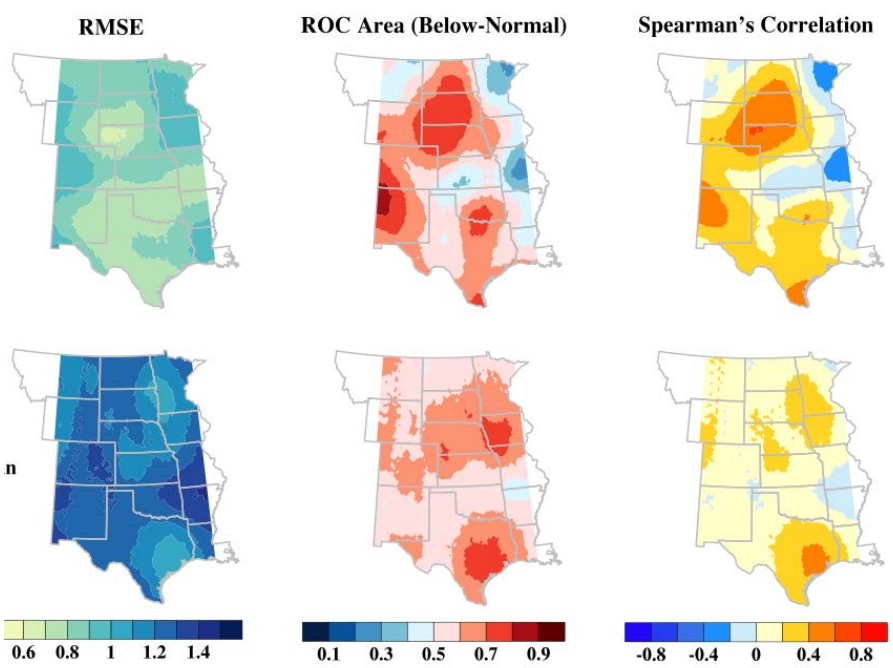

Fig. 5 The 3-months lead drought prediction by our process-based statistical model (top) showing generally higher skills than those of the NMME ensemble prediction (bottom) over the Great Plains, as measured by the Root Mean Squared Error (RMSE, left column), ROC Area (below-normal, middle column), and Spearman's correlation (right column) for July SPI6 using April initial conditions.

4. Conclusions and future works

Severe-to-exceptional summer droughts over the US Great Plains require persistent drought memory from spring to summer. Observations suggest that such persistent spring-to-summer droughts memory is initiated by a strong anomalous barotropic-like anticyclonic circulation in spring, and re-enforced by the coupled land surface, clouds and precipitation feedbacks.

The spring-to-summer drought memory could provide improved drought predictability, as demonstrated by our process-based statistical drought prediction model using three key predicting factors in spring. The drought early warning based on these predicting factors in spring and multivariate EOF statistical model has shown better skill than the dynamic prediction. It has been recommended by state water resource agency and begun to enable society to transition from emergence response to the drought preparedness.

Our results suggest that the cloud feedbacks play as important a role as the precipitation feedbacks to the land surface dryness in sustaining persistent large-scale subsidence, and spring to summer drought memory. Thus, comprehensive evaluations of the drought mechanisms in climate models, especially the impact of uncertainty in capturing the coupling between cloud, precipitation and land surface is an important first step for improving the summer drought prediction over the US Great Plains.

Acknowledgements. This work was supported by the NOAA's Climate Program Office's Modeling, Analysis, Predictions, and Projections Program (Grant Award NA10OAR4310157), the NASA Indicators for the National Climate Assessment Program (Grant NNX13AN39G) and the Jackson School of Geosciences.

[1] The CCA prediction Tool (CPT) available at http://iri.columbia.edu/our-expertise/climate/tools/cpt/ is used.

References

Carson, D. J., and A. B. Sangster, 1981: The influence of land-surface albedo and soil moisture on general circulation model simulations. *Numerical Experimentation Programme Report*, No. 2, 5.14-5.21.

Cayan, D. R., K. T. Redmond, and L. G. Riddle, 1999: ENSO and hydrologic extremes in the western United States. *J. Climate*, **12,** 2881-2893.

Dirmeyer, P. A., 1994: Vegetation stress as a feedback mechanism in midlatitude drought. *J. Climate*, **7,** 1463-1483.

Hoerling, M., and A. Kumar, 2003: The perfect ocean for drought. *Science*, **299,** 691-694.

——, and Coauthors, 2013: Anatomy of an extreme event. *J. Climate*, **26,** 2811-2832.

——, and Coauthors, 2014: Causes and predictability of the 2012 Great Plains drought. *Bull. Amer. Meteor. Soc.*, **95,** 269-282.

Hong, S. Y., and E. Kalnay, 2000: Role of sea surface temperature and soil-moisture feedback in the 1998 Oklahoma-Texas drought. *Nature*, **408,** 842-844.

Hu, Q., and S. Feng, 2007: Decadal variation of the southwest US summer monsoon circulation and rainfall in a regional model. *J. Climate*, **20,** 4702-4716.

Karl, T. R., 1983: Some spatial characteristics of drought duration in the United-States. *J. Clim. Appl Meteorol.*, **22,** 1356-1366.

Kushnir, Y., R. Seager, M. F. Ting, N. Naik, and J. Nakamura, 2010: Mechanisms of tropical Atlantic SST influence on North American precipitation variability. *J. Climate*, **23,** 5610-5628.

Lau, K. M., and L. Peng, 1990: Origin of low-frequency (intraseasonal) oscillations in the tropical atmosphere, Part III: Monsoon dynamics. *J. Atmos. Sci.*, **47,** 1443-1462.

McCabe, G. J., M. A. Palecki, and J. L. Betancourt, 2004: Pacific and Atlantic Ocean influences on multidecadal drought frequency in the United States. *Proc. Natl. Acad. Sci. USA*, **101,** 4136-4141.

Mintz, Y., 1984: The sensitivity of numerically simulated climates to land-surface conditions. *The Global Climate*, J. Houghton, Ed., Cambridge University Press, 79-105.

Mo, K. C., J. K. E. Schemm, and S. H. Yoo, 2009: Influence of ENSO and the Atlantic Multidecadal Oscillation on drought over the United States. *J. Climate*, **22,** 5962-5982.

Myoung, B., and J. W. Nielsen-Gammon, 2010: The convective instability pathway to warm season drought in Texas. Part I: The role of convective inhibition and its modulation by soil moisture. *J. Climate*, **23,** 4461-4473.

Namias, J., 1982: Anatomy of Great Plains protracted heat waves (Especially the 1980 United-States summer drought). *Mon. Wea. Rev.*, **110,** 824-838.

——, 1991: Spring and summer 1988 drought over the contiguous United-States - Causes and prediction. *J. Climate*, **4,** 54-65.

Nigam, S., B. Guan, and A. Ruiz-Barradas, 2011: Key role of the Atlantic Multidecadal Oscillation in 20th century drought and wet periods over the Great Plains. *Geophys. Res. Lett.*, **38,** L16713, doi:10.1029/2011GL048650.

Oglesby, R. J., and D. J. Erickson, 1989: Soil-moisture and the persistence of North-American drought. *J. Climate*, **2,** 1362-1380.

——, 1991: Springtime soil-moisture, natural climatic variability, and North-American drought as simulated by the NCAR Community Climate Model-1. *J. Climate*, **4,** 890-897.

Quan, X. W., M. P. Hoerling, B. Lyon, A. Kumar, M. A. Bell, M. K. Tippett, and H. Wang, 2012: Prospects for dynamical prediction of meteorological drought. *J. Appl. Meteorol. Clim.*, **51,** 1238-1252.

Rind, D., 1982: The influence of ground moisture conditions in North-America on summer climate as modeled in the GISS GCM. *Mon. Wea. Rev.*, **110,** 1487-1494.

Schubert, S. D., M. J. Suarez, P. J. Pegion, R. D. Koster, and J. T. Bacmeister, 2004: Causes of long-term drought in the US Great Plains. *J. Climate*, **17,** 485-503.

Seager, R., L. Goddard, J. Nakamura, N. Henderson, and D. E. Lee, 2014: Dynamical causes of the 2010/11 Texas-Northern Mexico drought. *J. Hydrometeorol.*, **15,** 39-68.

Smith, A. B., and R. W. Katz, 2013: US billion-dollar weather and climate disasters: data sources, trends, accuracy and biases. *Nat. Hazards*, **67,** 387-410.

Trenberth, K. E., G. W. Branstator, and P. A. Arkin, 1988: Origins of the 1988 North-American drought. *Science*, **242,** 1640-1645.

Wang, H. L., S. Schubert, R. Koster, Y. G. Ham, and M. Suarez, 2014: On the role of SST forcing in the 2011 and 2012 extreme U.S. heat and drought: A study in contrasts. *J. Hydrometeorol.*, **15,** 1255-1273.

Science and Technology Infusion Climate Bulletin
NOAA's National Weather Service
39th NOAA Annual Climate Diagnostics and Prediction Workshop
St. Louis, MO, 20-23 October 2014

An Enhanced Seasonal Transition That Could Have Intensified Droughts in the Central U.S.

S.-Y. Simon Wang[1], Joseph Santanello[2], Hailan Wang[2], Daniel Barandiaran[1], Rachel Pinker[3], Siegfried Schubert[2], Robert R. Gillies[1], Robert Oglesby[4], Kyle Hilburn[5], Ayse Kilic[6], and Paul Houser[7]

[1]*Utah Climate Center / Dept. Plants, Soils and Climate, Utah State University, Logan, UT*
[2]*NASA Goddard Space Flight Center, Greenbelt, MD*
[3] *Dept. Atmospheric and Oceanic Science, University of Maryland, College Park, MD*
[4]*Dept. Earth and Atmospheric Sciences, University of Nebraska-Lincoln, Lincoln, NE*
[5]*Remote Sensing Systems, Santa Rosa, California*
[6]*Dept. Civil Engineering and School of Natural Resources, University of Nebraska-Lincoln, Lincoln, NE*
[7]*Dept. Geography and GeoInformation Science, George Mason University, Fairfax, VA*

1. Introduction

The summer drought of 2012 in the central United States is instructive regarding one unique feature, that is, its rapid intensification during the early summer (Hoerling *et al.*, 2013; Hoerling *et al.*, 2014). A figure from the NOAA report (Hoerling *et al.*, 2013), shown here in Fig. 1a, depicts the rapid expansion of drought conditions in Wyoming, Colorado, Kansas, Nebraska and South/North Dakota, evolving over a mere month from moderate to severe status (categorized as per the U.S. Drought Monitor). The timing of this drought's rapid intensification coincided with a subseasonal feature of widespread drying: Climatologically, precipitation in the central U.S. generally is reduced by about 25% from June to July, as shown in Fig. 1b by the long-term monthly rainfall averaged over the central U.S. Such a rainfall reduction occurs in association with the development of the North American Monsoon (NAM) and the concurrent formation of the upper-level anticyclone over the western U.S., nudging the jet stream northward. The precipitation difference of July minus June (Fig. 1c), **denoted hereafter as "July-June"**, depicts a distinct zone of rainfall reduction to the north and east of the NAM region, covering the Central Plains and the Great Plains. While this seasonal rainfall reduction is a well-known phenomenon (Barlow *et al.*, 1998; S.-Y. Wang and Chen, 2009), the extent to which a progression of

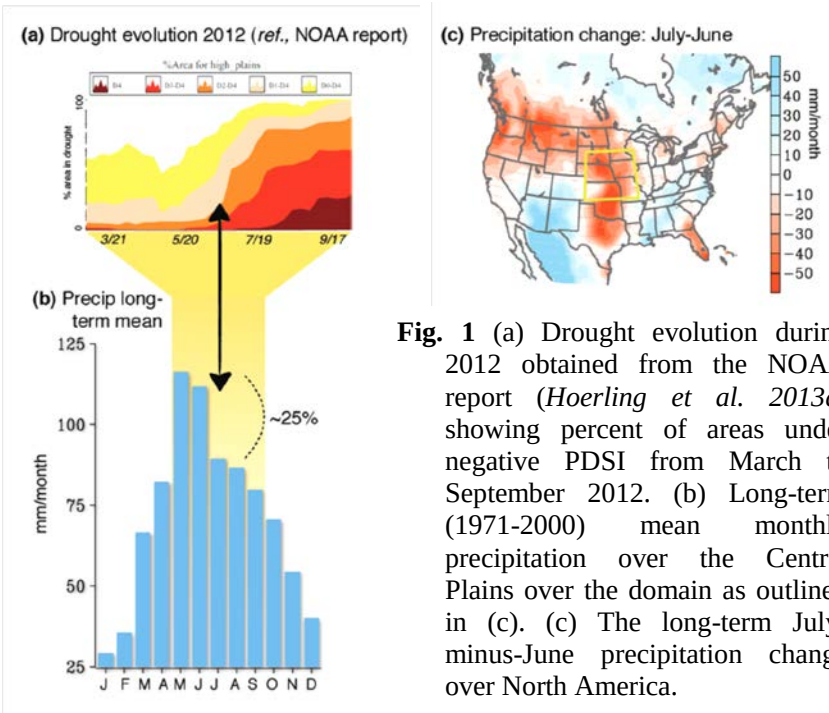

Fig. 1 (a) Drought evolution during 2012 obtained from the NOAA report (*Hoerling et al. 2013a*) showing percent of areas under negative PDSI from March to September 2012. (b) Long-term (1971-2000) mean monthly precipitation over the Central Plains over the domain as outlined in (c). (c) The long-term July-minus-June precipitation change over North America.

Correspondence to: S.-Y. Simon Wang, Utah Climate Center / Dept. Plants, Soils and Climate, Utah State University, Logan, UT; Email: simon.wang@usu.edu

drying may have amplified has not been examined.

The extremity and extensive impacts of summer droughts such as was the case in 2012 have prompted a number of studies. It was thought that the lack of prominent large-scale forcing factors in the tropics, such as that of ENSO, is a probable reason that has impeded climate forecast models' prediction of the 2012 drought (Hoerling *et al.*, 2014; H. Wang *et al.*, 2014). In this study, our goal was to examine possible forcing factors other than ENSO, with emphasis on regional drivers and mechanisms that may be related to the rapid advancement/expansion of drought (such as that in 2012) including the role of land-atmosphere interactions, circulation patterns, their interaction and, subsequently, how some or all of these may have changed.

2. Surface conditions

The linear trend of the post-1979 change in the July-June (*i.e.* July minus June) precipitation difference (*from Climatic Research Unit monthly precipitation dataset, (Harris et al., 2014)*) is shown in Fig. 2a. In comparison with Fig. 1c, the precipitation deficit from June to July is noticeably intensified in the northern part of the U.S., covering both the Central Plains and the northern Rockies. Around Iowa, Nebraska and part of Illinois, the precipitation reduction has diminished twofold when compared to that of the 1980s. Likewise, the linear trend of the July-June PDSI difference (Fig. 2b, *derived from PRISM temperature and precipitation data, (Daly et al., 1994)*) indicates that drought conditions have tended to intensify over the Central Plains and the northern Rockies during the June-to-July transition. A trend analysis conducted on the difference between the averages of May and June (MJ) and July and August (JA) (not shown) also yielded a similar result in both precipitation and PDSI.

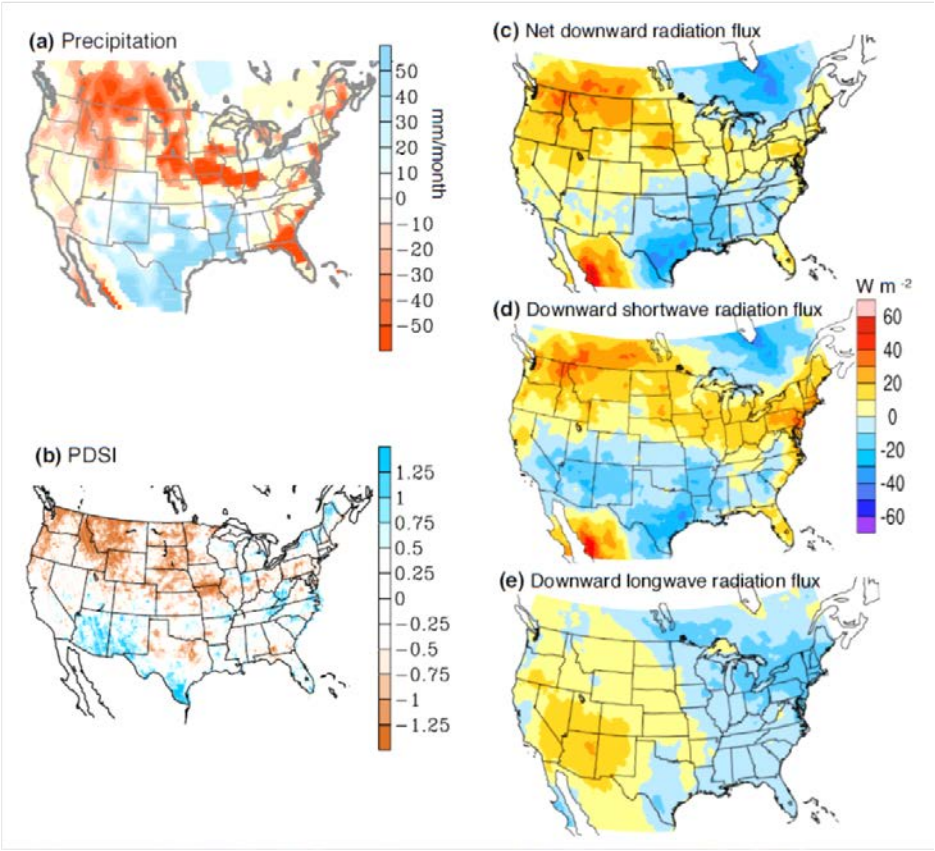

Fig. 2 Linear trends in the July-June difference of (a) precipitation (CRU data), (b) PDSI (PRISM data), (c) net downward radiation flux, (d) downward shortwave radiation flux, and (e) downward longwave radiation flux (NLDAS-2 data). (In (a) the red and blue colors are significant at the 99% level.)

Another factor worth noting is the trend in the July-June net downward radiation flux at the surface (Fig. 2c) – derived from NLDAS-2 data (Xia *et al.*, 2012). The increased (positive) trend in the July-June net downward radiation flux reveals a pattern very similar to the decreased (negative) trend in precipitation, i.e. meridionally elongated pattern with a particularly strong increase in the northern Rockies and the northern Great Plains. The pattern of net downward radiation flux results primarily from the change in downward shortwave radiation (DSWR) flux (Fig. 2d) caused by change in cloud cover or cloud thickness. In comparison, the trend in the July-June downward longwave radiation (DLWR; Fig. 2e) depicts an east-west dipole pattern with increased radiation in the southwest and decreased radiation in the northeast. The net

result indicates that the central U.S. received either increased shortwave radiation in July or decreased radiation in June, or a combination of both. These changes are accompanied by a concurrent increase in 2-m air temperature (T2m) and 700-200mb thickness (not shown), suggesting enhanced ridge formation in this region.

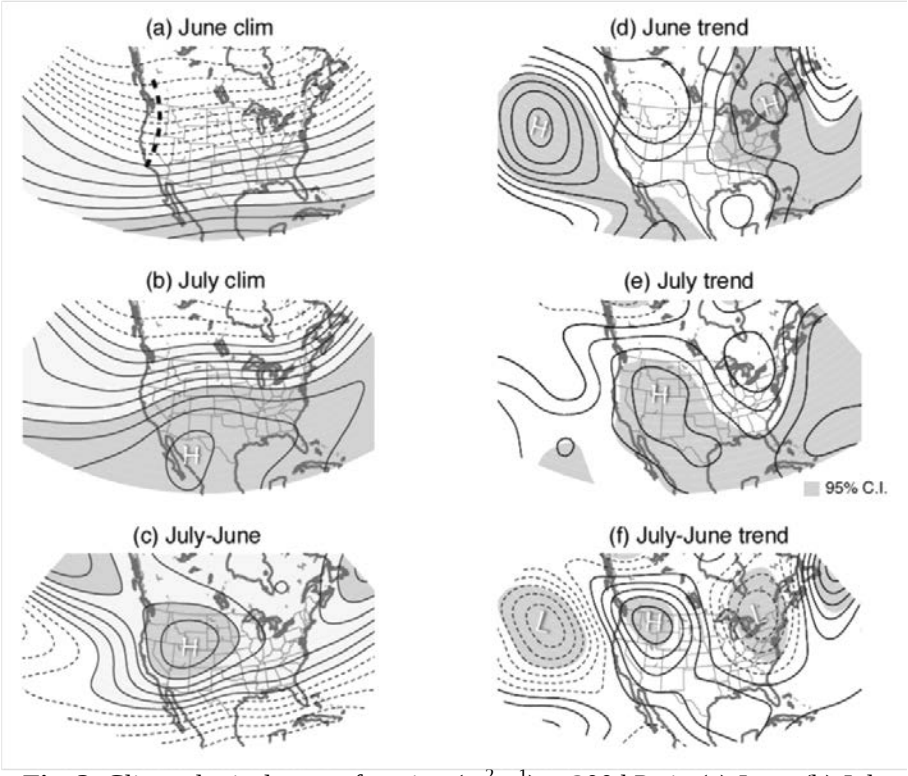

Fig. 3 Climatological streamfunction ($m^2 s^{-1}$) at 200 hPa in (a) June, (b) July and (c) July-June transition, with a contour interval of 5x106 in (a),(b) and 2.5x106 in (c). The monthly streamfunction anomaly of the post-1979 trend in (d) June, (e) July, and (f) July-June transition, with a contour interval of 1.5x106 (total change of 1979-2011). Shadings in (d)-(f) indicate the regression coefficients significant at the 95% confidence interval. The bold dashed line in (a) indicates the stationary trough, while "H" and "L" indicates high and low pressure anomalies, respectively.

3. Circulations vs. remote forcing

As previously noted, the development of the NAM is associated with a noticeable transition in upper-level circulations from the cold season regime (trough) to mid-summer regime (ridge); this is illustrated in Fig. 3 (*Circulation data: ensemble of MERRA, CFSR, ERA-Interim, and NCEP/DOE R-2*). In June, a stationary trough near the West Coast characterizes the upper-level circulation with the jet exit located over the Central Plains (Fig. 3a). In July, the monsoonal anticyclone develops, pushing the jet stream northward to about 50°N (Fig. 3b); consequently the circulation change from June to July forms an anticyclonic anomaly over the western U.S. (Fig. 3c) and creates subsidence over the Central Plains (Barandiaran *et al.*, 2013). The linear trends in these circulations (Figs. 3d-f) reveal an intensification manifest as a deepened western trough in June and enhanced western ridge in July. As a result, the July-June shift in the circulation (Fig. 3f) depicts an amplified ridge in the northwestern U.S. and a deepened trough in the northeastern U.S. The ridge corresponds well with increased surface warming and tropospheric thickening (noted earlier), and is also accompanied by increased subsidence at 500-hPa (*ref.*, Fig. 3). Such a change in the circulation is apparent as a distinct short-wave pattern with a zonal wave-5 structure, a feature of which has been found to suppress summer moisture in the central U.S. (S.-Y. Wang *et al.*, 2014).

Summer anticyclonic anomalies in western North America are frequently connected to remote forcing in the North Pacific and Asia (Barandiaran *et al.*, 2013). Thus, to explore the climatic forcing of the circulation patterns, Fig. 4a displays the trends in the July-June SST (*obtained from NOAA Extended Reconstructed SST*) and 200-hP streamfunction and reveals a marked similarity with the 2012 situation, suggesting a contribution of the post-1979 trend. The distinct short-wave train across the midlatitudes implies a link with remote forcing that triggers a circumglobal teleconnection, from which wave energy propagates zonally along the jet stream and affects North America (S.-Y. Wang *et al.*, 2014). Noteworthy is the weak tropical SST anomalies, and this feature is consistent with the lack of prominent tropical forcing in 2012 (Barlow *et al.*, 1998). By comparison, trends in the June and July circulation and SST (Figs. 4b and 4c) reveal a La Niña type of SST change in both months, consistent with previous studies of the global SST trends (Barlow *et al.*, 2001; S.-Y. Wang and Chen, 2009). However, July is accompanied by a stronger warming over the central North Pacific

in comparison to June, while the circulation anomalies between the two months are quite different. June circulation exhibits a teleconnection emanating from the central tropical Pacific through the "PNA route", yet such a teleconnection is lacking in July.

4. Concluding remarks

Climatologically, precipitation in the central U.S. decreased by about 25% during the June-to-July seasonal transition. Since 1979, this precipitation reduction in the central U.S. has become more severe, having decreased twice as much in recent years. At the larger scale, examination of T2m and tropospheric circulation change indicated that dynamical forcing was present that enhanced subsidence in the central U.S. while, at the same time, suppressing rainfall. Such a long-term change has a potential effect to aggravate summer droughts. In particular, the analyses presented here indicated a marked resemblance between the June-to-July PDSI, precipitation, temperature and circulation shifts in their long-term change and those associated with the 2012 drought – one which was characterized by a rapid expansion over the Central Plains in early summer. As far as drought development is concerned, one important factor revealed from this study was land-atmosphere feedbacks over the U.S., *i.e.* the enhanced anticyclonic anomalies stationed over the western U.S. can lead to further reductions in precipitation and soil moisture in the Central U.S. In turn, the long-term changes in land surface moisture and temperature can sustain or amplify the evolution of the overlying anticyclonic circulation and precipitation deficit. In the long run, the land surface feedback to the atmospheric circulation anomalies is strong and can affect future drought expansion in the central U.S. These processes could help anticipate the evolution and extent of future drought in the central U.S., especially those that occur in spring and can worsen in summer.

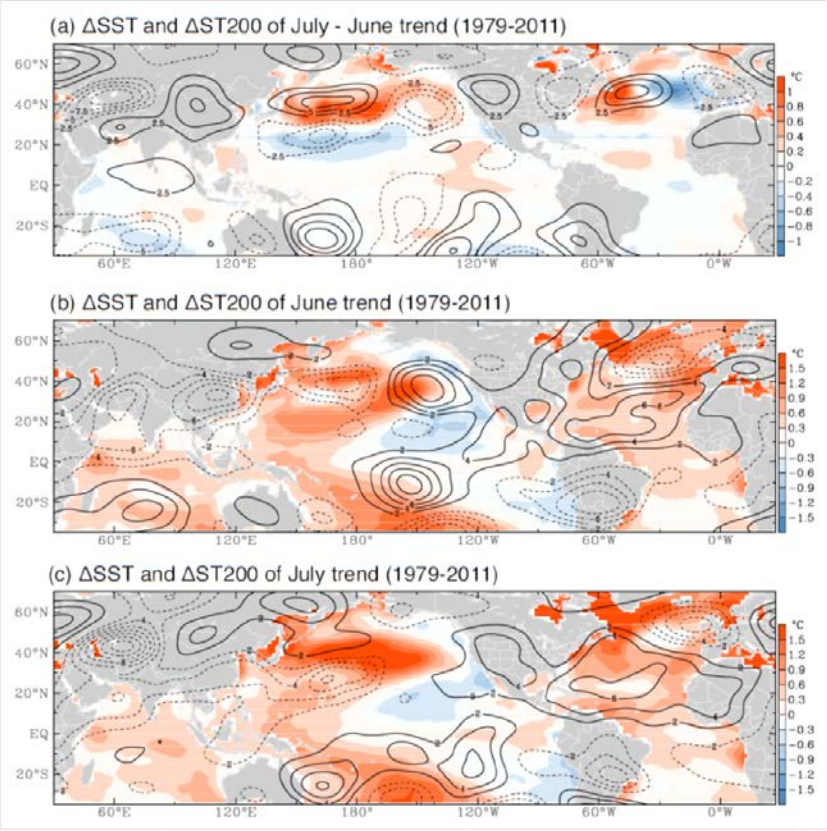

Fig. 4 (a) The anomalies of the July-June changes in 200-hPa streamfunction (contours) and SST (shadings) from the post-1979 trends, and the trends in monthly streamfunction and SST during (b) June and (c) July. Zero contours of the streamfunction are omitted. Contour intervals are 2.5x106 m^2 s^{-1} in (a) and 2x106 m^2 s^{-1} in (b) and (c).

Acknowledgements. This study was supported by the NASA Energy and Water cycle Study (NEWS).

References

Barandiaran, D., S.-Y. Wang, and K. Hilburn, 2013: Observed trends in the Great Plains low-level jet and associated precipitation changes in relation to recent droughts. *Geophys. Res. Lett.*, **40**, 2013GL058296.

Barlow, M., S. Nigam, and E. H. Berbery, 1998: Evolution of the North American Monsoon System. *J. Climate*, **11**, 2238-2257.

——, ——, and ——, 2001: ENSO, Pacific decadal variability, and US summertime precipitation, drought, and stream flow. *J. Climate*, **14**, 2105-2128.

Daly, C., R. P. Neilson, and D. L. Phillips, 1994: A statistical-topographic model for mapping climatological precipitation over mountainous terrain. *J. Appl. Meteor.*, **33**, 140-158.

Harris, I., P. D. Jones, T. J. Osborn, and D. H. Lister, 2014: Updated high-resolution grids of monthly climatic observations – the CRU TS3.10 Dataset. *Int. J. Climatol.*, **34**, 623-642.

Hoerling, M., S. Schubert, K. Mo, and H. B. A. AghaKouchak , J. Dong, M. Hoerling, A. Kumar, V. Lakshmi, R. Leung, J. Li, X. Liang, L. Luo, B. Lyon, D. Miskus, K. Mo, X. Quan, S. Schubert, R. Seager, S. Sorooshian, H. Wang, Y. Xia, and N. Zeng, 2013: An Interpretation of the origins of the 2012 central Great Plains drought. Edited by NOAA/CPO/MAPP, 44 pp. [Available online at http://cpo.noaa.gov/ClimatePrograms/ModelingAnalysisPredictionsandProjections/MAPPTaskForces/DroughtTaskForce/2012CentralGreatPlainsDrought.aspx]

——, J. Eischeid, A. Kumar, R. Leung, A. Mariotti, K. Mo, S. Schubert, and R. Seager, 2014: Causes and predictability of the 2012 Great Plains drought. *Bull. Amer. Meteor. Soc.*, **95**, 269–282.

Wang, H., S. Schubert, R. Koster, Y.-G. Ham, and M. Suarez, 2014: On the role of SST forcing in the 2011 and 2012 extreme U.S. heat and drought: A study in contrasts. *J. Hydrometeor.*, (in press).

Wang, S.-Y., and T.-C. Chen, 2009: The late-spring maximum of rainfall over the U.S. Central Plains and the role of the low-level jet. *J. Climate*, **22**, 4696-4709.

——, D. Barandiaran, K. Hilburn, P. Houser, B. Oglesby, M. Pan, R. Pinker, J. Santanello, S. Schubert, and H. Wang, 2014: Could the 2012 drought have been anticipated?–A NASA NEWS initiative. *Climate Prediction S&T Digest*, 38th NOAA Annual Climate Diagnostics and Prediction Workshop, College Park, MD, National Oceanic and Atmospheric Administration. 58-63. [Available online at http://docs.lib.noaa.gov/noaa_documents/NWS/NCEP/CDPW/38th_2014.pdf]

Xia, Y., K. Mitchell, M. Ek, J. Sheffield, B. Cosgrove, E. Wood, L. Luo, C. Alonge, H. Wei, and J. Meng, 2012: Continental-scale water and energy flux analysis and validation for the North American Land Data Assimilation System project phase 2 (NLDAS-2): 1. Intercomparison and application of model products. *J. Geophys. Res.: Atmospheres (1984–2012)*, **117**, D03109, doi:10.1029/2011JD016048.

Science and Technology Infusion Climate Bulletin
NOAA's National Weather Service
39th NOAA Annual Climate Diagnostics and Prediction Workshop
St. Louis, MO, 20-23 October 2014

Why Do Some La Niña Years in the Southern Great Plains Have Droughts and Other Not?

Bing Pu, Rong Fu, Robert E. Dickinson, D. Nelun Fernando

Department of Geological Sciences, Jackson School of Geosciences,
The University of Texas at Austin, Austin, Texas 78712

1. Introduction

La Niña has long been related to the droughts in the Great Plains (*e.g.*, Trenberth *et al.*, 1988; Ting and Wang, 1997; Dai *et al.*, 1998; Schubert *et al.*, 2004; Seager *et al.*, 2005a; Seager *et al.*, 2005b; Schubert *et al.*, 2009 ; Seager *et al.*, 2014). Such abnormal SSTs and their consequent diabatic heating excite wave trains from the tropical Pacific to North America, placing an anomalous high over the southern U.S. and also shifting the Pacific storm track northward and reducing local moisture transport by the Great Plains low-level jet and thus summer precipitation. The recent severe 2010-2011 drought over the Southern Great Plains (SGP) is related to a strong La Niña event during the winter and spring, along with other factors such as atmospheric internal variability (Seager *et al.*, 2014).

However, not all La Niña events lead to droughts in the SGP. For example the 1973-1975 La Niña event actually led to increased rainfall over the eastern Plains and the Gulf coast, and climate models failed to reproduce this rainfall change probably due to their strong sensitivity to ENSO (Schubert *et al.*, 2004; Lau *et al.*, 2006; Seager and Hoerling, 2014). What factors lead to the different rainfall responses in the area during La Niña years? Seager and Hoerling (2014) have suggested that random atmosphere variability and other SST anomalies, *e.g.*, tropical Atlantic and Indian ocean, may overcome the influence of the tropical Pacific. This issue is examined here in more details. We focus on the circulation and SSTA patterns that lead to dry conditions in the SGP during La Niña years.

2. Methodology

2.1 Datasets

To understand how circulation pattern and moisture convergence differ for the La Niña dry and non-dry years, winds, geopotential height, and specific humidity are analyzed from the NCEP/NCAR reanalysis

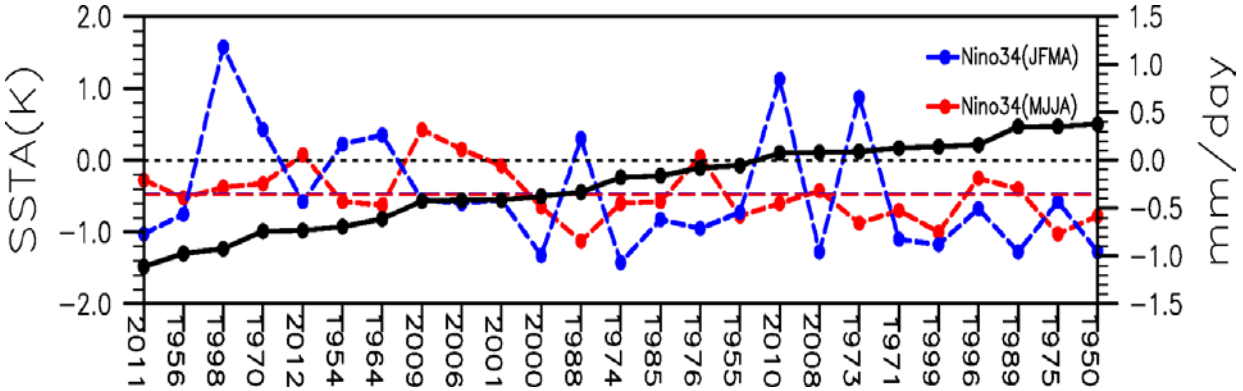

Fig. 1 Time series MJJA precipitation of La Niña years averaged in the SGP (see the black box in Fig. 2) along with CPC 3-month running mean Niño3.4 SSTA during JFMA (*i.e.*, centered in JFMA; blue) and MJJA (red) from 1950-2012. Rainfall anomalies are reordered from the driest to the wettest years.

Correspondence to: Bing Pu, Department of Geological Sciences, Jackson School of Geosciences, The University of Texas at Austin, Austin, Texas 78712; Email: bing.pu@jsg.utexas.edu

(Kalnay *et al.*, 1996; Hereafter NCEP1) from 1948-2013. The reanalysis is chosen because of its long data record. Its horizontal resolution is 2.5º by 2.5º.

The climatic Research Unit (CRU) TS3.21 (UEACRU, Jones and Harris, 2013) monthly precipitation on a 0.5º latitude by 0.5º longitude grid from 1901-2012 is used to examine precipitation variations. The Niño3.4, Atlantic Multidecadal Oscillation (AMO), Pacific Decadal Oscillation (PDO) and North Atlantic Oscillation (NAO) indices from Climate Prediction Center (CPC) from 1948 (or 1950) to 2013 are used to identify La Niña years and SST and circulation anomalies. The Hadley Centre Sea Ice and Sea Surface Temperature data set (HadISST; Rayner *et al.*, 2003) on a 1º by 1º grid from the UK Met Office is used to examine SST patterns.

2.2 Criteria for La Niña dry and non-dry years

Three-month running mean ERSST.v3bSST anomalies in the Niño3.4 region from the CPC are used to identify La Niña years. Since we are interested in La Niña events that occurred before or simultaneously with SGP summer rainfall anomalies, the following two criteria are used to decide such events: i) from DJF-MAM there are at least three consecutive over-lapping seasons with negative SSTA greater than -0.5 ºC, or ii) from AMJ-JAS there are at least two consecutive over-lapping seasons with negative SSTA greater than -0.5 ºC. Twenty-five La Niña years are so identified from1950-2013 (Figure 1).

To understand different rainfall responses during these La Niña events, two composites, namely, LaDry and LaNonDry, are formed corresponding to seven driest and wettest MJJA rainfall anomalies for the twenty-five La Niña years. MJJA average is chosen because SGP rainfall peaks from May to September, and MJJA precipitation contributes to about 44% of the total annual precipitation. The averaging also includes the early peak in May that may be more useful for agriculture planning.

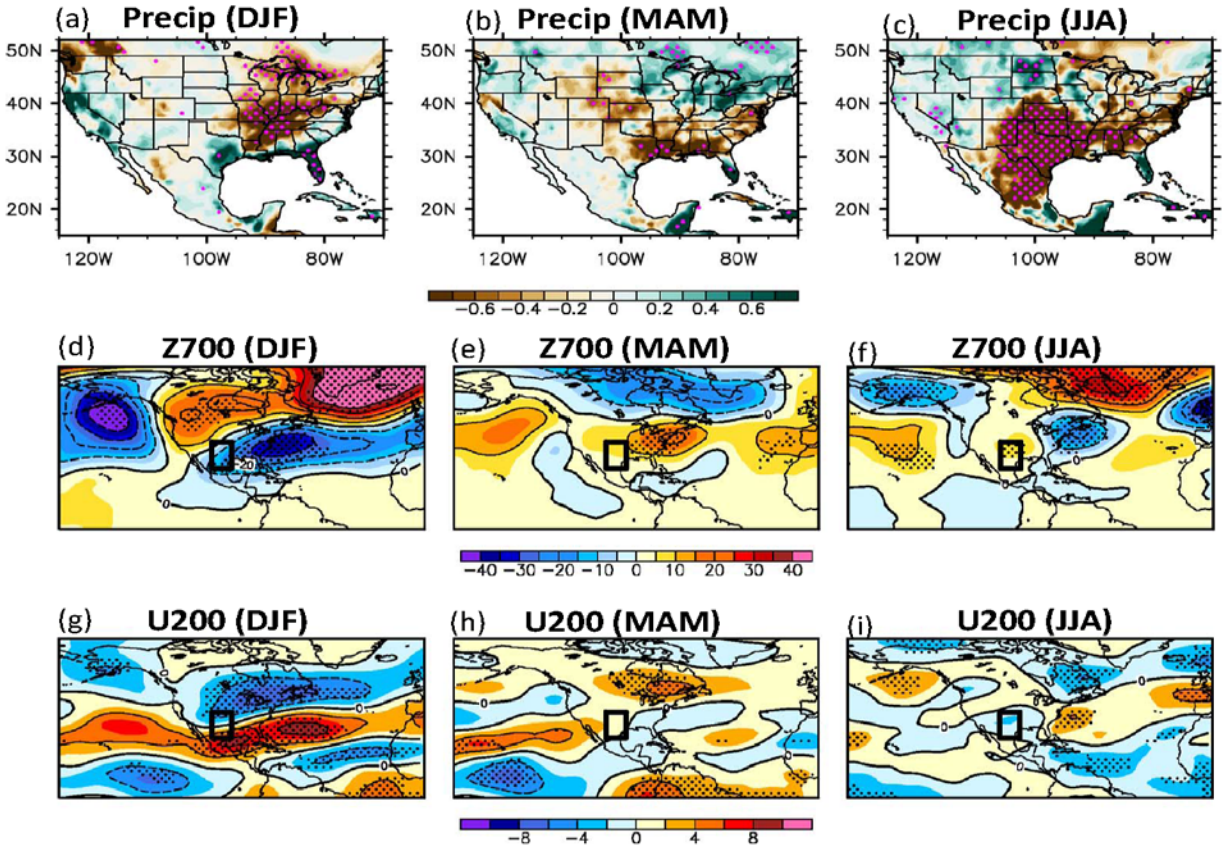

Fig. 2 (a)-(c) Precipitation (mm day^{-1}), (d)-(f) 700 hPa geopotential height (gpm) and (g)-(i) 200 hPa zonal wind (m s^{-1}) anomalies between the LaDry and LaNonDry composites from DJF to JJA. Areas significant at the 95% confidence level are dotted (Monte Carlo test).

3. Analysis

SGP MJJA rainfall anomalies along with the Niño 3.4 SSTA in JFMA (blue) and MJJA (red) are shown in Figure 1. MJJA Rainfall deceases in about two-thirds of La Niña years，consistent with previous results that La Niña contributes to SGP drought. However, the linear relationship between Niño 3.4 SST and rainfall magnitude in these La Niña years is not very strong. MJJA rainfall has a weak negative correlation of -0.37 (significant at the 90% confidence level) with concurrent Niño 3.4 SSTA. In other words, drought is more likely to occur in weak La Niña years. Niño 3.4 SSTA in JFMA shows an even weaker negative influence (not significant) on MJJA rainfall.

The rainfall differences between the dry and non-dry years (Figs. 2a-c) generally resemble the patterns in dry years (not shown) but with greater magnitudes. Rainfall reduces over the Mississippi river basin and Midwest in DJF. The dry anomaly in the SGP establishes in MAM and intensifies in JJA.

The low-level circulation pattern in MAM shares some similarity with that in typical La Niña years (not shown). The main difference is that the location of anomalous high over the U.S. is centered at the east coast instead of the Gulf coast while the geopotential height over the subtropical and tropical Atlantic is increased (Fig. 2e), suggesting an influence from the North Atlantic. The upper-level jet stream is shifted northward over the U.S. but slightly southward over the Atlantic (Fig. 2h). In JJA, an anomalous high is located over the SGP with a low center over the eastern U.S. (Fig. 2f), while the Pacific jet stream is also shifted northward and thus favors the drought development (Fig. 2i).

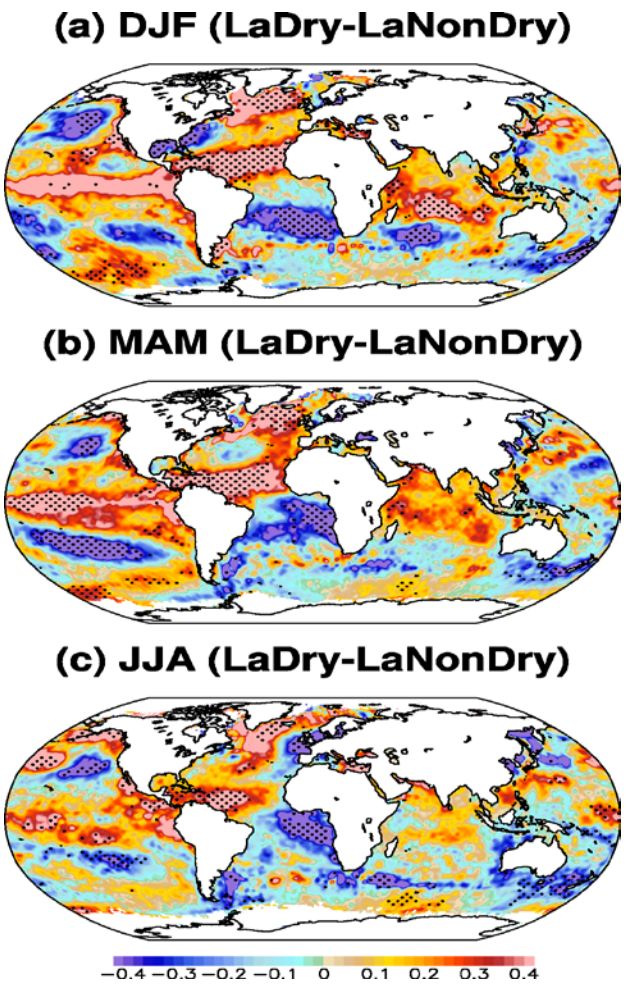

Fig. 3 Differences of SST (K) between the LaDry and LaNonDry composites. Areas significant at the 95% confidence level are dotted (Monte Carlo test).

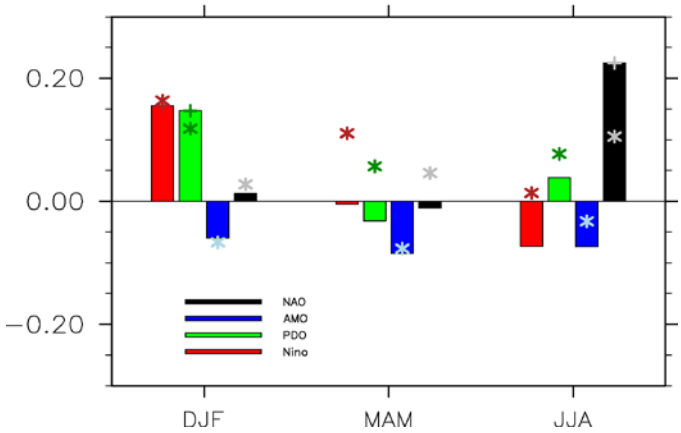

Fig. 4 Regression coefficients of SGP rainfall onto the standardized Niño 3.4 (red), PDO (green), AMO (blue), and NAO (black) indices in 25 La Niña years (bars) and from 1950-2012 (stars). Regression coefficients in La Niña years significant at the 90% confidence level are topped with a "+" sign.

The differences of SST between the LaDry and LaNonDry composites show an anomalously warm SST over the tropical and high-latitude North Atlantic, resembling a positive AMO pattern (Figure 3). This pattern persists from winter to summer but with a weaker magnitude in summer. SST also decreases over the Gulf of Mexico in DJF but not in other seasons, which may contribute to the anomalous northerly flow from land to the Gulf. Southern Atlantic SST also decreases from DJF to JJA, indicating a northward shift of Atlantic ITCZ.

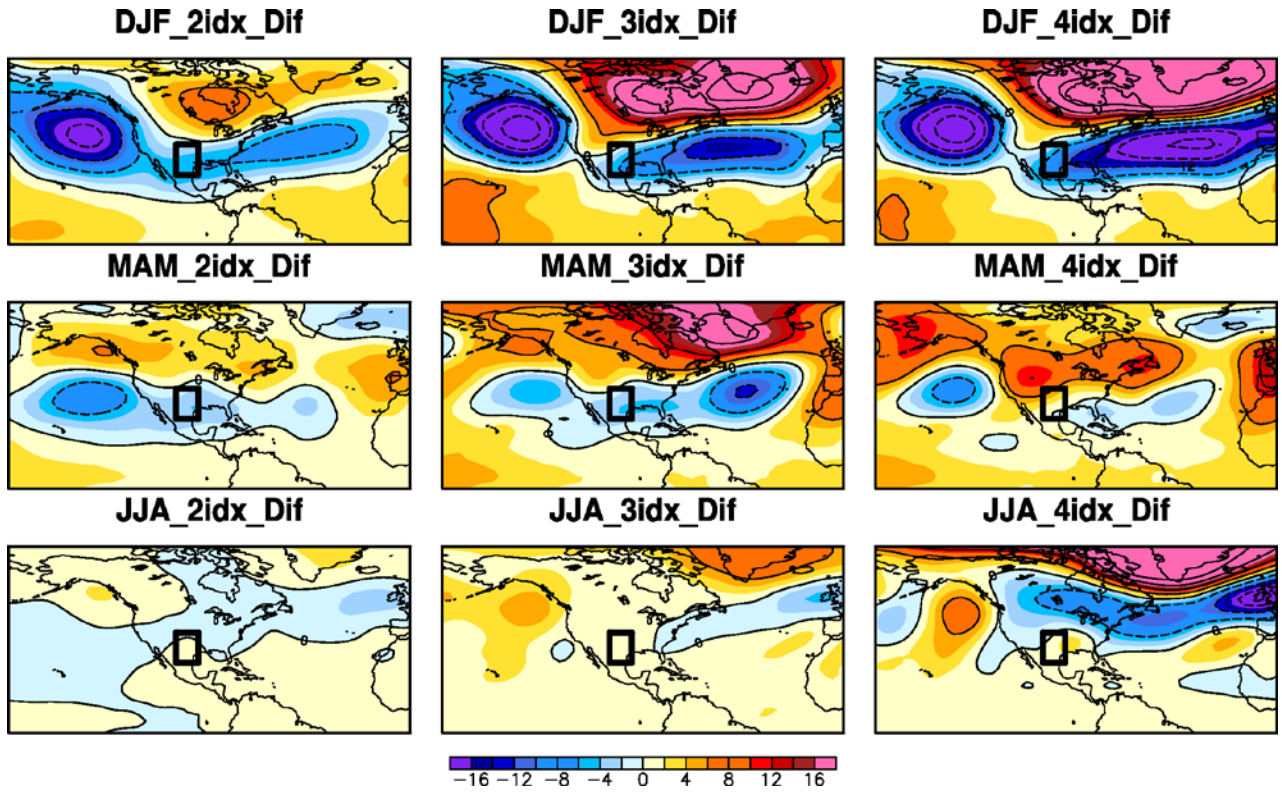

Fig. 5 Regressed 700 hPa geopotential height anomalies (gpm) between the LaDry and LaNonDry composites using PDO and Niño3.4 indices (left column), three SST based indices (middle column), and four indices (right columns).

The tropical Pacific SST is slightly warmer in dry years than non-dry years, mainly in DJF and MAM. In typical La Niña years, dry anomaly is located over the SGP in DJF and shifts northward to the northern Plains in JJA. A warmer Niño 3.4 SST indicates a weaker/slower seasonal northward migration of dry anomalies, favoring the development of drought in the SGP. An anomalous low SST over the mid-latitude North Pacific also persists from DJF to JJA, resembling a positive PDO pattern, while a symmetric negative SSTA is located over the South Pacific.

Figure 4 shows the regression coefficients of SGP rainfall onto the three SST based indices and NAO index during 1950-2012 (stars) and during 25 La Niña years (bars). This further verifies a weak but persistent influence of AMO on SGP rainfall in La Niña years from winter to summer. Influence of Niño 3.4 SST on rainfall is very weak in spring during La Niña and reverses to a negative relationship in summer. The NAO is the most important factor in JJA regardless of whether it is a La Niña year or not.

Figure 5 shows regressed 700 hPa geopotential height using different linear combinations of indices discussed above for the differences between the LaDry and LaNonDry composites. The left column shows the influences from the Pacific Ocean (*i.e.*, Niño3.4+PDO), middle column includes the influences of the North Atlantic and Pacific oceans (*i.e.*, Niño3.4+PDO +AMO) while the right column includes the influence of NAO.

The regressed pattern using Pacific indices shows relatively high correlations with the NCEP1 reanalysis in winter over the North Pacific-North America-North Atlantic (NPAA, 10º-60ºN, 30º-150ºW) region (uncentered pattern correlations 0.66) and the southern U.S. and its surroundings (USS, 20º-43ºN, 80º-120ºW; 0.63), but quite low or even negative correlations for spring and summer. Regressions using four indices have largely increased the correlations in both NPAA (*e.g.*, 0.87 in DJF and 0.62 in JJA) and USS (*e.g.*, 0.93 in DJF and 0.65 in MAM) regions except in summer when the patterns over the USS is better captured without the NAO index.

In La Niña dry years the above indices can explain about 63% of rainfall anomaly in MAM and 38% in JJA. Such a decrease of explanation from spring to summer suggests a contribution from factors other than SSTAs and NAO, such as soil moisture feedbacks and radiative feedbacks from the reduction of cloud that can amply the drought, and from random atmospheric variability. The wet anomaly in the summer is not captured and may also due to these factors. Overall, the rainfall differences between the dry and non-dry composites are explained by 36% in MAM and 23% in JJA with these indices.

4. Conclusions and discussion

- There are distinct circulation patterns between La Niña dry and non-dry years in the SGP. Droughts are associated with anomalous high geopotential height and subsidence over the SGP, along with an intensified northward moisture flux that transports moisture to the northern Plains and Midwest and a northward displacement of the North Pacific and Atlantic jet streams.
- Anomalous SST patterns are found between dry and non-dry years: i) a warm SSTA over the North Atlantic that resembles a positive AMO pattern; ii) a relatively warm Niño3.4 SST. Such an anomalous positive AMO pattern enhances the geopotential height over the northern Atlantic and thus strengthens and shifts the high center over the SGP toward the southeast, and it also modifies the location of subtropical jet streams. A weaker La Niña, by delaying the seasonal northward shift of the dry anomaly during MAM and JJA, also contributes to the development of drought in the SGP.
- Niño 3.4, PDO, AMO and NAO indices can largely reproduce the anomalous geopotential height patterns between dry and non-dry years in DJF but less in MAM and JJA mainly due to a worse representation of anomalous wet condition.
- Although previous studies have identified the role of the AMO in SGP drought, this analysis highlights its influences in La Niña years that contribute to the anomalous large-scale patterns that favor the development of drought. Thus improving model performance in simulating the influence of Atlantic SST on SGP rainfall may enhance the capability of drought modeling and prediction in this region.

References

Dai, A., K. E. Trenberth, and T. R. Karl, 1998: Global variations in droughts and wet spells: 1900-1995. *Geophys. Res. Lett.*, **25**, 3367-3370.

Kalnay, E., and Coauthors, 1996: The NCEP/NCAR 40-year reanalysis project. *Bull. Amer. Meteorol. Soc.*, **77**, 437-471.

Lau, N. C., A. Leetmaa, and M. J. Nath, 2006: Attribution of atmospheric variations in the 1997-2003 period to SST anomalies in the Pacific and Indian ocean basins. *J. Climate*, **19**, 3607-3628.

Rayner, N. A., and Coauthors, 2003: Global analyses of sea surface temperature, sea ice, and night marine air temperature since the late nineteenth century. *J. Geophys. Res.-Atmos*, **108.**

Schubert, S., and Coauthors, 2009: A US CLIVAR Project to Assess and Compare the Responses of Global Climate Models to Drought-Related SST Forcing Patterns: Overview and Results. *J. Climate*, **22**, 5251-5272.

——, M. J. Suarez, P. J. Pegion, R. D. Koster, and J. T. Bacmeister, 2004: Causes of long-term drought in the US Great Plains. *J. Climate*, **17**, 485-503.

Seager, R., N. Harnik, Y. Kushnir, W. Robinson, and J. Miller, 2003: Mechanisms of hemispherically symmetric climate variability. *J. Climate*, **16**, 2960-2978.

——, N. Harnik, W. A. Robinson, Y. Kushnir, M. Ting, H. P. Huang, and J. Velez, 2005a: Mechanisms of ENSO-forcing of hemispherically symmetric precipitation variability. *Q. J. Roy. Meteor. Soc.*, **131**, 1501-1527.

——, Y. Kushnir, C. Herweijer, N. Naik, and J. Velez, 2005b: Modeling of tropical forcing of persistent droughts and pluvials over western North America: 1856-2000. *J. Climate*, **18**, 4065-4088.

——, L. Goddard, J. Nakamura, N. Henderson, and D. E. Lee, 2014: Dynamical causes of the 2010/11 Texas-Northern Mexico drought. *J. Hydrometeorol.*, **15**, 39-68.

——, and M Hoerling, 2014: Atmosphere and ocean origins of North American droughts. *J. Climate*, **27**, 4581–4606. doi: http://dx.doi.org/10.1175/JCLI-D-13-00329.1.

Smith, T. M., R. W. Reynolds, T. C. Peterson, and J. Lawrimore, 2008: Improvements to NOAA's historical merged land-ocean surface temperature analysis (1880-2006). *J. Climate*, **21**, 2283-2296.

Ting, M. F., and H. Wang, 1997: Summertime US precipitation variability and its relation to Pacific sea surface temperature. *J. Climate*, **10**, 1853-1873.

Trenberth, K. E., G. W. Branstator, and P. A. Arkin, 1988: Origins of the 1988 North-American drought. *Science*, **242**, 1640-1645.

University of East Anglia Climatic Research Unit (UEACRU); P.D. Jones, and I. Harris, 2013: CRU TS3.21: Climatic Research Unit (CRU) Time-Series (TS) Version 3.21 of high resolution gridded data of month-by-month variation in climate (Jan. 1901- Dec. 2012). NCAS British Atmospheric Data Centre, 24th September 2013. doi:10.5285/D0E1585D-3417-485F-87AE-4FCECF10.

2. EXTREME EVENTS: PREDICTION, ATTRIBUTION AND ASSESSMENT

Science and Technology Infusion Climate Bulletin
NOAA's National Weather Service
39th NOAA Annual Climate Diagnostics and Prediction Workshop
St. Louis, MO, 20-23 October 2014

CPC's New Week-2 Probabilistic Hazards Forecast and Extremes Tool

Melissa Ou, Ken Pelman, Mike Charles, and Jon Gottschalck

Climate Prediction Center, NCEP/NWS/NOAA

1. Introduction

For the last 13 years, the Climate Prediction Center (CPC) has been issuing days 3-14 hazards forecasts daily. This is a manually produced forecast in deterministic format highlighting areas that have elevated risk of various hazards, such as wildfires, flooding, much above/below normal temperatures, heavy precipitation, etc. Model improvements in daily weather forecasts have enabled weather centers (such as the Weather Prediction Center, Storm Prediction Center, *etc*.) to issue national forecasts with longer lead times, mainly up to 7 days. Therefore, CPC is now focusing on improving the national hazards forecasts beyond week-1, from days 8-14, which will be referred to as week-2 in this article.

Beyond week-1, it is more useful and robust to present forecasts in a probabilistic format, rather than deterministic due to the greater uncertainty associated with models at longer lead times. CPC is now issuing experimental manual forecasts daily of hazards presented in a probabilistic format, similar to the majority of CPC's outlooks. The underlying probabilistic threshold used to issue a deterministic hazard is intrinsically high. Shifting the paradigm to a probabilistic format allows CPC's forecasters to highlight more areas with lower probabilities, thus providing users with more information about potential hazards during week-2. The probabilistic hazards outlook has three risk levels slight, moderate, and high corresponding to a 20%, 40%,

Fig. 1 Sample screenshot of the CPC probabilistic extremes tool for September 16, 2014. Probabilities of daily maximum temperatures on day 8 exceeding the 15th percentile are shown. Various features of the tool are highlighted in purple boxes.

Correspondence to: Melissa Ou, Climate Prediction Center, NCEP/NWS/NOAA, 5830 University Research Court, College Park, MD 20740-3818; Email: Melissa.Ou@noaa.gov

and 60% chance of occurring. This additional information about the probability of an event occurring may significantly add value to the forecast for decision makers.

The main guidance used to produce the new probabilistic hazards forecast is a newly developed extremes tool at CPC. This tool has probabilities retrieved from the CPC reforecast tool, which involves post-processing ensemble model guidance using historical reforecasts to produce calibrated week-2 daily probabilistic forecasts of daily maximum and minimum temperatures at varying climatological percentiles and threshold values, including those deemed as extreme. This tool will also be made available publicly in the future.

A main motivation for this project was the need by CPC hazards forecasters for more guidance and tools in the week-2 period. Much of the available guidance is presented as deterministic model run output from both deterministic models and ensemble means. Additionally, there is a growing need and interest in extremes and hazards outlooks, especially in the subseasonal timescale beyond week-1. These extreme/hazardous events often have the most impact to life, property, and commerce. More interests want longer lead times for early detection and preparedness. The hope is that this new extremes tool and probabilistic hazards outlook will be beneficial to a wide variety of users, especially decision makers.

The main goal of this article is to introduce the new probabilistic hazards forecast product and extremes tool and discuss the transition of the hazards product. Both the extremes tool and probabilistic hazards outlook are currently being produced for daily forecasts of 2-m minimum and maximum temperatures (which will be referred to as Tmin, and Tmax, respectively, in this article). CPC is planning to use a phased approach to add more variables in the future, such as for winds and precipitation. Some initial verification results are also shown from the probabilistic extremes tool for week-2 daily forecasts of Tmin being less than the 15th

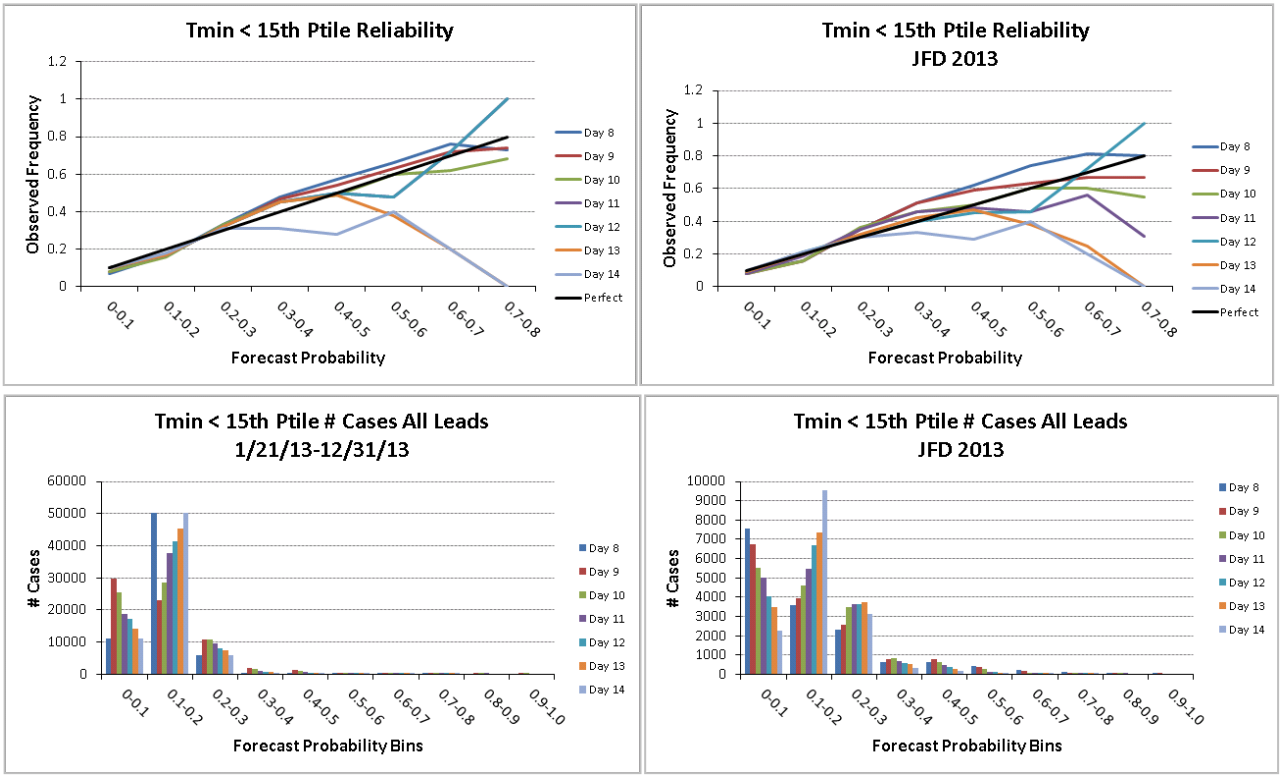

Fig. 2 Reliability diagrams are shown on the top row for daily minimum temperature forecasts produced by the extremes tool for probabilities less than the 15th ptile for all day leads including all forecasts from 2013 (left) and just the winter months (Jan, Feb, and Dec) of 2013 (right). The black line indicates what would be considered a perfectly reliable forecast. The bottom row shows histograms of the number of cases for all the probability bins for the associated reliability plots above. The '# Cases' on the y-axis refers to the fact that this shows the number of forecasts in each probability bin over time and space.

percentile, over the CONUS domain for a year (January 2013 to December 2013). We focused on Tmin because we wanted to get an idea of how skillful the tool was since CPC would be using it as guidance to produce probabilistic hazards forecasts for the upcoming winter season. The 15th percentile was evaluated because CPC typically uses this as the general threshold for deeming an event as hazardous.

2. Data

2.1 Training and forecast data

The underlying data for the extremes tool is from the CPC Reforecast Tool for daily minimum and maximum 2-m temperatures. These are formatted as the probabilities of a location being greater than a specified range of percentiles. The extremes tool software performs further postprocessing to convert this data for being less than or greater than varying thresholds for temperature values as well as percentiles. The reforecast tool calibrates realtime ensemble forecasts from the Global Ensemble Forecast System (GEFS), with physics operational during 2012, using the ensemble regression method (Unger 2009). Longterm statistics are derived using the 25-year GEFS reforecast dataset (past forecasts produced by the frozen 2012 GEFS model), provided by the Earth System Research Laboratory (ESRL), and the associated observations (the "day zero" analysis from GEFS). The reforecast dataset includes 11 ensemble members (including a control run) for each day of the 25 years, and the realtime GEFS has 21 members, daily. Further details regarding these datasets can be found in the 38th CDPW Digest summary article, "Sensitivity Study of the Skill of the CPC Week-2 Reforecast Tool to Reforecast Sampling" (Ou *et al.* 2014).

2.2 Verification data

The observational data used to produce verification results is 1 degree global, gridded, daily minimum temperature values that merges land and ocean observations from 2 different datasets from 1985 to 2010. Land data uses 1/6 degree gridded data that is derived from the Global Telecommunication System (GTS), which contains observations from about 600 US stations; data over oceans comes from the GEFS analyses, taken as the mean from 4 update cycles of the GEFS day zero analyses (forecast hours F006, F012, F018, and F024). The observation and forecast percentiles were determined using a climatology dataset derived from this merged observation dataset using all 25 years. CPC typically uses 30year climatologies, but due to the fact that reforecast data only goes back to 1985, a 25year dataset was created and used.

3. About the Week-2 CPC Probabilistic Extremes Tool

A week-2 probabilistic extremes outlook tool was developed to provide guidance to forecasters for producing probabilistic hazards forecasts. This tool was also developed with the intention for the public to eventually be able to access and utilize it across various interests via a web interface, hopefully aiding decision makers in planning. As a change in the typical paradigm to product development at CPC, feedback was sought prior to the development of the tool, in the hopes that the end product would be more userfriendly and that the content would be found useful to a wide variety of interests. Mockup designs of the user interface were presented to a number of users, including the Federal Emergency Management Agency (FEMA) and at the 11th Climate Prediction Applications Science Workshop (CPASW). This feedback was the driving factor for the design, features, and content, such as the set of percentile and temperature thresholds.

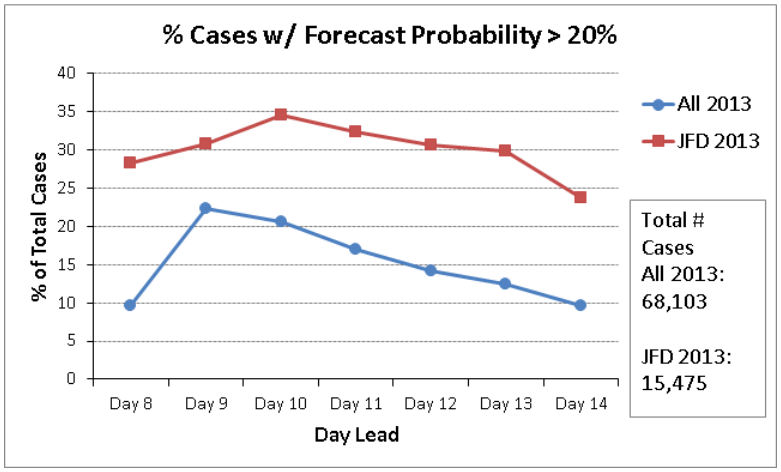

Fig. 3 Percent of total cases with forecast probabilities greater than 20% for all leads, including all dates in 2013 (blue line) and only the winter months (red line).

The extremes web tool presents the forecast as the probabilities of minimum or maximum temperatures being less than or greater than a set of thresholds. Thresholds are available as both percentiles and temperature values. Figure 1 shows a sample screenshot of the extremes tool. Below is a list of the current features and options in the web tool (highlighted in purple in Figure 1):

- Minimum and maximum temperatures
- Thresholds in percentiles and temperature values
- Daily outlooks for days 8 to 14
- Probabilities based on the calibrated GEFS reforecast tool and uncalibrated GEFS forecasts
- Ability to click on any location and retrieve the latitude, longitude, and probability associated with that location
- Zoom-in and zoom-out functionality

This tool is currently available for the U.S. domain, including Alaska and Hawaii. Based on further evaluation results and quality control tests, the global domain of forecasts may be made available publicly as well.

4. Verification results

The skill of daily week-2 probabilistic forecasts of minimum temperatures being less than the 15th percentile is evaluated using the ranked probability skill score (RPSS) and reliability. These skill metrics were chosen because they have been shown to be appropriate scores for assessing the skill of probabilistic forecasts. Results are presented for using all dates from January 21, 2013 to December 31, 2013 as well as only the winter months (Jan, Feb, and Dec) for 2013.

Overall, reliability (Fig. 2) was pretty good until day 13, for including all dates in the assessment period and only the winter months. There was poorer reliability at higher probabilities (*i.e.* greater than 60%), which may be due to the fact that there are less forecasts in this probability range and that it is typically inherently

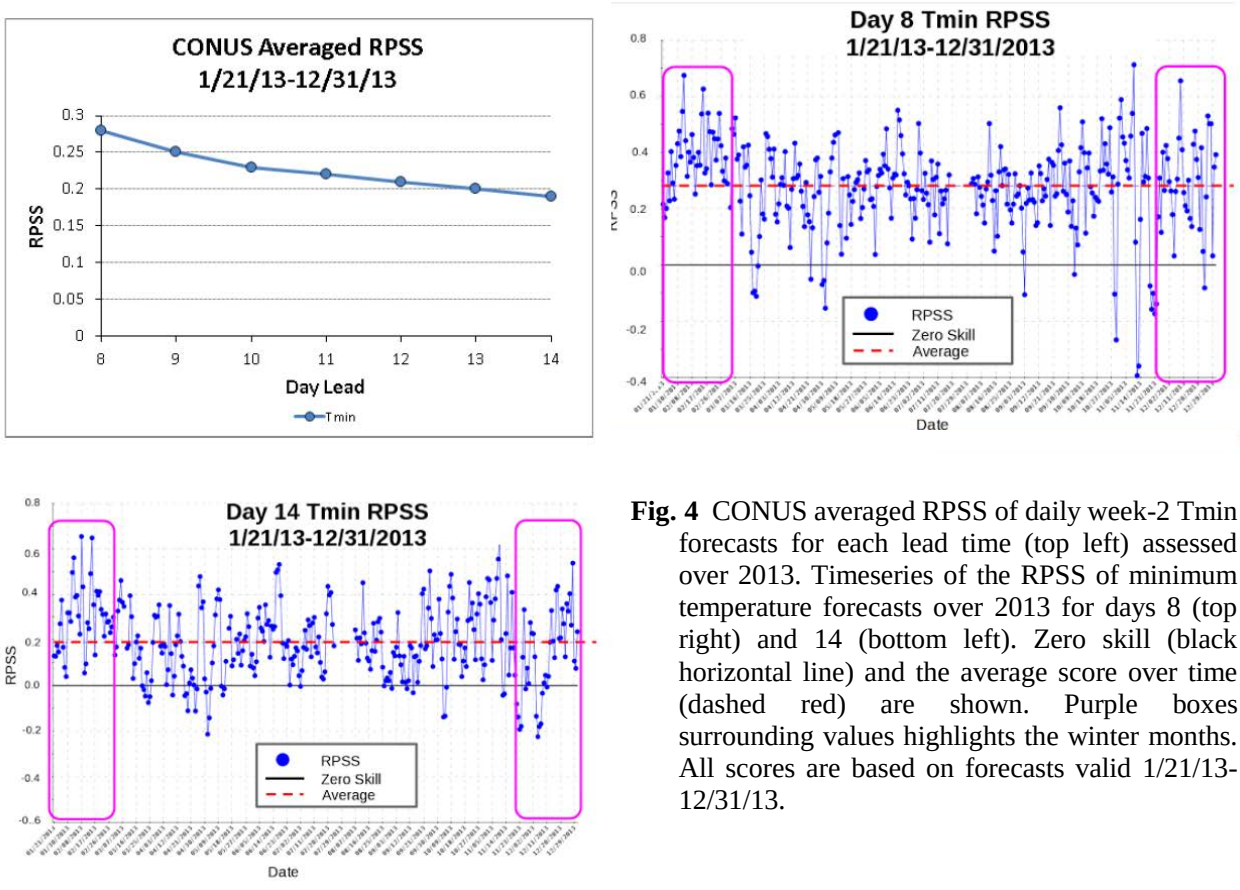

Fig. 4 CONUS averaged RPSS of daily week-2 Tmin forecasts for each lead time (top left) assessed over 2013. Timeseries of the RPSS of minimum temperature forecasts over 2013 for days 8 (top right) and 14 (bottom left). Zero skill (black horizontal line) and the average score over time (dashed red) are shown. Purple boxes surrounding values highlights the winter months. All scores are based on forecasts valid 1/21/13-12/31/13.

harder to have accurate reliability at higher probabilities.

For a forecaster, what would be useful is knowing that at days 8 and 9, forecast probabilities tend to be underconfident, potentially indicating that they should slightly bump up probabilities at i.e. the 20-50% range. Beyond day 9, forecasts tend to be overconfident at probabilities of 40% or greater, so they should be cautious of putting higher probabilities. One possible explanation for the underconfidence of the days 8 and 9 forecasts is that the ensemble regression method (used to produce the forecasts) does not widen the distribution about the members at the tails relative to near the ensemble mean. Therefore, the probabilities at the tails of the distribution are not increased sufficiently. From our experience it would appear that the probabilities do increase in the calibrated versus uncalibrated GEFS forecasts, but perhaps not enough. The overconfidence of forecasts at longer lead times likely stems from the fact that the spread of the ensemble is higher at those leads, resulting in probabilities that are more confident in the tails of the distribution, but not with more skill.

The associated histograms (Fig. 2) showing the number of forecasts (referred to as cases in the plots) in each probability bin indicates that the winter season of 2013 had a greater portion of occurrences of higher probabilities than when including all dates from all seasons, where cases are over time and space. This is most likely due to better predictability during the winter season because it is typically harder to predict summer convective events.

One concern that we had when we first started discussing a probabilistic hazards product and extremes tool was that the tool may produce a very low frequency of forecasts for the tails of the distribution, especially with probabilities that we deem high enough to consider drawing an associated probabilistic hazards contour on the forecast map. For our purposes, we chose 20% as the minimum forecast probability to consider as a potential hazard.

Our results show that a significant number of cases predicted forecasts with probabilities greater than 20 percent. Figure 3 shows the percent of forecasts (over time and space) in 2013 that had probabilities of greater than 20 percent, for both all dates and winter months only. This plot indicates that 24 to 35 percent of the winter forecasts had probabilities greater than 20%. Day 10 had the greatest percent of > 20% probabilities (35%), and day 14 had the least (24%). Day 8 and 9 fell somewhere in the middle. When considering all dates in 2013, the percent of >20% probabilities was much lower than only winter months, ranging from 10% (days 8 and 14) to 23% (day 9). This is again, likely due to the inclusion of seasons (such as summer) with less predictability, although the day 8 value for all 2013 looks suspiciously low compared to the other longer leads.

To evaluate the RPSS and reliability, we created 3 categories to represent the distribution of percentiles associated with the 15th percentile (RPSS requires multiple categories to be used). The 3 categories are Tmin < 15th percentile, 15-85th percentile, > 85th percentile.

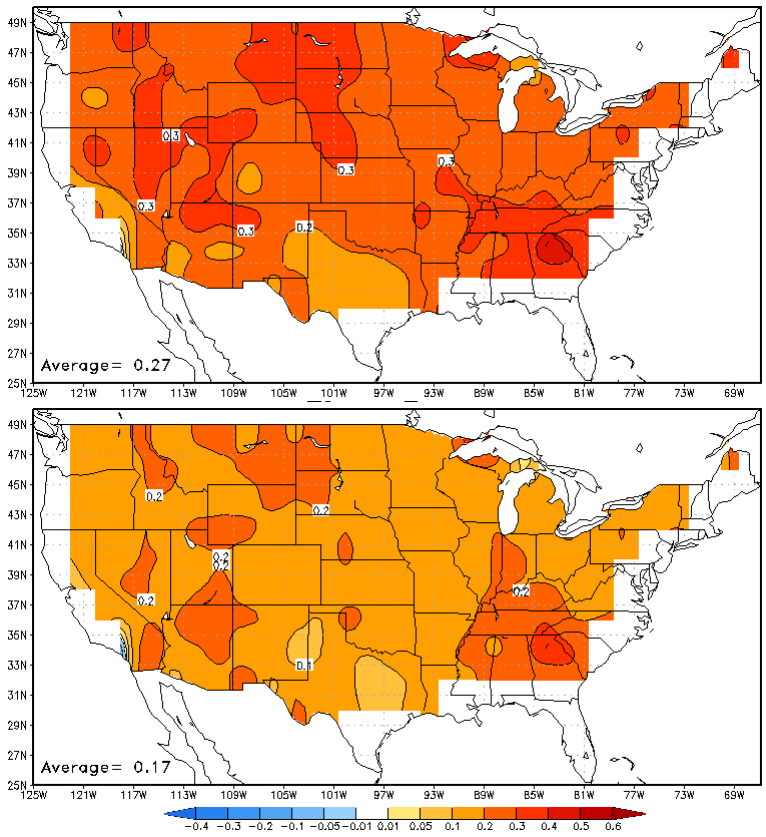

Fig. 5 RPSS over the CONUS for Tmin forecasts for days 8 (upper) and 14 (lower) for 1/21/13-12/31/13.

The RPSS averaged over the CONUS (Fig. 4) for 2013 yielded pretty good results, with the highest skill for forecasts on day 8 at about 0.28, and just below 0.2 by day 14. RPSS was positive for all leads, meaning the forecasts performed better than climatology for all leads. These results showed minimal loss in skill, even out to day 14, which is promising. For comparison, CPC's official 8-14 day tercile, probabilistic forecasts for the 7day mean temperature, had an RPSS of 0.12 for the same period. The higher skill for the extremes compared to the mean temperature may be attributed to the fact that there is more reward in RPSS for the tails of the percentile distribution. The timeseries of RPSS for days 8 and 14 shows that almost all of the forecasts had positive RPSS, with the highest scores during fall and winter.

Spatial evaluation of the RPSS of Tmin forecasts reveals positive skill across the entire CONUS for days 8 and 14 (other leads in the middle not shown), excluding a small area in southern California (which may be due to a bad data issue associated with the land border). This shows that there is an improvement upon climatology for all locations of the CONUS. The spatial distribution of skill was relatively uniform, with the least skill across the Southern Plains for both leads, and the most skill across the Southeast. The majority of the CONUS had skill of 0.2 or greater at day 8, and 0.1 or greater at day 14.

Reliability diagrams (Fig 6) reveal pretty good reliability for all three categories at day 8. The lower category (< 15th percentile) was underconfident for all probabilities, whereas the middle category (15-85th percentile) and above category (> 85th percentile) have better reliability, although somewhat overconfident at higher probabilities. At day 14, reliability is significantly worse than day 8, as expected. The lower category at day 14 is overconfident, which is the opposite of the day 8 results. This may be in part due to the fact that the model often produces higher probabilities at a longer leads, thinking it has more skill than would really

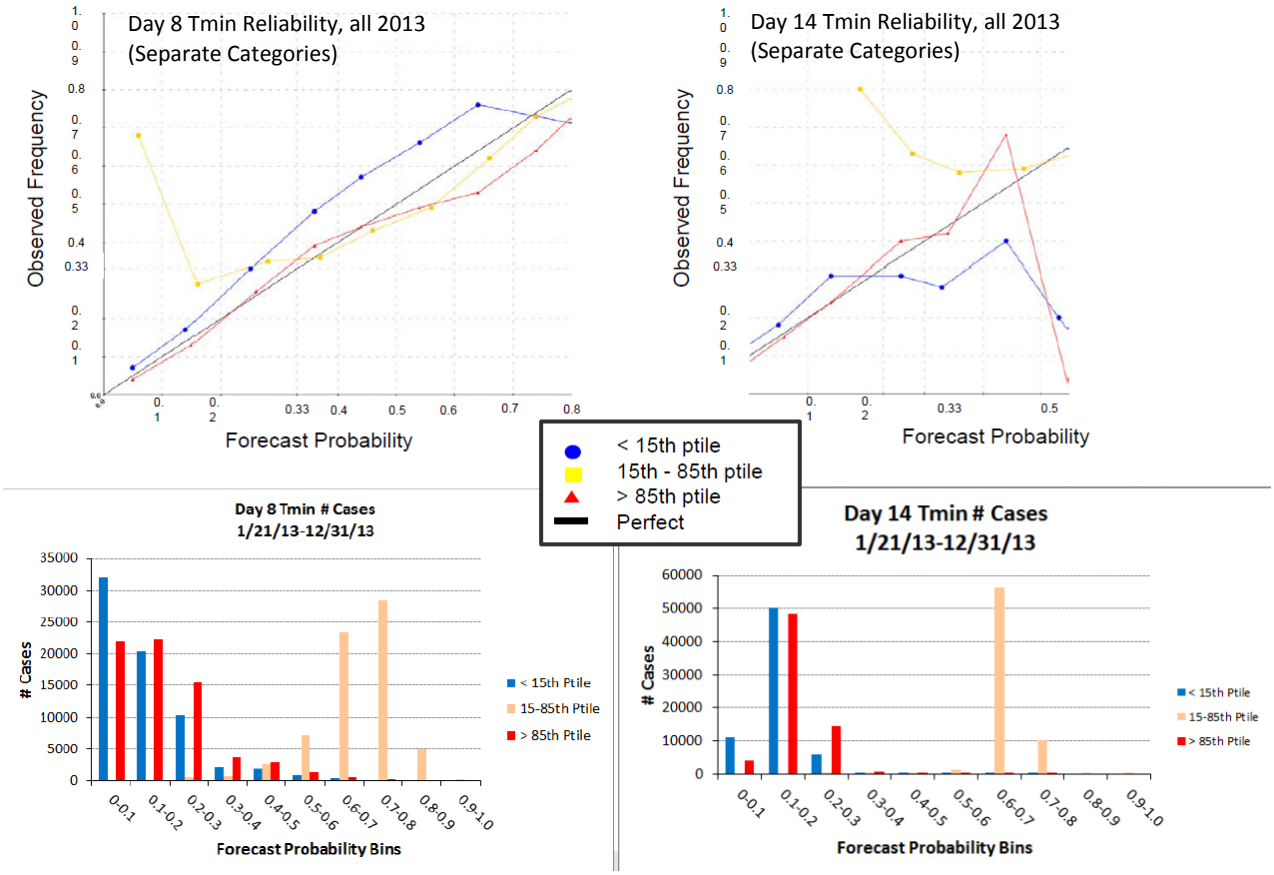

Fig. 6 The top row shows reliability diagrams for days 8 (top left) and 14 (top right) for 3 categories of percentile thresholds. The black diagonal line indicates what would be considered perfect reliability. The bottom row shows associated histograms (with the reliability diagrams above) with the number of forecasts associated with each of the probability bins for days 8 (bottom left) and 14 (bottom right) for the same categories.

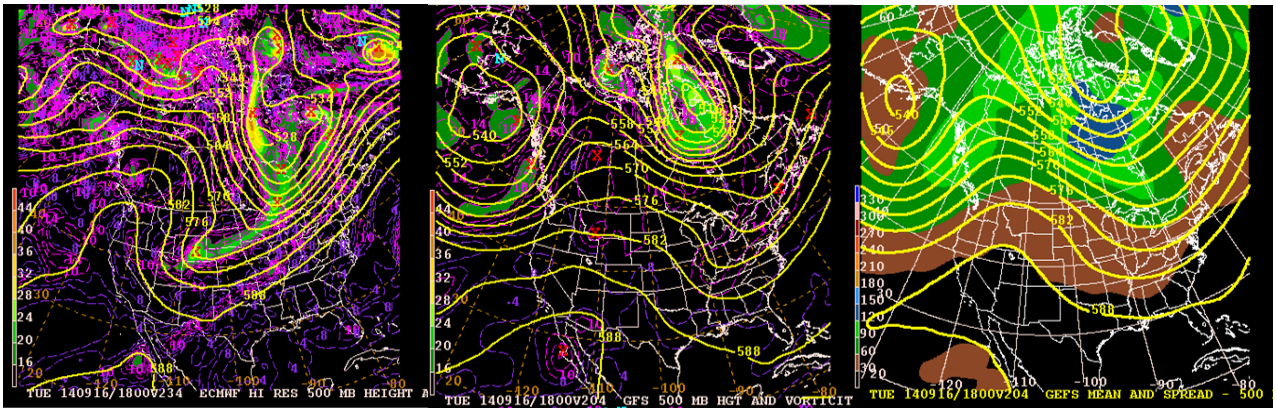

Fig. 7 Model run 500MB heights (yellow contours) and vorticity (shaded) from the deterministic 0Z ECMWF (left) and deterministic 6Z GFS (center). 500MB heights (yellow contours) and ensemble spread (shaded) are shown from the 6Z GEFS (right). All maps are valid 9/16/14, 18Z.

exist at that lead. There is likely less calibration performed at shorter leads than longer leads because skill is typically higher at shorter lead times. Therefore, the probabilities get scaled back more for shorter leads compared to the longer (calibration tends to lower the typically higher forecast probabilities from raw, uncalibrated ensemble forecasts). Results also indicate that at lead 8, there are more cases in the extreme categories (< 15th and >85th percentiles) with higher probabilities than day 14, as expected. There is better skill at shorter lead times, producing sharper probability distributions by the model. For both leads, the outlying reliability values for lower probabilities are likely due to the small sample sizes of forecasts in those probability bins. Curves in the reliability diagram are not shown in the day 14 diagram for probability bins greater than 0.6 because there were no forecasts of any category in those bins at that lead.

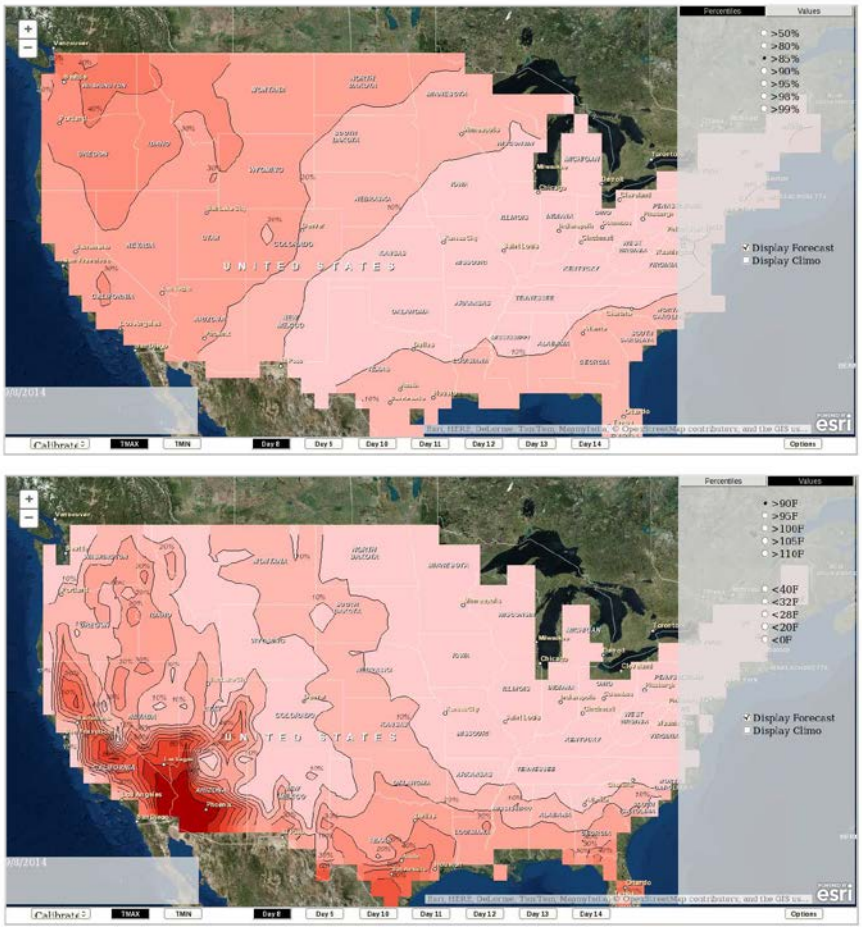

Fig. 8 Extremes tool forecast valid day 8, showing the probabilities of the daily maximum temperatures exceeding the 85th percentile (upper) and 90 degrees F (lower) based on CPC's GEFS reforecast tool.

5. Week-2 Probabilistic Hazards Forecast

a. About the forecast

CPC has been issuing daily probabilistic week-2 (days 8-14) hazards forecasts over the CONUS and Alaska since July 2014, in addition to the week-2 deterministic map, which has been issued for a number of years. These are manually drawn by the forecaster and are publicly available on the CPC

website. The probabilistic week-2 maps represent the probabilities of a daily minimum or maximum temperature reaching what we deem as hazardous criteria for each of the days in week-2, which is by nature a subjective forecast. Forecasters use the previously discussed probabilistic extremes tool as the main guidance regarding the probabilities, looking at both the percentiles and temperature value thresholds. They additionally evaluate the daily synoptic pattern and temperatures from various models. The hazards highlighted on the map are based on the forecasters' previous experiences and base knowledge and agreement amongst forecasters of what are considered regional thresholds and conditions for hazardous events. This information is often obtained from discussions and criteria provided by external regional interests and forecasters, such as the local weather forecast offices (WFOs). As mentioned earlier, CPC typically uses the upper and lower 15th percentiles as guidance for possibly deeming an event as hazardous, in combination with the probabilities of a temperature being below or above a certain threshold, which varies based on the location and time regime. Every Tuesday, a briefing is hosted by the hazards forecaster in which various interests dial-in, providing feedback and suggestions regarding the forecast. This enables local and regional weather service offices to provide valuable information to the hazards forecaster regarding whether an event should be highlighted or not, in addition to ensuring forecast coordination on various National Weather Service levels.

There are 3 levels of probabilities of a hazardous event occurring that are included in the forecast. Each level is denoted on the map with a qualitative description which has underlying probabilities associated with them. Qualitative versions of describing the risk level were used because it may convey the concept of varying probabilities better to the public. These categories are similar to those used by the Storm Prediction Center (SPC). The risk levels and their associated forecast probabilities are slight risk (20%), moderate risk (40%), and high risk (60%). Any contours greater than or equal to 40% (moderate or high risk) are automatically included on the week-2 deterministic hazards map. The web page for this product is http://www.cpc.ncep.noaa.gov/products/predictions/threats/threats.php.

b. Example forecast case

An example case of a forecast valid September 16, 2014 is discussed here. The daily model runs from the deterministic 0Z ECMWF and 6Z GFS, and 6Z GEFS (18Z) (Fig. 7) all indicated the possibility of an amplified ridge developing across the northwestern CONUS, with some variation in the level of amplification and ridge axis orientation. The 0Z ECMWF had the most amplified pattern, with the ridge axis focused over the Pacific Northwest, while the GFS and GEFS had the ridge shifted slightly eastward and not as amplified. Overall, this pattern would indicate the potential for warmer temperatures across the northwestern CONUS.

The probabilistic extremes tool for this day (Fig. 8) showed a 30-40% chance of Tmax being greater than the 85th percentile for the Pacific Northwest, and 30% chance of this area being greater than 90 degrees F. This temperature would be considered unusually high for this time of year with respect to the region. Therefore, the forecaster decided to issue a slight risk for much above normal temperatures for parts of Washington and Oregon for this day, as well as a moderate area embedded within this slight risk contour, focused over the central portion of this region (Fig. 9).

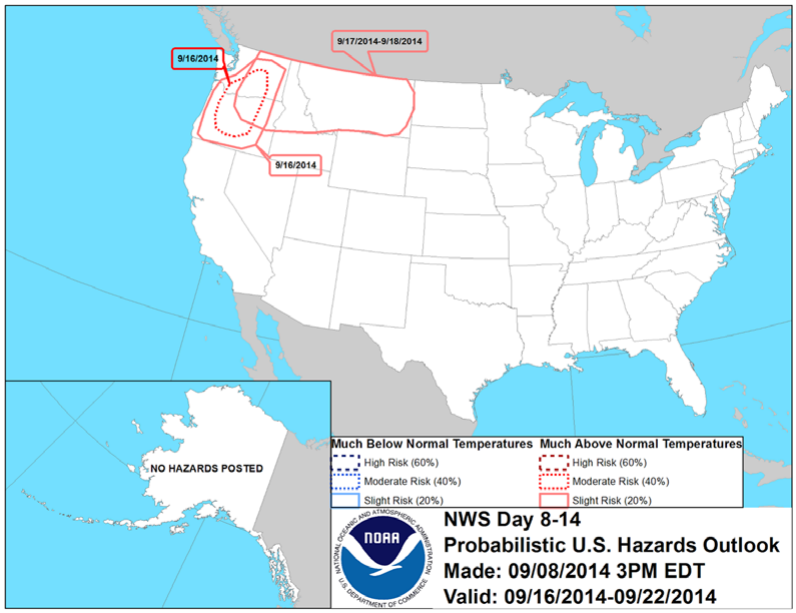

Fig. 9 Week-2 CPC probabilistic hazards forecast issued 9/8/2014, valid 9/16/2014-9/22/2014. Contours represent slight (light red solid line), moderate (medium red dotted line), and high risk (dark red dashed line) of much above normal temperatures.

An additional area was highlighted across the Pacific Northwest eastward into Montana for days 9 and 10 (not shown).

The verifying observations (Fig. 10) show that on 9/16/2014 temperatures were above normal that day across the Pacific Northwest, with anomalies in the 10-12 degrees F range and temperatures reaching 85 to 90 degrees. Overall, this would be considered a pretty good forecast, in that it did highlight the main areas that these temperatures would be considered very anomalous. The forecast area probably could have been extended slightly eastward into Idaho as well.

For the following day, the highlighted area for slight risk was not too bad either. The greatest temperature anomalies occurred over western Montana, which was included in the contour, although temperatures were only around 80 to 85 degrees F.

An example screenshot of CPC's hazard webpage that includes the week-2 probabilistic hazards forecast is shown in figure 11. There are options on the page to view the days 3-7 and 8-14 hazards forecast as well as the days 8-14 probabilistic forecast.

6. Summary

CPC has a new week-2 probabilistic hazards forecast, issued daily, which highlights potential hazards in probabilistic format. Currently this is done for Tmin and Tmax, but additional variables are planned to be added in the future. There are 3 categories representing the levels of likelihood of an event occurring. The thinking is that as the lead time shortens for an event, the probabilities of the event occurring may increase

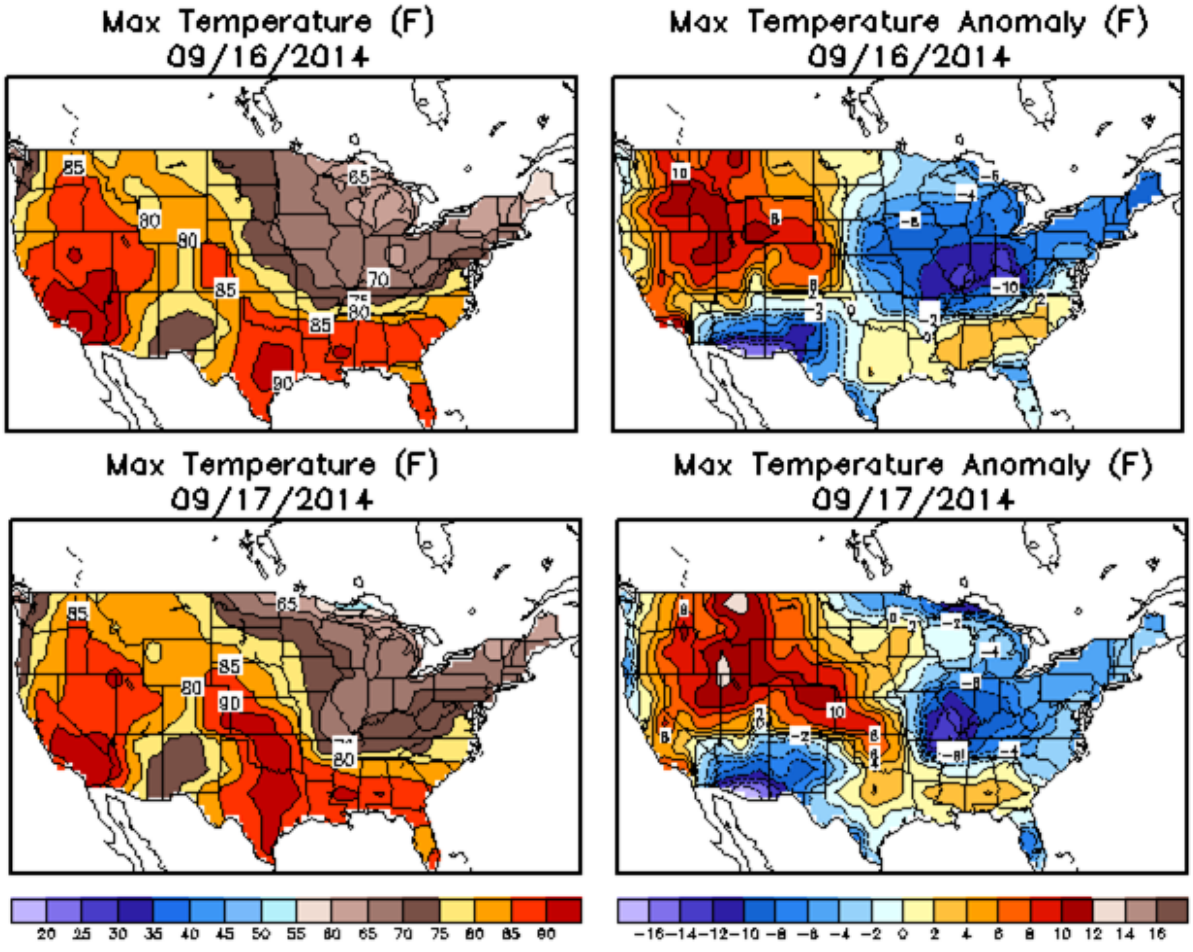

Fig. 10 Verifying observations of Tmax (left column) and Tmax anomalies (right column), for 9/16/2014 (top row) and 9/17/2014 (bottom row). All values are in degrees F.

due to higher certainty, finally enabling the hazard to be included on the deterministic map. The main guidance for this product is the newly developed probabilistic extremes tool at CPC, which provides an objective probabilistic outlook of extreme temperatures at varying percentile and temperature thresholds. The underlying data of the tool is currently from the reforecast tool at CPC, which calibrates GEFS model output using long term statistics from the 25year GEFS reforecast dataset.

The benefit of having the week-2 hazards in probabilistic format is that it enables more hazards to be put on the map. Previously, when CPC only issued the deterministic days 8-14 hazards, forecasters were often unable to put hazards on the map because of the inherent higher confidence/probabilities required to delineate a hazard deterministically would be very high. By expressing hazards as probabilities with varying tiers of likelihood, forecasters are able to include lower certainty/probability events at a longer lead. Extra information associated with these levels of likelihood will hopefully add value to the forecasts, especially for decision makers.

Overall, the initial verification of the probabilistic extremes tool shows positive skill (reliability and RPSS). There is decent improvement over climatology and shows the best skill for the winter season, which is expected since winter typically has better predictability. The tool produces significant probabilities (defined

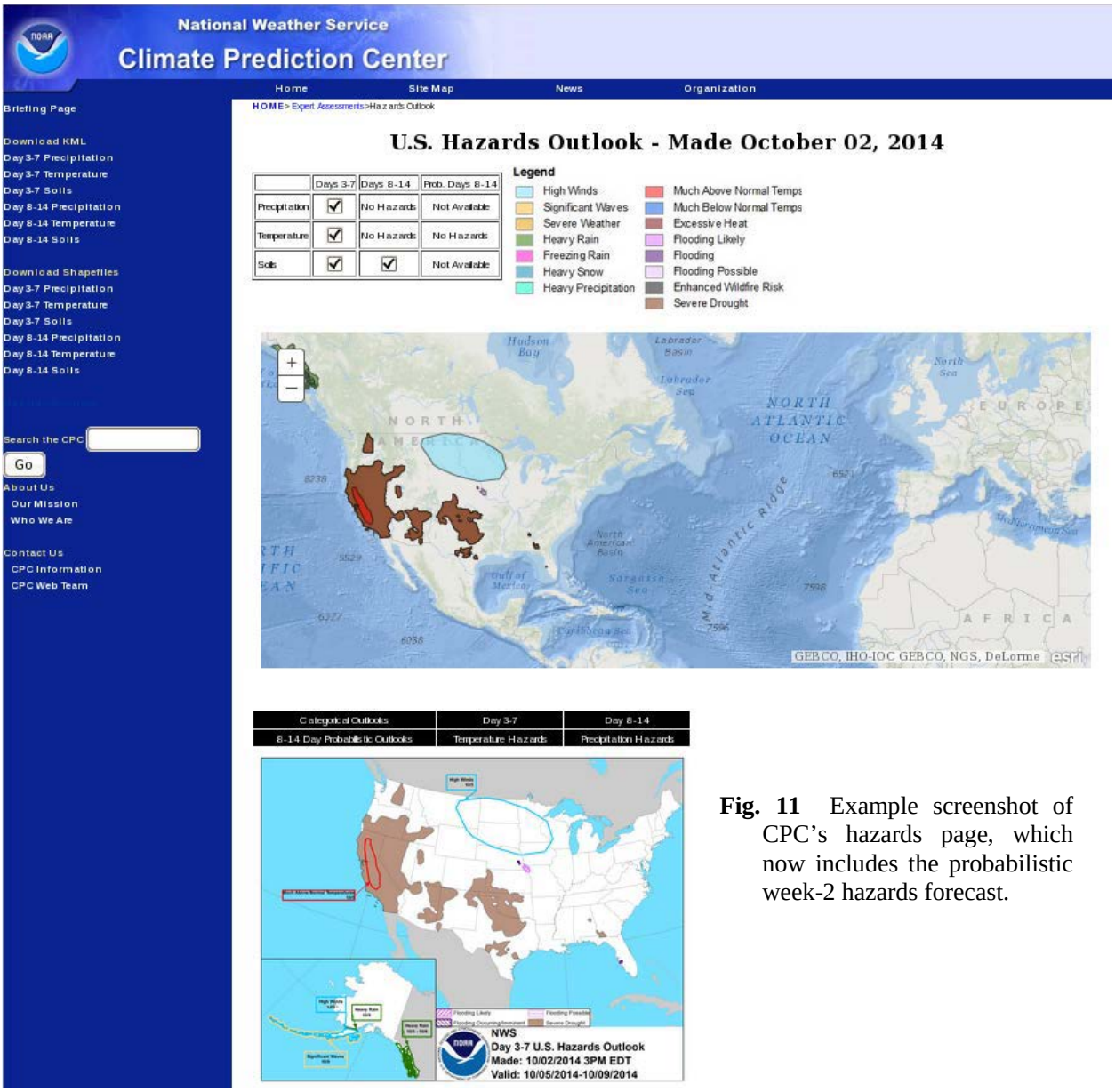

Fig. 11 Example screenshot of CPC's hazards page, which now includes the probabilistic week-2 hazards forecast.

as 20% or greater) of extremes at a pretty good frequency, enabling forecasters to potentially include an event on the probabilistic hazards forecast 10 to 20% of the time (based on a year's worth of evaluation over 2013). There are especially good opportunities for hazardous Tmin probabilities to be issued during the winter season.

7. Ongoing/future work

This project is planned to have a phased approach for adding new features, such as more variables (precipitation, wind, *etc*.), thresholds, and models. Another tool is currently being developed at CPC, which consolidates forecasts from different sources (dynamical and statistical models), by which the weights used for combination are determined by the past skill of the model/tool. CPC plans to utilize this consolidated forecast to derive a multimodel forecast for probabilistic extremes in the future. This would hopefully improve the skill of the probabilistic extremes tool, and thus the manually issued forecasts.

Additional skill evaluation of the extremes tool is planned to be extended for Tmax, Alaska, and other percentiles and temperature values. Verification of the tool will also likely be performed on forecasts produced by the calibrated versus uncalibrated GEFS reforecast tool and impacts associated with the relationship of spread to skill. Global or other regional verification may also be done by other members of CPC, such as to evaluate the ability to use this tool to support the global tropical hazards forecasts, as well as external users.

References

Ou, M., M. Charles, D. Collins, and E. Riddle, 2014: Sensitivity study of the skill of the CPC week-2 reforecast tool to reforecast sampling. *Climate Prediction S&T Digest*, 38th NOAA Annual Climate Diagnostics and Prediction Workshop, College Park, MD, National Oceanic and Atmospheric Administration, 36-43. [Available online at http://docs.lib.noaa.gov/noaa_documents/NWS/NCEP/CDPW/38th_2014.pdf]

Unger, D., A., and Co-authors, 2009: Ensemble regression. *Mon. Wea. Rev.*, **137**, 2365-2379.

Science and Technology Infusion Climate Bulletin
NOAA's National Weather Service
39th NOAA Annual Climate Diagnostics and Prediction Workshop
St. Louis, MO, 20-23 October 2014

Assessment of the Predictability of September Sea Ice Concentration Using Sea Ice Thickness

Thomas W. Collow[1, 2], Wanqiu Wang[2], and Arun Kumar[2]

[1]*INNOVIM, LLC*

[2]*Climate Prediction Center, NCEP/NWS/NOAA*

1. Introduction

According to the 5th assessment report from the Intergovernmental Panel on Climate Change (IPCC), annual Arctic sea ice extent (SIE) is very likely (90%-100% confident) to have decreased at a rate of 0.45 to 0.51 million km^2 per decade during the 1979-2012 period due to anthropogenic influences (Vaughan et al. 2013) leading to projections of an ice free Arctic by the 2030's (Wang and Overland 2012). On a seasonal time scale, accurate sea ice prediction is important for oil and shipping interests, wildlife protection, and ecosystems management. Changes in sea ice can also influence atmospheric variability. For example, it has been observed that because Arctic sea ice melt decreases the albedo, which exacerbates the warming, there has been a faster rate of warming in the Arctic than in the lower latitudes (Kumar *et al.* 2010; Screen and Simmonds 2010). Some studies (Francis and Varvus 2012; Liu *et al.* 2012) have proposed this polar amplification in the warming trend as a mechanism for changes in the geopotential height structure and upper level jet stream pattern, which are then linked to more extreme weather events across the globe.

Blanchard-Wrigglesworth *et al.* (2011) and Wang *et al.* (2013) demonstrated that Arctic sea ice cover is potentially predictable beyond 9 months using the Community Climate System Model version 4 (CCSM4) and Climate Forecast System Version 2 (CFSv2) respectively. However, assessments also show small actual predictive skill for sea ice beyond 2-3 months (Merryfield *et al.* 2013; Wang *et al.* 2013). The difference between potential predictability and actual skill raises interesting questions for possible causes, for example, errors in the initialization of sea ice thickness. Wang *et al.* (2013) show that changes in sea ice thickness during the spring months had a large impact on forecasts of September SIE using CFSv2, with thickness increases resulting in higher SIE forecasts and vice versa, which agreed with observations. Low March 2007 sea ice thickness anomalies were cited by Kauker *et al.* (2009) as a factor leading to the record low sea ice cover the following September. Therefore, because sea ice thickness is argued to be an important predictor to forecast September sea ice cover, it is plausible that an improvement in the initial condition sea ice thickness dataset used in models could yield an improvement in September sea ice forecasts, even those initialized in the spring, narrowing the gap between prediction skill and potential predictability. However, before modeling experiments are carried out, this work aims to simply test the relationship between lagged sea ice thickness from two different datasets and September sea ice cover to assess the feasibility of such experiments.

2. Data and methods

Pan-Arctic Ice Ocean Modeling and Assimilation System (PIOMAS) monthly averaged sea ice thickness data (Zhang and Rothrock 2003) from the Polar Science Center at the University of Washington were used, in addition to Climate Forecast System Reanalysis (CFSR; Saha *et al.* 2010) sea ice thickness data from the National Centers of Environmental Prediction (NCEP). Sea ice components in both PIOMAS and CFSR assimilate satellite measurements of sea ice concentration. Sea ice thickness is derived from internal dynamics and thermodynamics without assimilating observed thickness information. Both CFSR and PIOMAS data were interpolated to 0.5° x 0.5° Arctic grid spacing. Separate time series of Arctic sea ice

Correspondence to: Thomas W. Collow, INNOVIM, LLC | Climate Prediction Center, NOAA/NWS/NCEP, 5830 University Research Court, College Park, MD; Email: Thomas.collow@noaa.gov .

volume (SIV) for each month of the period 1982-2013 were created for each dataset by multiplying the sea ice thickness of each grid cell by the respective grid cell area and taking a sum across the northern hemisphere.

First it is shown that PIOMAS sea ice thicknesses are more accurate in both magnitude and trend than CFSR data with respect to Ice, Cloud, and land Elevation Satellite (ICESat) data. Then, 2nd order polynomial detrended, lagged PIOMAS and CFSR SIV were temporally correlated with a common dataset of September SIE and sea ice area (SIA) from the National Snow and Ice Data Center which was generated with the National Aeronautics and Space Administration (NASA) Team Sea Ice Algorithm based on satellite observations (Cavalieri and Gloersen 1984), and also interpolated to a 0.5° x 0.5° grid (native NASA Team grid spacing is 25 km). The NASA Team observations have a region close to the pole that cannot be observed due to the orbit inclination of the satellites. This area, known as the polar hole, is removed from all datasets for a concise evaluation. Following the IPCC report (Vaughan *et al.* 2013), SIE is defined as the region encompassed by the edge of sea ice, represented by a concentration of at least 15%. Because of this, regions with small gaps in the sea ice with a concentration still greater than the 15% threshold are still counted as part of the SIE. SIA is different, as these gaps between sea ice are not included. For this reason SIE is always greater than SIA. In this analysis, Arctic SIE was computed by taking the cumulative sum across the northern hemisphere of the area of each grid cell with a sea ice concentration at or above 15%. SIA was calculated by multiplying the sea ice concentration in each grid cell by the area of the respective grid cell and taking a northern hemisphere sum of the results for grid cells with a sea ice concentration at or greater than 15%.

Temporal correlations were also computed on a grid point scale, using only monthly sea ice thickness and September sea ice concentration values at individual grid cells with the idea that regional patterns could exist that cannot be explained by a single hemispheric parameter like SIE or SIA. To assess the significance of the differences between the correlations, the Steiger's Z test (Steiger 1980) was employed. The test takes into account the number of data points as well as the correlation between the two datasets being compared, in this case PIOMAS and CFSR sea ice thicknesses. Because of the small size of the dataset, significance is based on an 80% confidence interval, rather than the more traditional 95%.

3. ICESat volume comparison

SIV is difficult to evaluate due to a lack of uniform observations. However, ICESat was able to provide measurements of ice thickness using a laser altimeter (Schultz *et al.* 2005). The satellite had an acquisition period each spring 2004-2008 covering roughly 35 days each, which vary slightly in their exact coverage dates. There is also a set of autumn retrievals, but because this study is concerned with prediction of September sea ice, the spring acquisition periods were of particular interest to us. For each period, from the sea ice thickness retrieved by the satellite (available from http://rkwok.jpl.nasa.gov/icesat), total SIV was calculated in the same manner as it was for PIOMAS and CFSR. The same interpolation and common mask described in the previous section was used and no detrending was applied as the time period was too short to establish any coherent trend. The ICESat data were compared with daily PIOMAS and CFSR data which were averaged to match the exact dates of the ICESat acquisition periods. Only PIOMAS and CFSR data within the ICESat domain were considered for this comparison. Figure 1 illustrates the comparison of spatial sea ice thickness and hemispheric SIV between the ICESat data and the two modeled datasets. Averaging over the spring acquisition periods, ICESat sea ice thickness patterns were closer to PIOMAS sea ice thickness patterns than to CFSR sea ice thickness patterns (Figure 1a-c). It is also apparent from Figure 1d that the ICESat SIV trends are more in line with PIOMAS trends than with CFSR trends. Root mean square errors (RMSE) relative to ICESat SIV were 2143 km^3 and 825 km^3 for CFSR and PIOMAS SIVs respectively.

4. Correlation between September sea ice cover and lagged sea ice thickness

Using detrended monthly data, no significant differences were seen in the performance of PIOMAS and CFSR when hemispheric scale SIV was correlated with September SIE and SIA over the period. However, using PIOMAS SIV showed a slightly stronger relationship with September SIA at a 1-3 month lead. Changes were more apparent on a grid point scale as there was a larger region that showed significant

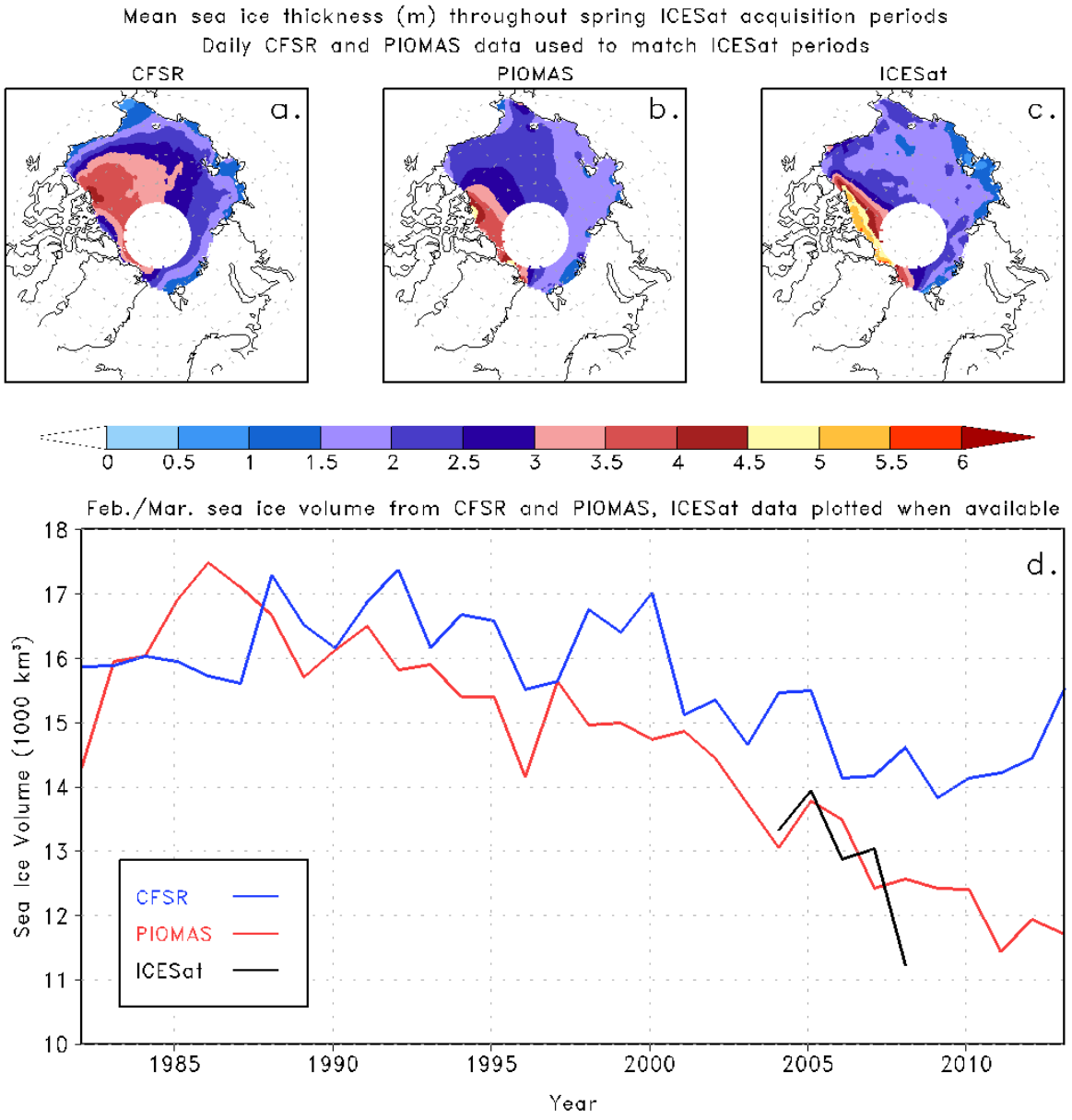

Fig. 1 Mean sea ice thickness throughout the five ICESat spring acquisition periods. Daily CFSR (panel a) and PIOMAS (panel b) data used to exactly match ICESat (panel c) periods. Panel d shows mean February-March SIV from CFSR and PIOMAS for 1982-2013 with the ICESat volume for the five acquisition periods plotted where applicable (Only grid cells common to the three datasets are used in the calculation of SIV).

increases in correlation at an 80% confidence interval than decreased skill at all lead times except zero. The area of the region with significant increases versus that with significant decreases are shown under each panel of Figure 2 and plotted as a function of lag month in panel h to further convey this point. Positive differences between increases and decreases were highest for -2 to -4 months lag (correlating May, June, or July sea ice thickness to September sea ice concentration, Figure 2c-e). Even for a lag of -6 months (March sea ice thickness, Figure 2g), increases were prevalent suggesting improvements could still be obtained out to 6 months.

5. Summary and conclusion

An assessment of the potential usefulness of PIOMAS SIV to improve the predictability of Arctic SIE and SIA in September was conducted using detrended lagged correlations. The same geographical masks

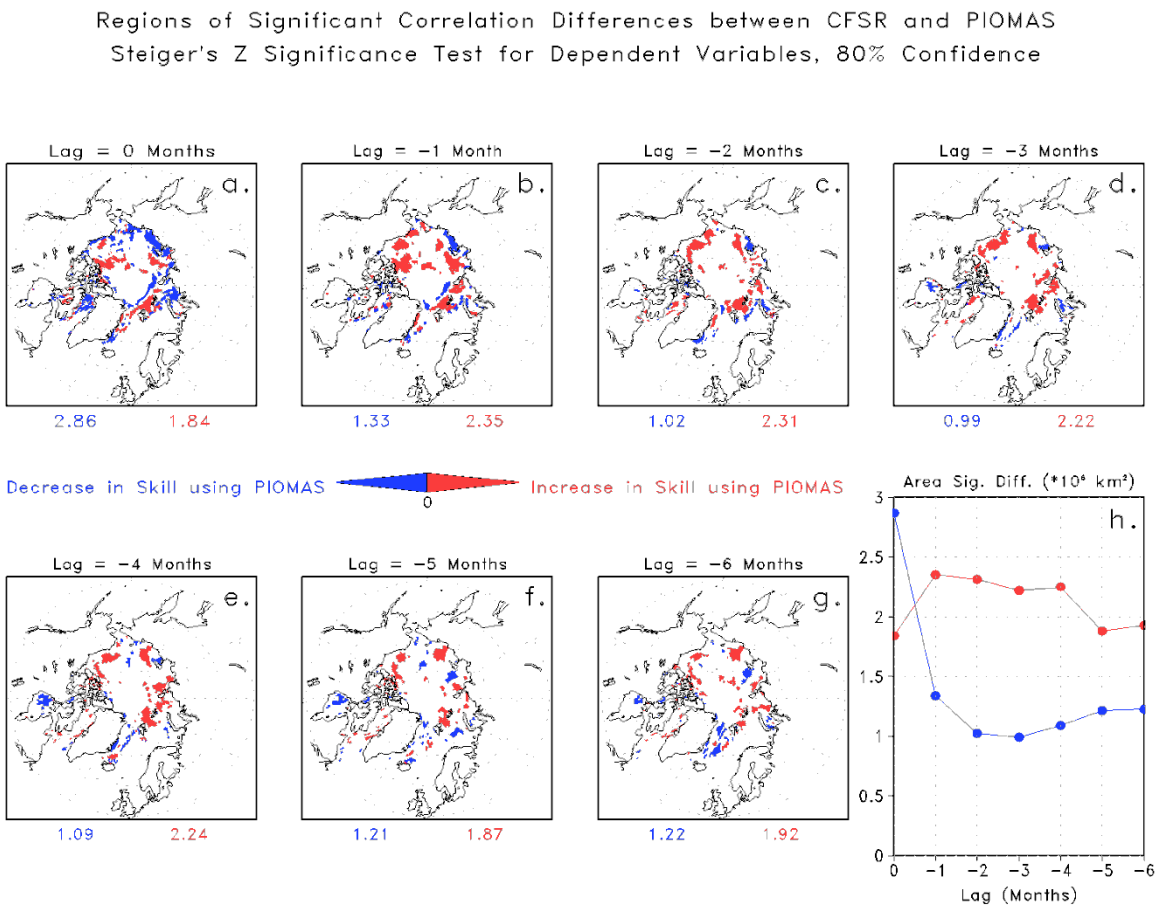

Fig. 2 Significant changes in correlation at 80% confidence that result from using PIOMAS lagged sea ice thickness to correlate with September sea ice concentration from NASA Team relative to using CFSR sea ice thickness. Red shading represents locations with a significant increase in skill using PIOMAS and blue signifies locations with a significant decrease in skill. Numbers at the bottom of each plot denote the area (10^6 km^2) of each colored region. Panels a through g are for 0 to -6 lag months. Panel h is a time series showing the area encompassed by each color (y-axis) as a function of lag month (x-axis).

were applied to all datasets to ensure consistency. Comparison with ICESat as an observational benchmark for SIV yielded PIOMAS as a more realistic dataset (within the limitation that the assessment was based on only 5 data points in time). We show that although little improvements were seen in correlating September SIE and SIA using PIOMAS SIV as opposed to CFSR SIV, significant improvements were seen when grid cell scale ice thickness and concentration were looked at. The area with significant improvements was larger than the area with significant decrease in skill in all lag months except the initial month for 80% confidence. The increase was most pronounced for correlations of May, June, and July sea ice thicknesses with the following September sea ice concentration in which the area of increase exceeded the area of decrease by a factor of near or greater than 2, which is important as this period was previously labeled as having a low predictability of September ice cover.

Because of the stronger relationship between the PIOMAS data and NASA Team observations, in addition to being more realistic as seen through comparisons with ICESat, it is plausible that utilization of PIOMAS sea ice thickness data could aid in improving prediction of September sea ice coverage, especially in the preceding June, but also as early as March. We are in the process of doing forecast experiments with the CFSv2 initialized using PIOMAS initial sea ice thickness as opposed to CFSR sea ice thickness, with the goal of producing a better sea ice forecast.

References

Blanchard-Wrigglesworth, E., C. M. Bitz, and M. M. Holland, 2011: Influence of initial conditions and climate forcing on predicting Arctic sea ice. *Geophys. Res. Lett.*, **38**, L18503, doi: 10.1029/2011GL048807.

Cavalieri, D. J., and P. Gloersen, 1984: Determination of sea ice parameters with the NIMBUS 7 SMMR. *J. Geophys. Res.*, **89(D4)**, 5355-5369.

Francis, J. A., and S. J. Varvus, 2012: Evidence linking Arctic amplification to extreme weather in mid-latitudes. *Geophys. Res. Lett.*, **39**, L06801, doi: 10.1029/2012GL051000.

Kauker, F., T. Kaminski, M. Karcher, R. Giering, R. Gerdes, and M. Voβbeck, 2009: Adjoint analysis of the 2007 all time Arctic sea-ice minimum. *Geophys. Res. Lett.*, **36**, L03707, doi :10.1029/2009GL036323.

Kumar, A., J. Perlwitz, J. Eischeid, X. Quan, T. Xu, T. Zhang, M. Hoerling, B. Jha, and W. Wang, 2010: Contribution of sea ice loss to Arctic amplification. *Geophys. Res. Lett.*, **37**, L21701, doi: 10.1029/2010GL045022.

Liu, J., J. A. Curry, H. Wang, M. Song, and R. M. Horton, 2012: Impact of declining Arctic sea ice on winter snowfall. *Proc. Natl. Acad. Sci.*, **109(11)**, 4074-4079. doi: 10.1073/ pnas. 1114910 199.

Merryfield, W. J., W.-S. Lee, W. Wang, M. Chen, and A. Kumar, 2013: Multi-system seasonal predictions of Arctic sea ice. *Geophys. Res. Lett.*, **40**, 1551-1556. doi: 10.1002/grl.50317.

Saha, S., and Co-authors, 2010: The NCEP Climate Forecast System Reanalysis. *Bull. Amer. Meteor. Soc.*, **91**, 1015-1067. doi: 10.1175/2010BAMS3001.1.

Schutz, B. E., H. J. Zwally, C. A. Shuman, D. Hancock, and J. P. DiMarzio, 2005: Overview of the ICESat Mission. *Geophys. Res. Lett.*, **32**, L21S01, doi:10.1029/2005GL024009.

Screen, J. A., and I. Simmonds, 2010: The central role of diminishing sea ice in recent Arctic temperature amplification. *Nature*, **464**, 1334-1337. doi: 10.1038/nature09051.

Steiger, J. H., 1980: Tests for comparing elements of a correlation matrix. *Psychol. Bull.*, **87(2)**, 245-251. doi: 10.1037/0033-2909.87.2.245.

Vaughan, D.G., J.C. Comiso, I. Allison, J. Carrasco, G. Kaser, R. Kwok, P. Mote, T. Murray, F. Paul, J. Ren, E. Rignot, O. Solomina, K. Steffen and T. Zhang, 2013: Observations: Cryosphere. In: Climate Change 2013: The Physical Science Basis. Contribution of Working Group I to the Fifth Assessment Report of the Intergovernmental Panel on Climate Change [Stocker, T.F., D. Qin, G.-K. Plattner, M. Tignor, S.K. Allen, J. Boschung, A. Nauels, Y. Xia, V. Bex and P.M. Midgley (eds.)]. Cambridge University Press, Cambridge, United Kingdom and New York, NY, USA, 317-382.

Wang, M., and J. E. Overland, 2012: A sea ice free summer Arctic within 30 years: An update from CMIP5 models. *Geophys. Res. Lett.*, **39**, L18501, doi: 10.1029/2012GL052868.

Wang, W., M. Chen, and A. Kumar, 2013: Seasonal prediction of Arctic sea ice extent from a coupled dynamical forecast system. *Mon. Wea. Rev.*, **141**, 1375-1394. doi: 10.1175/MWR-D-12-00057.

Zhang, J.L., and D.A. Rothrock, 2003: Modeling global sea ice with a thickness and enthalpy distribution model in generalized curvilinear coordinates. *Mon. Wea. Rev.*, **131**, 845-861.

Science and Technology Infusion Climate Bulletin
NOAA's National Weather Service
39th NOAA Annual Climate Diagnostics and Prediction Workshop
St. Louis, MO, 20-23 October 2014

Fire and Ice - California Drought and "Polar Vortex" in a Changing Climate

S.-Y. Simon Wang[1], Larry Hipps[1], Robert Gillies[1], and Jin-Ho Yoon[2]

[1]*Utah Climate Center / Dept. Plants, Soils and Climate, Utah State University, Logan, UT*
[2] *Pacific Northwest National Laboratory, Richland, WA*

ABSTRACT

The 2013–2014 California drought was initiated by an anomalous high-amplitude ridge system. The anomalous ridge was investigated by Wang *et al.* (2014) using reanalysis data and the Community Earth System Model (CESM). Analysis from observational data (NCEP/NCAR Reanalysis) showed that the ridge emerged from continual sources of Rossby wave energy in the western North Pacific starting in late summer and subsequently intensified into winter (Fig. 1). The ridge generated a surge of wave energy downwind and deepened further the trough over the northeast U.S., forming a dipole. The wavelength of this dipole is rather large (at zonal wave numbers 1-2 scale) surpassing the common short-wave patterns (zonal wave #4-6) accompanying heat waves and stormy weather (Chang and Wallace, 1987; Screen and Simmonds, 2014; Teng *et al.*, 2013; Wang *et al.*, 2013a). This long-wave feature of the dipole suggests a closer link with SST teleconnection from the tropical Pacific (Wallace and Gutzler, 1981), rather than with the higher-latitude forcing that tends to produce shorter waves (Branstator, 2002).

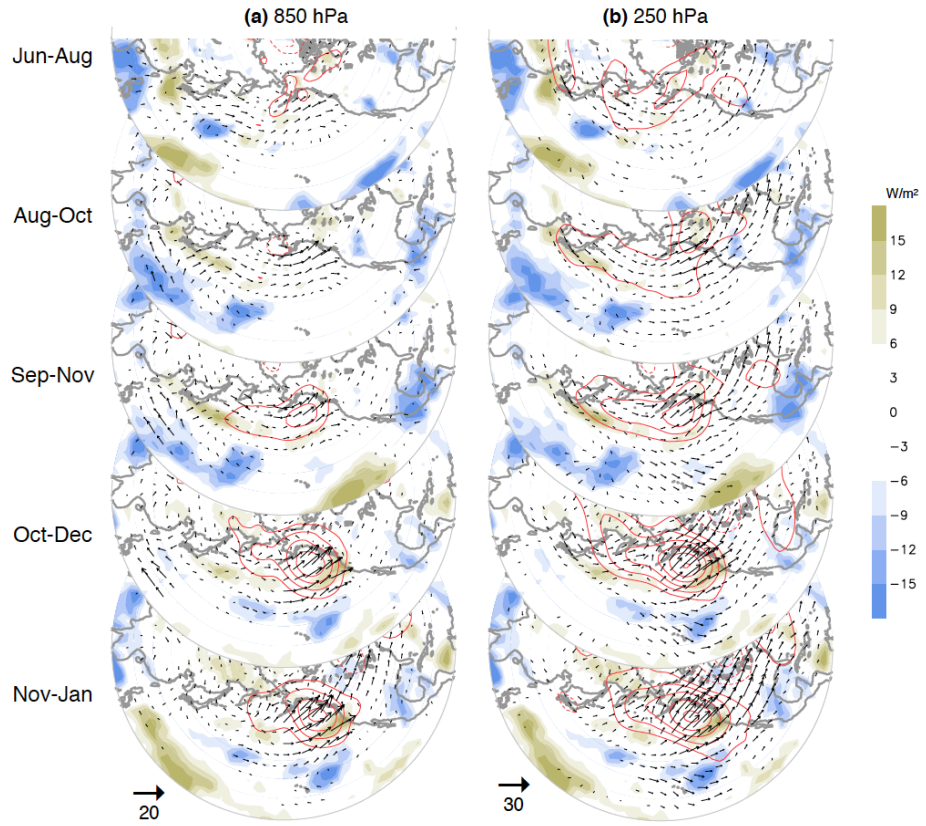

Fig. 1 NDJ 2013-14 anomalies of geopotential height (red contours) and OLR (color shadings) overlaid with the wave activity fluxes (vectors) for a three-month period from June-August to November-January as indicated, computed from the levels of (a) 850 hPa and (b) 250 hPa. Contour interval is 25 m for 850 hPa and 50 m for 250 hPa; the zero and the first positive and negative contours are omitted.

Furthermore, the study of Wang *et al.* (2014) indicated that the dipole and associated circulation pattern is not linked directly with either El Niño–Southern Oscillation (ENSO) or Pacific Decadal Oscillation. Instead, it is correlated with a type of ENSO precursor, one that has a predominant signal in the Western North Pacific (WNP) and this dynamical linkage has intensified in recent decades (Wang *et al.*,

Correspondence to: S.-Y. Simon Wang, 4820 Old Main Hill, Logan, UT 84322; Email: simon.wang@usu.edu

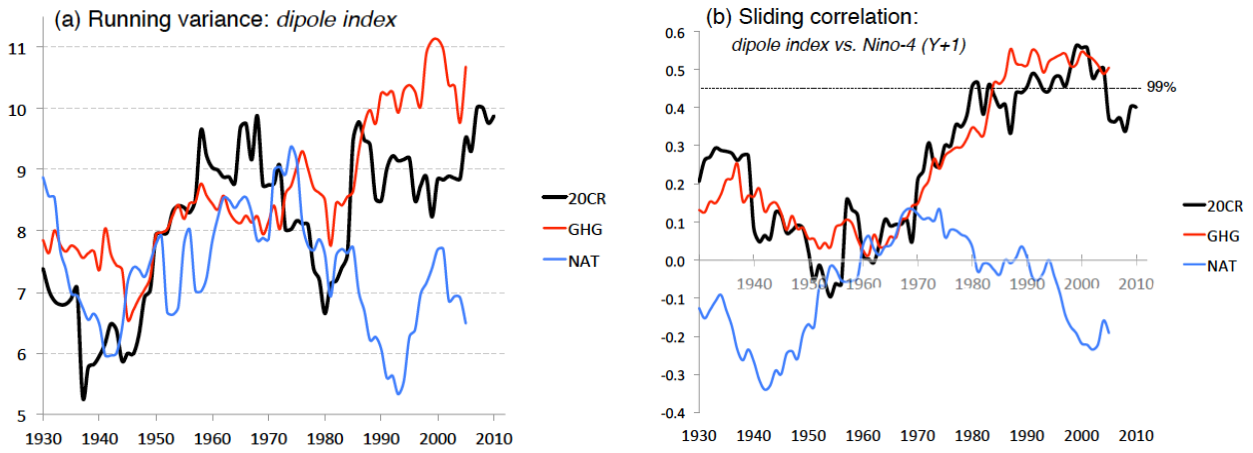

Fig. 2 (a) Running variance of the dipole index (x 10^4 m^2) with a 30-year window plotted at the end year beginning in 1900, derived from the 20CR (black), CESM1-GHG run (red) and CESM1-NAT run (blue). (b) Sliding correlations between the dipole index and Niño4 (Y+1) within a 30-year window corresponding to (a). The dashed line indicates significance at the 99% level.

2013b). The variance of the dipole has increased, while the connection between the dipole and ENSO precursor has become stronger since the 1970s; this is attributed to increased greenhouse gas loading as simulated by the CESM (Fig. 2). As further verification, a recent study (Wang *et al.*, 2015) using 17 models from the Coupled Model Intercomparison Project Phase 5 (CMIP5) found that most models capture the midlatitude circulation dipole, its association with El Niño precursor, and its intensification under anthropogenic greenhouse gas forcing (Fig. 3). Therefore, there is a traceable anthropogenic warming footprint in the enormous intensity of the anomalous ridge during winter 2013–2014 and the associated drought.

References

Branstator, G., 2002: Circumglobal teleconnections, the jet stream waveguide, and the North Atlantic Oscillation. *J. Climate*, **15**, 1893-1910.

Chang, F.-C., and J. M. Wallace, 1987: Meteorological conditions during heat waves and droughts in the United States Great Plains. *Mon. Wea. Rev.*, **115**, 1253-1269.

Screen, J. A., and I. Simmonds, 2014: Amplified mid-latitude planetary waves favour particular regional weather extremes. *Nature Clim. Change*, **4**, 704–709, doi:10.1038/nclimate2271.

Teng, H., G. Branstator, H. Wang, G. A. Meehl, and W. M. Washington, 2013: Probability of US heat waves affected by a subseasonal planetary wave pattern. *Nature Geoscience*, **6**, 1056-1061, doi:10.1038/ngeo1988.

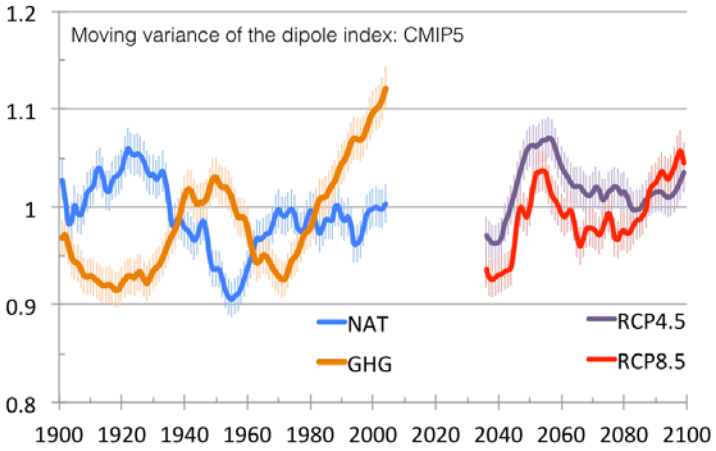

Fig. 3 Moving variance of the dipole index (see text) over a 30-year running window, plotted at the end year, for the ensemble of different experiments as indicated by the legend. Error bars indicate model spread from all members and all models. The dipole index was normalized (between -2 and 2) prior to computing the variance.

Wallace, J. M., and D. S. Gutzler, 1981: Teleconnections in the geopotential height field during the Northern Hemisphere winter. *Mon. Wea. Rev.*, **109**, 784-812.

Wang, S.-Y., R. E. Davies, and R. R. Gillies, 2013a: Identification of extreme precipitation threat across midlatitude regions based on short-wave circulations. *J. Geophys. Res.: Atmos.*, **118**, 11,059–11,074, doi:10.1002/jgrd.50841.

——, M. L'Heureux, and J.-H. Yoon, 2013b: Are greenhouse gases changing ENSO precursors in the western North Pacific? *J. Climate*, **26**, 6309-6322.

——, W.-R. Huang, and J.-H. Yoon, 2015: The North American winter 'dipole' and extremes activity: A CMIP5 assessment. *Atmos. Sci. Lett.*, in press.

——, L. Hipps, R. R. Gillies, and J.-H. Yoon, 2014: Probable causes of the abnormal ridge accompanying the 2013–2014 California drought: ENSO precursor and anthropogenic warming footprint. *Geophys. Res. Lett.*, **41**, 3220–3226, doi:10.1002/2014GL059748.

Science and Technology Infusion Climate Bulletin
NOAA's National Weather Service
39th NOAA Annual Climate Diagnostics and Prediction Workshop
St. Louis, MO, 20-23 October 2014

What caused the North America climate anomalies in 2013/14 winter?

Peitao Peng, Arun Kumar, Mingyue Chen, and Bhaskar Jha

Climate Prediction Center, NCEP/NWS/NOAA

North America experienced severe climate anomalies in the winter season of 2013/14. The anomalies are characterized with recorded warm and draught in west coast and extremely cold in the middle and east (Fig. 1). The associated circulation anomalies had a ridge off the west coast and a trough over the inner part of the land, representing a skewed polar vortex towards NA region (Fig. 2). In this study, we analyzed possible causes for the anomalies with both statistical and dynamical tools and AGCM simulations. It is found that in the observation, the seasonal mean circulation anomalies over North America was a part of wave train propagated from the jet exit region over the North Pacific (Fig. 2) . The lack of Gill-type heating-circulation in lower latitudes, however, suggests that the wave train may not be directly forced by tropical heating for the whole season. A further examination of monthly mean data suggests that the wave train was likely initiated by tropical heating in December and maintained by internal dynamics in following three months (Fig. 3). On the other hand, a set of AMIP-type experiments successfully simulated the climate anomalies in North America for the winter season. Diagnostics showed that the corresponding circulation anomalies in the model were forced by tropical SST. Major differences in circulation anomalies between model and observation are in lower latitudes, where model circulation matches well with tropical heating in Gill-type relationship. In order to see the possibility that a 4-month persistence of circulation over North America could happen without persistent external forcing, we conducted a pattern persistence analysis with the monthly mean data from reanalysis and the ensemble AMIP-type simulation data. It is found that 4-month or longer circulation persistence in that region could occur in ENSO-neutral winters, though with minor probability. In addition, contribution from recent climate trend is also analyzed.

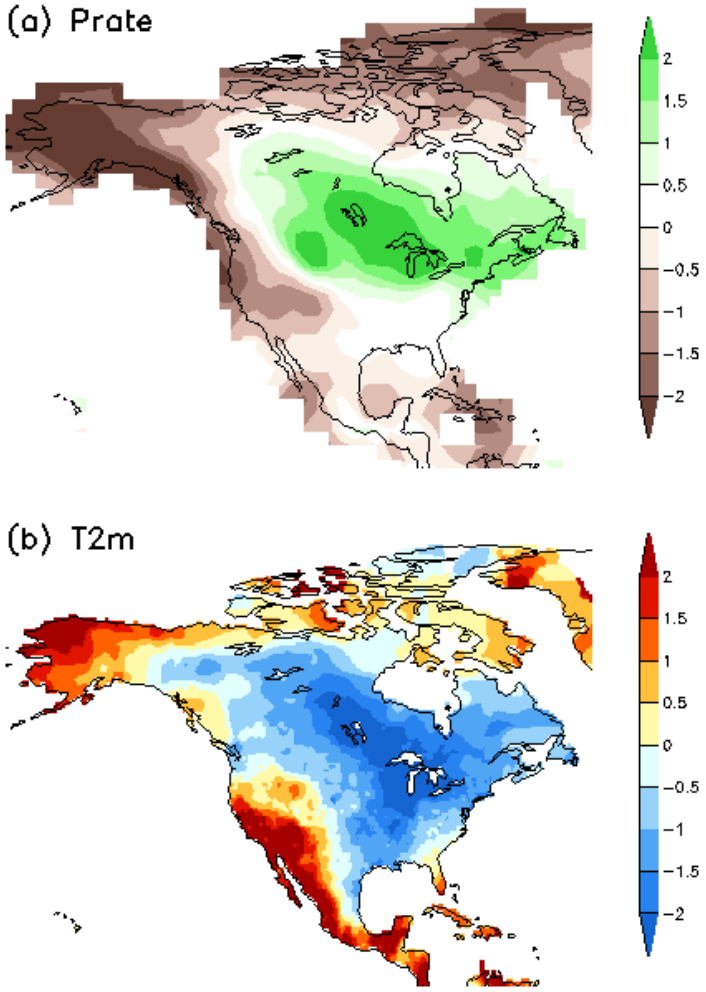

Fig. 1 Standardized seasonal mean precipitation and 2-meter temperature anomalies of 2013/14 winter (Dec-Jan-Feb-Mar). The unit is the standard deviation of the seasonal mean anomalies over the period of 1981-2010.

Correspondence to: Peitao Peng, Climate Prediction Center, NCEP/NWS/NOAA, 5830 University Research Court, College Park, MD 20740-3818; Email: Peitao.Peng@noaa.gov

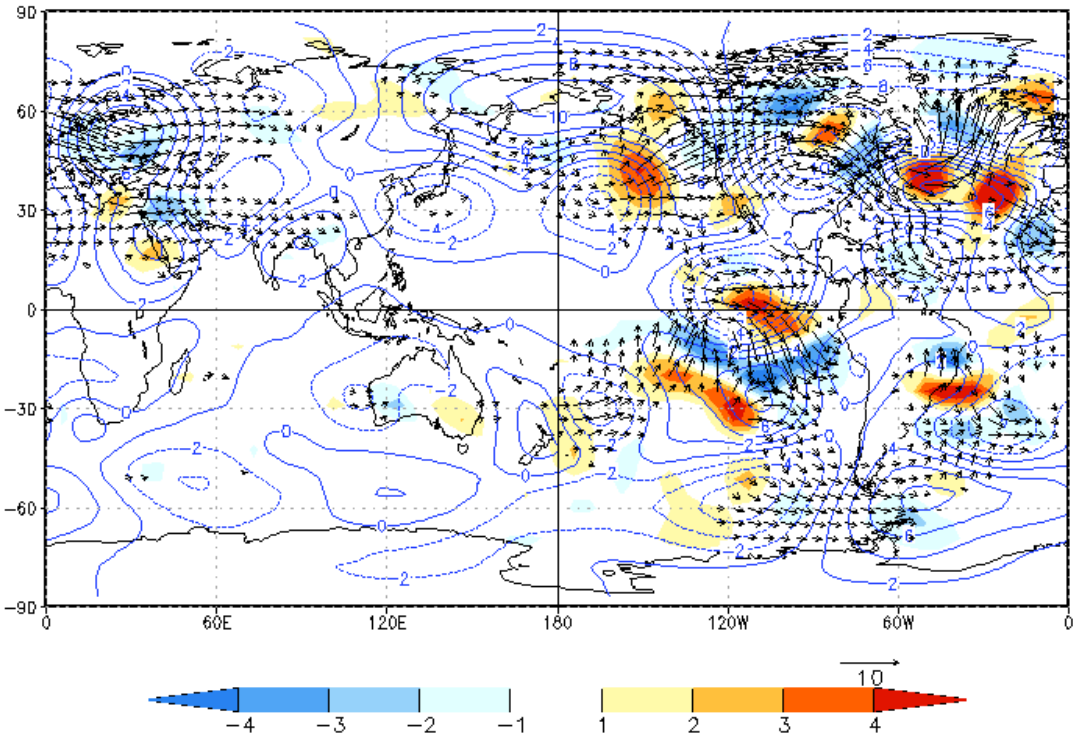

Fig. 2 200 hPa stream function anomaly (contours), wave-activity fluxes (arrows) and their divergence (shadings) for DJFM mean of 2013/14 winter. Units: 10^6 m^2 s^{-1} for stream function, m^2s^{-2} for wave activity fluxes, and m s^{-2} for divergence of wave-activity fluxes.

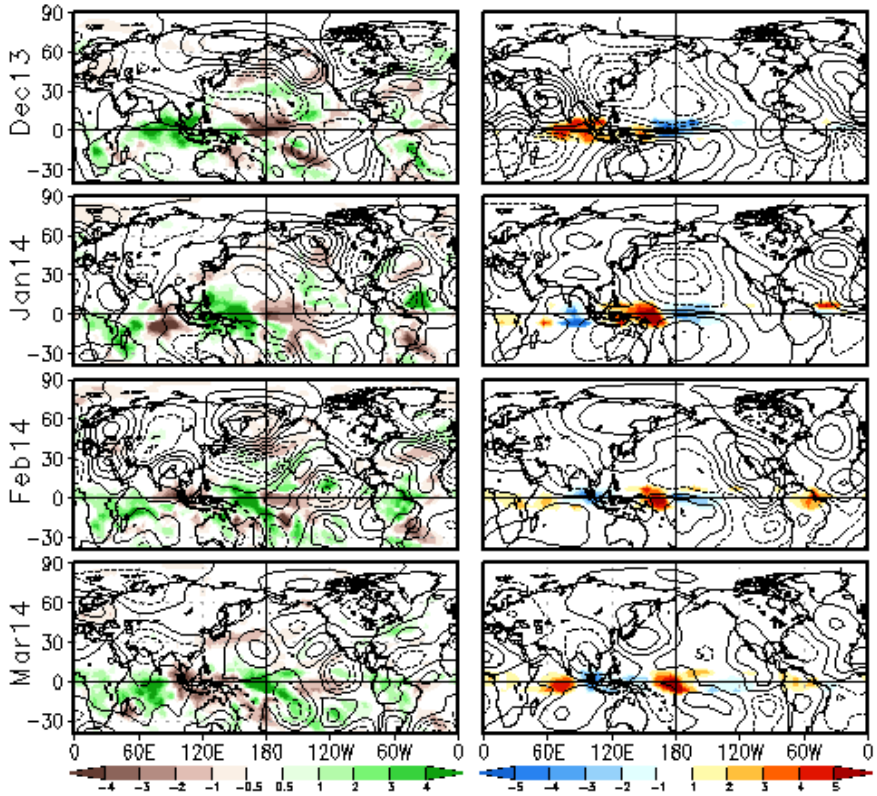

Fig. 3 Left column: Observed 200 hPa stream function (contours) and precipitation rate anomalies (shadings) for individual months of 2013/14 winter. Right column: Linear model response to tropical divergence (shadings) in a linear model with 200 hPa climatological basic state of the month. The divergence anomalies are specified with the same patterns of the precipitation rate in equatorial region. Units: 10^6 m^2s^{-1} for stream function, mm/day for precipitation rate, and 10^{-6} s^{-1} for divergence anomalies.

3. NORTH AMERICAN MULTI MODEL ENSEMBLE

Science and Technology Infusion Climate Bulletin
NOAA's National Weather Service
39th NOAA Annual Climate Diagnostics and Prediction Workshop
St. Louis, MO, 20-23 October 2014

Probabilistic Forecasting with NMME

Emily J. Becker, Huug van den Dool, and Qin Zhang

Climate Prediction Center, NCEP/NWS/NOAA

The North American Multi-Model Ensemble (NMME, http://www.cpc.ncep.noaa.gov/products/NMME/) forecasting system has been continuously producing seasonal forecasts since August, 2011. The NMME, with its suite of diverse models, provides a valuable opportunity for characterizing forecast confidence using probabilistic forecasts. The realtime forecasts have become an important tool for NOAA Climate Prediction Center seasonal forecasters, as well as many others. This study will serve as a baseline assessment before a series of improvements are attempted for the forecast construction method.

The current experimental probabilistic forecast product (in map format, Fig. 1) presents the most likely tercile for the monthly mean value, chosen out of "above normal", "near normal", or "below normal", using a non-parametric counting method to determine the probability of each class.

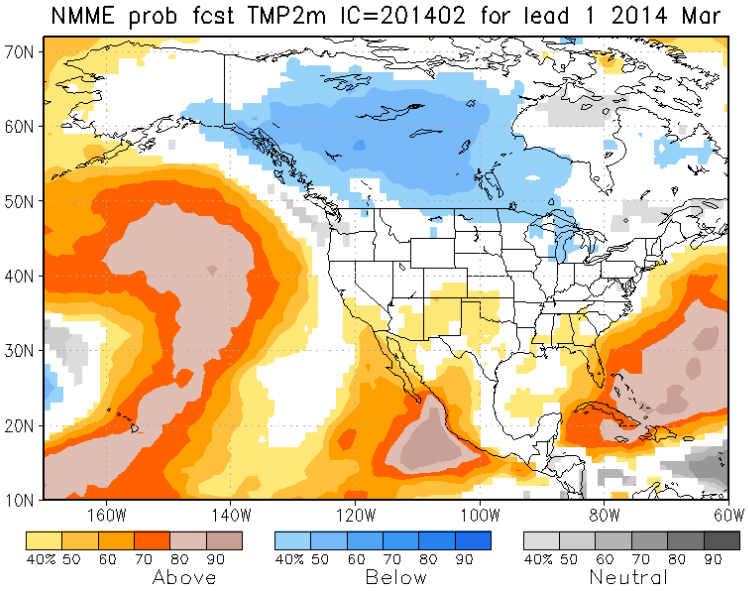

Fig. 1 Real-time 2 m surface temperature probabilistic forecast for March, 2014.

a. SST Niño 3.4 Region				
	A	**N**	**B**	**AC**
NMME	0.61	0.25	0.58	0.89
mini-NMME	0.60	0.24	0.59	0.89
CFS	0.45	0.05	0.43	0.82
6-mem CFS	0.41	-0.02	0.41	0.81

Table 1 Brier skill scores (BSS) and anomaly correlation coefficients (AC) for lead-1 forecasts from the NMME and CFSv2 of sea-surface temperature in the Niño3.4 region. Columns show BSS for forecasts in the above- (A), below- (B), and near-normal (N) categories; the last column is AC. Values are averaged over all 12 initial condition lead-1 forecasts. "Lead-1" seasonal forecast is for the first complete 3-month period following the initial month: for example, from June initial conditions, the lead-one seasonal forecast is for the July-August-September period.

A first-order bias correction is applied when the hindcast based local model climatology is removed (for each model separately) and replaced with the climatology from observations. A 2nd order bias correction is applied when forecasts are expressed in terciles derived from model hindcast data.

This study assesses the skill of the current method used to produce NMME realtime probabilistic forecasts using 29 years of cross-validated hindcasts. Probabilistic forecasts from a 6-model NMME, the full, 24-member CFSv2, a mini-NMME (4 members from each of 6 models), and a mini-CFS (6 members) are assessed using the Brier Skill Score (BSS), and the anomaly correlation of deterministic forecasts is included for comparison

Correspondence to: Emily J. Becker, Climate Prediction Center, NCEP/NWS/NOAA, 5830 University Research Court, College Park, MD 20740-3818; Email: emily.becker@noaa.gov

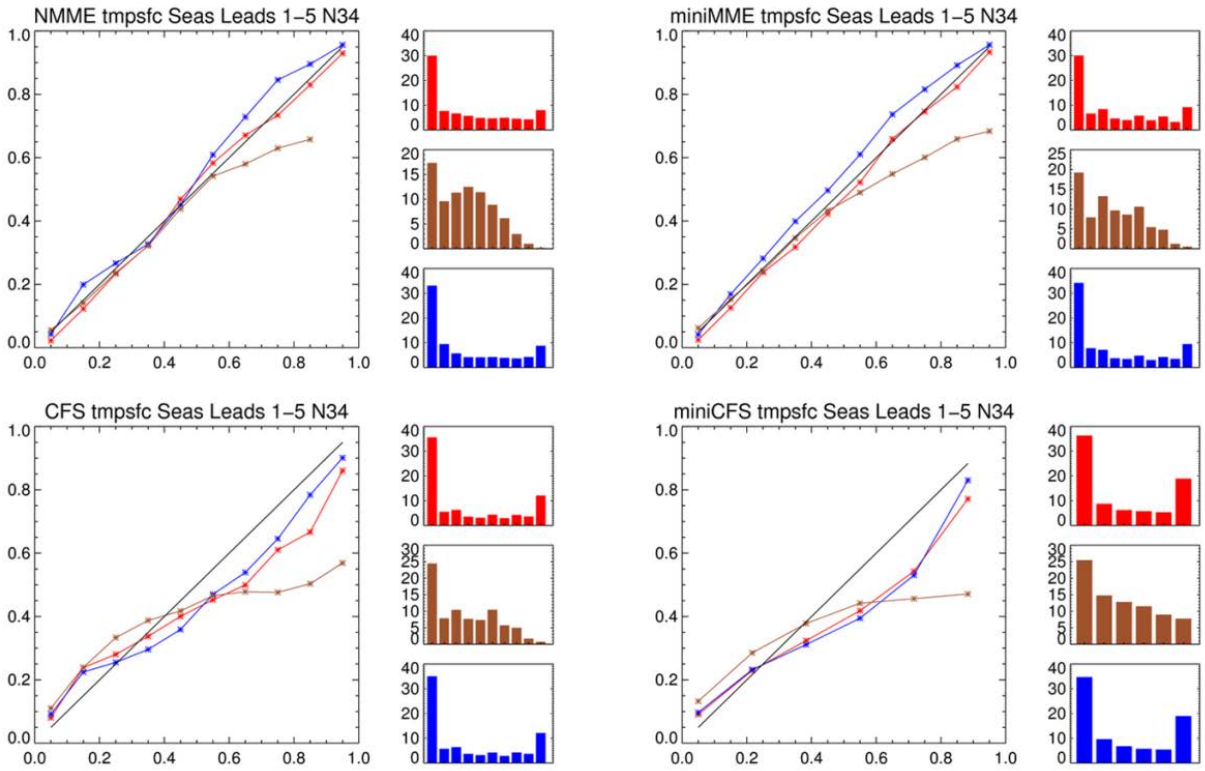

Fig. 2 Reliability diagrams for probabilistic forecasts of sea-surface temperature (SST) in the Niño3.4 region (190°E - 240°E, 5°S – 5°N) for the NMME (top L), mini-NMME (top R), CFS (lower L), and mini-CFS (lower R). Red lines indicate forecasts in the "above" tercile, blue the "below", and brown the "near-neutral". Lines closer to the black diagonal mean the observed event frequency (y-axis) is close to the forecast probability (x-axis), and therefore the forecasts are more reliable. Histograms indicate how often each forecast bin is used; numbering on the y-axis has been divided by 1000. All diagrams use 10 bins of size 0.1.

(Table 1). The hindcast assessment is employed due to the relatively short time that real-time probabilistic forecasts have been issued (less than two years.)

We also employ reliability diagrams, which allow for visual comparison of the conditional event frequency and the forecast probability; the associated "sharpness diagrams" indicate how often a given probability bin is used in the forecast. The "event" is an observation falling in a particular tercile. Probability forecasts are assigned to one of 10 bins (0 – 0.1, etc.). Reliability diagrams show the aggregated results for the lead-1 through lead-5 seasons (Fig. 2).

For all of the areas and fields (2 m land-only surface air temperature in the northern hemisphere, sea surface temperature in the Niño3.4 region and the extratropical northern hemisphere, and precipitation in the tropics) BSS for NMME forecasts are higher than those of CFSv2 forecasts. Forecasts in the near-normal tercile are near or below zero for all fields except sea surface temperature in the Niño3.4 region; BSS of the near-normal tercile is nevertheless much lower than the above and below categories. This preliminary study lends confidence that the NMME probabilistic forecasts, even as-is, provide value beyond that of the CFSv2 alone. The NMME benefits from both a higher number of ensemble members and model diversity. Further study is required to assess the sources of improved skill in the various fields and regions.

This work has been submitted to the Journal of Climate and is currently under review.

4. SUBSEASONAL TO INTERANNUAL PREDICTABILITY

Science and Technology Infusion Climate Bulletin
NOAA's National Weather Service
39th NOAA Annual Climate Diagnostics and Prediction Workshop
St. Louis, MO, 20-23 October 2014

Using the Bering Sea and Typhoon Rules to Generate Long-Range Forecasts

Joseph S. Renken[1], Joshua Herman[2], Daniel Parker[3], Travis Bradshaw[4], and Anthony R. Lupo[5]

[1]*KOPN Radio, Columbia, MO*

[2]*University of Wisconsin, Fox Valley, WI*

[3]*Western Illinois University, Macomb, IL*

[4] *Moberly Area Community College, Columbia, MO*

[5]*Department of Soil, Environmental, and Atmospheric Science, University of Missouri, Columbia, MO, and Belgorod State University, Belgorod, Russia 308015*

1. Introduction

Weather forecasting in the short range and long range has improved dramatically over the years (Anderson *et al.* 1999; Barnston *et al.* 2005; Lupo and Market, 2002, 2003). Weather forecasts in the short range are routinely issued for as long as seven to ten days. Long range forecasts are routinely issued at least one month to more than a year in advance. Short range forecasting is an initial value problem, which is performed within the framework of the primitive equations, whether these are made observationally, or with the aid of numerical models. Long range forecasting relies on a variety of methods, but are generally constructed using statistical methods, and is considered a boundary value problem. The methods used can be persistence, model of the day, contingency, analogues, or using more sophisticated statistical methodologies. There are medium range products available through the cooperation between the National Weather Service (NWS) regional and local offices and the Climate Prediction Center (CPC) in the range of 8 – 14 days (http://www.cpc.ncep.noaa.gov/products/predictions/814day/interactive/index.php). However, there are few products available that provide forecasts in the 6 – 30 day range, especially beyond 14 days, which is considered the dynamical limit for weather forecasting based on the size and rotation rate of the planet as well as the gasses that make up our atmosphere.

The Bering Sea (BSR) and Typhoon (TR) rules are two observations used by weather forecasters. The former was introduced in 2011, while the latter has been used since at least the 1940s and are based on the idea of teleconnectivity within the Pacific Ocean region which was defined statistically by Wallace and Gutzler (1981). For example, the Pacific North American (PNA) pattern will be associated with alternating trough-ridge patterns from the Central Pacific to the East Coast of the US. A ridge-trough pattern from west to east over the US is a positive PNA configuration, while the opposite pattern is negative. Teleconnection is thought to be the result of downstream propagation of Rossby Wave activity in the North and South Pacific basins (*e.g.*, Renwick and Revell, 1999; Wang *et al.* 2011, and references therein). The Bering Sea region is close to one teleconnective centers in the PNA pattern, which should make these rules useful indicators of weather downstream.

Atmospheric blocking, which generally persists for 7-10 day has also been associated with downstream influence on North America's weather (*e.g.* Quiroz, 1984; Wiedenmann *et al.* 2002). Blocking can have a substantial impact on the conditions over a region for an entire month or even a season as many researchers have demonstrated (*e.g.*, Lupo *et al.* 2014). Birk *et al.* (2010) demonstrated the influence of sea surface temperatures associated with El Niño and Southern Oscillation (ENSO) will be influential on the predominant temperature and precipitation regimes of the central USA, and that these are modified by longer term variability such as the Pacific Decadal Oscillation. Blocking is generally associated with troughing over the middle part of the USA, and a dramatic recent example occurred during November, 2014. Thus, the goal of

Correspondence to: Joseph S. Renken, KOPN Radio, Columbia MO; Email: jdrenken7@gmail.com

this research is to develop statistical tools based on the BSR and/or the TR that demonstrate their value and are better than climatology for prediction in the period of 6 to 30 days.

2. Data and methodology

a. data

The data used for this project come from a variety of sources, however the general source of this information is through the National Oceanic and Atmospheric Administration (NOAA), including the National Centers for Environmental Prediction / National Centers for Atmospheric Research (NCEP/NCAR) re-analyses (500 hPa heights) and the National Climactic and Data Center (NCDC) climatic information (climatological normals), and the Weather Underground (www.wunderground.com) for surface information.

b. Methods and definitions

The forecast verification method was based on the methods used by Lupo and Market (2003), and can be described generally as a skill score. In that paper, skill was measured using the formula:

Skill = (Forecast – Base) / (Verification – Base). (1)

For example, in their work, which was originated by Thornes and Proctor (1999), they converted actual temperature information into a point system for use in Eqn. (1), where a forecast within +/- 2^o F of the observed was considered perfect (2 points), and a forecast within +/-2 to +/-4^o F was given 1 point, and 0 was given to forecasts outside the 4^o F range. Here we modified this score system by awarding two, one, and zero point(s), respectively, for a forecast that was within one, two, or more than two seasonal standard deviation(s) (2σ), respectively away from observations.

A quick analysis demonstrated that the scores for the BSR, TR, and climatology were similar for the entire study period as well as within each season. Each method produced a similar number of perfect forecasts (two points) and busted forecasts (zero points). It is apparent that climatology would be difficult to improve upon, since the climatology in theory would result in a normal distribution, or a theoretical score of 1.63. However, anecdotal evidence indicated that the BSR and TR performed well when the temperatures were greater than 2σ from the normal. Scoring long range forecasts based on skill may not be the right way to show value, since climatology would be difficult to improve upon using statistical methods. This, however, does not preclude improvement via dynamical forecasting. Additionally, forecasts that involved 1 point scored can be considered partial successes and there were more contingencies that would fit into this type of analysis.

In this study, a methodology usually used by the National Weather Service and others in short range forecasting and severe weather was borrowed, which is based on a contingency table for events forecast and observed (*e.g.*, http://www.nws.noaa.gov/mdl/scan/test2/awipssvr.htm) (Table 1). Using this methodology will allow the scoring of the BSR and TR independent of climatology, and demonstrate value in abnormal (2σ) weather conditions. Here we will calculate success / probability of detection (POD – X / (X+Y)), false alarm rate (FAR – Z / (X +Z)), success ratio (SRO – X / (X+Z)), critical success (CSI – X / (X + Y + Z)), correct negatives (CRN – W / (W+ Y)), failures (FFR – Y / (W + Y)), and bias (BIAS – (X+Z) / (X + Y)).

Observed (below) / Forecast (right)	Yes	No
Yes	X	Y
No	Z	W

Table 1 The contingency table for BSR and TR forecasts of 2σ events and observations.

The definitions for blocking follow those used in Wiedenmann *et al.* (2002), and the definitions for the teleconnections examined are consistent with the work of Wallace and Gutzler (1981) or definitions found on the NWS and CPC websites. Here we examined the East (West) Pacific Oscillations (EPO(WPO)), the North Pacific Oscillation (NPO), the PNA, the North Atlatnic Oscillation (NAO), and the Arctic Oscillation (AO). The blocking occurrences were obtained from http://weather.missouri.edu/gcc. All statistics were tested using standard methods, which can be found in any elementary statistics text book.

3. Analysis and results

a. The Bering Sea and typhoon rules

In order to examine the BSR and TR, forecasts were made in the 17-21 day time period. These results demonstrate that the BSR and TR performed similarly to climatology during 2013 and 2014 (not shown). Thus, to examine the value of the BSR and TR during extreme events independent of climatology, the method in Table 1 was used, where X is the number of events were forecast correctly and occurred (two points), and Y is the number of events not forecast, but did occur (zero points). The value Z is the number of forecasted events that did not occur (0 points), and W the number of events that did not occur, but not forecast (two points). These results are shown in Tables 2 and 3.

Observed (below) / Forecast (right)	Yes	No
Yes	5 (10)	3 (3)
No	7 (4)	5 (9)

Table 2 As in Table 1, except for the outcome of BSR (TR) forecasts.

Index	BSR	TR
POD	62.5	76.9
FAR	58.3	28.6
SRO	41.7	71.4
CSI	33.3	58.8
CRN	62.5	75.0
FFR	38.5	25.0
BIAS	150.0	107.7

Table 3 The calculated indexes from section 2 for the BSR and TR expresses as a percentage (times 100).

The results demonstrated that the TR in general was more successful than the BSR, but both showed some success in forecasting 2σ events. Both the TR and BSR showed good scores for POD, CRN, but the BSR showed significantly less success in SRO and CSI. The TR showed low scores in FRA and FFR, and showed little bias in the forecasts, whereas BSR was higher in all these negative indicators. In the future this group will continue to track the progress of these forecasts in order to acquire a larger data set. Also, it would be desirable to identify an objective method for discerning those conditions that presage the effective use of the BSR and TR.

b. Blocking

All blocking events in the Pacific Region (140° E – 100° W) and Atlantic Region (80°W – 40° E) were compared over a three year from Sept 2011 – Aug. 2014 period with various teleconnection indexes and the monthly temperature and precipitation anomalies. The results of this preliminary study are shown in Table 4. Pacific (Atlantic) region blocking correlated strongly with the Pacific (Atlantic) Basin teleconnection patterns as expected. Pacific region blocking also correlated strongly with central US temperature and precipitation anomalies, although the temperature correlation was stronger. This might be expected as precipitation anomalies can be influenced by more localized factors as well as large-scale flow regimes. In general, Pacific Region blocking correlated with cooler and drier conditions. Atlantic Region blocking correlated with only the temperature. The correlation with colder temperatures is especially marked in the cold season.

Teleconnectivity	Correlation
At 99% confidence level	
East Pacific Oscillation	-0.60
West Pacific Oscillation	-0.60
Midwest monthly temperature anomaly	-0.45
At 95% confidence level	
Pacific North American	-0.42
North Pacific	0.42
North Atlantic Oscillation*	-0.39
At 90% confidence level	
Arctic Oscillation*	-0.33
Midwest monthly temperature anomaly*	-0.35
Midwest monthly precipitation anomaly	-0.30

Table 4 The correlation between Pacific (*Atlantic) blocking occurrences and days to teleconnectivity influencing Midwest region temperatures and/ or precipitation.

The strong Pacific Blocking event of early to mid-November 2014 was encouraging forecasts of a cooler than normal November within the first ten days of the month. Even one month before, the 30 day outlook projected a warmer than normal November for the far Northern Tier of states (http://www.cpc.ncep.noaa.gov/products/archives/long_lead/llarc.php). This blocking event was not foreseen, but was the result of the development of Super Typhoon Nuri in the west Pacific. Nuri became extratropical, and deepened to about 924 hPa, which is the strongest North Pacific extratropical cyclone on record. This cyclone strengthened a weak blocking event, that forced strong troughing over North America during the week of November 10th.

4. Conclusions

This study examined the utility of the BSR and TR for extended outlooks in the 6 – 30 day time frame. Data from NOAA and CPC were used primarily. The results of this study are preliminary and further study will be done in order to develop usable forecasting tools and a larger data base for performance statistics.

Examining the skill for the BSR and TR over the period the results demonstrate initially that both were consistent with climatology and did not show skill in the classic sense. However, a cursory examination demonstrated that both were able to forecast time periods when the temperatures were greater than two standard deviations from the mean. Thus, a contingency analysis typically used in synoptic and mesoscale meteorology was used in order to test the efficacy of each method for the detection of extreme events. Both methods demonstrated utility in identifying these periods, however the TR was consistently high (low) in those measures associated with positive (negative) performance, and showed small biases. The BSR scored high in false alarm rate as well as displaying more bias.

As expected, blocking in the North Pacific and Atlantic blocking correlated strongly with teleconnections in their respective ocean basins over a three year period of study. While Atlantic region blocking is correlated to central USA monthly temperature anomalies, Pacific region blocking correlated more strongly, and even correlated to monthly precipitation anomalies. As blocking is very difficult to forecast more than a day or two in advance (*e.g.*, Wiedenmann *et al*., 2002), these events can result in monthly forecasts that are busted by their occurrence as evidenced by November 2014, which showed a forecast of normal to warm conditions. Strong blocking in the early part of the month led to a strong cold wave in the central USA for the last two-thirds of the month.

References

Anderson, J., and Coauthors, 1999: Present-day capabilities of numerical and statistical models for atmospheric extratropical seasonal simulation and prediction. *Bull. Amer. Meteor. Soc.*, **80,** 1349-1362.

Barnston, A.G., A. Kumar, L. Goddard, and M.P. Hoerling, 2005: Improving seasonal prediction practices through attribution of climate. *Bull. Amer. Meteor. Soc.*, **86,** 59-72.

Birk, K., A.R. Lupo, P.E. Guinan, and C.E. Barbieri, 2010: The interannual variability of Midwestern temperatures and precipitation as related to the ENSO and PDO. *Atmofera*, **23**, 95 - 128.

Lupo, A.R., and P.S. Market, 2003: First Conference on Weather Analysis and Forecasting Issues in the Central United States. *Bull. Amer. Meteor. Soc.*, **84**, 1245-1247.

——, and P.S. Market, 2002: The verification of weather forecasts in central Missouri and seasonal variations in forecast accuracy. *Wea. Forecasting*, **8,** 891 - 897.

——, I.I. Mokhov, Y.G. Chendev, M.G. Lebedeva, M. Akperov, and J.A. Hubbart, 2014: Studying summer season drought in western Russia. *Advances in Meteorology, Special Issue: Large Scale Atmospheric Science*, Article ID 942027. 9 pp.

Quiroz, R.S., 1984: The climate of the 1983-1984 winter - a season of strong blocking and severe cold over North America. *Mon. Wea. Rev.*, **112,** 1894-1912.

Renwick, J.A., and M.J. Revell, 1999: Blocking over the south Pacific and Rossby wave propagation. *Mon. Wea. Rev.*, **127,** 2233-2247.

Thornes, J. E., and E. A. J. Proctor, 1999: Persisting with persistence: The verification of Radio 4 weather forecasts. *Weather*, **54,** 311-320.

Wallace, J.M., and D.S. Gutzler, 1981: Teleconnections in the geopotential height field during the northern hemisphere winter. *Mon. Wea. Rev.*, **109,** 784-812.

Wang, Y., X. Xu, A.R. Lupo, P. Li, and Z. Lin, 2011: The remote effect of the Tibetan Plateau on downstream flow in early summer. *J. Geophys. Res.: Atmospheres*, **116,** *D19108, doi:10.1029/2011JD015979.*

Wiedenmann, J.M., A.R. Lupo, I.I. Mokhov, and E. A. Tikhonova, 2002: The climatology of blocking anticyclones for the northern and southern hemisphere: Block intensity as a diagnostic. *J. Climate*, **15,** 3459-3474.

Science and Technology Infusion Climate Bulletin
NOAA's National Weather Service
39th NOAA Annual Climate Diagnostics and Prediction Workshop
St. Louis, MO, 20-23 October 2014

Influence of ENSO SSTs on the Spread of the Probability Density Function for Precipitation and Surface Temperature

Mingyue Chen, and Arun Kumar

Climate Prediction Center, NCEP/NWS/NOAA

ABSTRACT

The impact of the interannual variations in ENSO SSTs on the spread of probability density function (PDF) for the seasonal mean of variables of societal relevance are analyzed based on a large set of the hindcasts from NCEP CFSv2. The study is focused on the analysis of rainfall and 2-meter temperature (T2m) for December-January-February (DJF) seasonal mean.

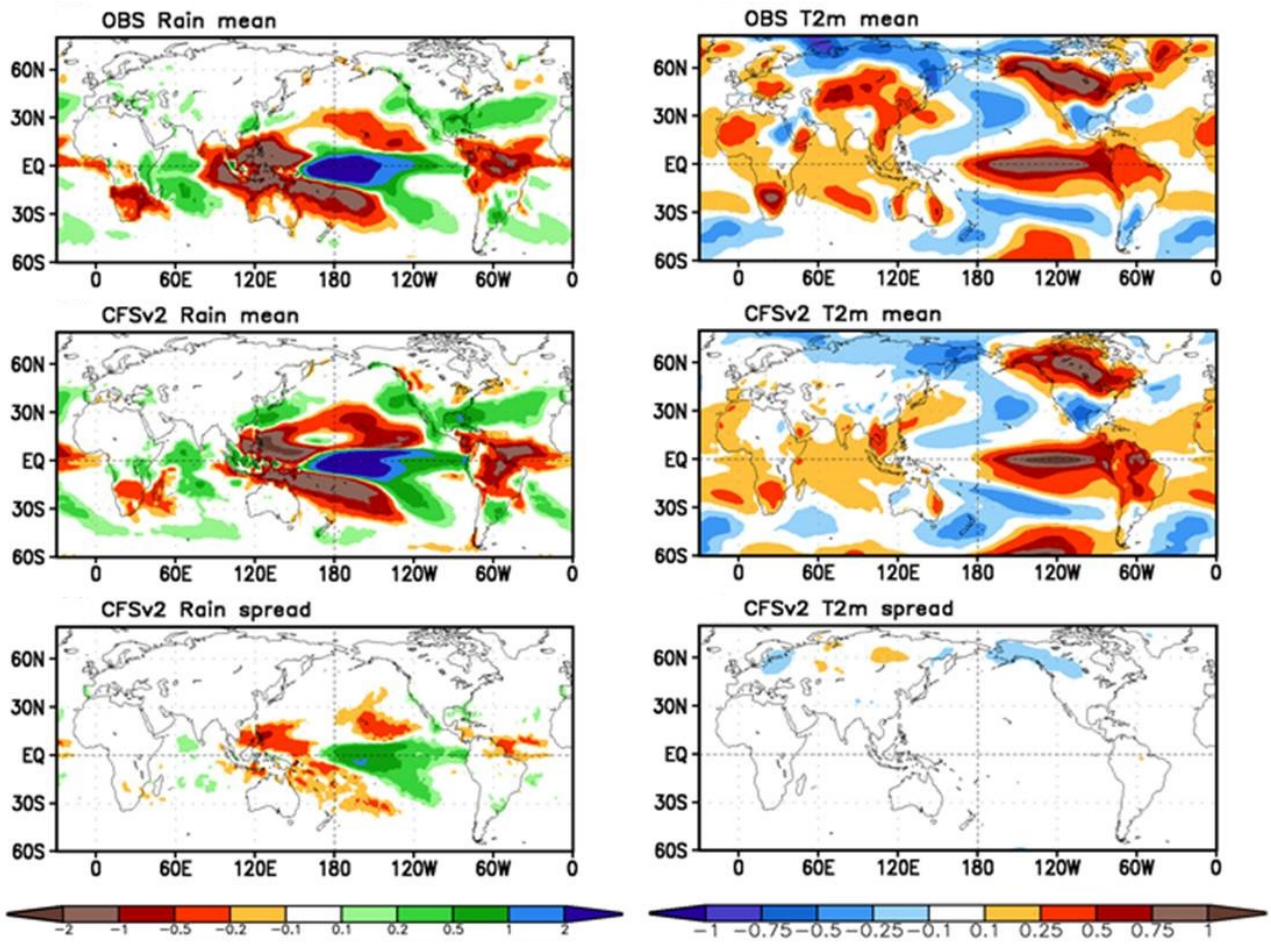

Fig. 1 Left column: Spatial patterns of the linear regression between Niño 3.4 SST index and the DJF seasonal mean rainfall from observation (top), the model forecasted ensemble mean (middle), and the model forecasted ensemble spread (bottom). The unit is mm/day per degree K of Niño 3.4 SST. Right column: The same as the left column but for T2m. The unit is degree K per degree K of the Niño 3.4 SST index.

Correspondence to: Mingyue Chen, Climate Prediction Center, NCEP/NWS/NOAA, 5830 University Research Court, College Park, MD 20740-3818; Email: Mingyue.Chen@noaa.gov

For rainfall, the spatial distribution of the ENSO SSTs induced changes on the spread of PDF strongly resembles changes in the mean but with smaller amplitude. Over the central-eastern equatorial Pacific, changes in the spread lead to a reduction in signal-to-noise ratio (SNR) during El Niño years while to an increase in the SNR during La Niña years. Over extratropics, year to year changes in the spread are relatively small. For T2m, the changes in spread have little systematic dependence on the ENSO SSTs and the amplitudes of the changes in spread are much smaller than corresponding changes in the ensemble mean.

The results demonstrate small systematic year to year variations in the PDF spread, for example over extratropics for rainfall and over most of global areas for T2m, and indicate that it might be a good practice in seasonal predictions to assume that the spread of seasonal means from year to year is constant and the skill in seasonal forecast information resides primarily in the shift of the first moment of the seasonal mean of the PDF.

This work has been published in Climate Dynamics in 2014.

References

Chen M, and A. Kumar, 2014: Influence of ENSO SSTs on the spread of the probability density function for precipitation and land surface temperature. *Clim Dyn.*, doi: 10.1007/s00382-014-2336-9.

Science and Technology Infusion Climate Bulletin
NOAA's National Weather Service
39th NOAA Annual Climate Diagnostics and Prediction Workshop
St. Louis, MO, 20-23 October 2014

Modulation of Atlantic Basin Tropical Cyclone Activity by the Madden-Julian Oscillation (MJO) from 1905-2011

Philip Klotzbach

Department of Atmospheric Science, Colorado State University, Fort Collins, CO

Eric Oliver

Institute for Marine and Arctic Studies
Australian Research Council Centre of Excellence for Climate System Science
University of Tasmania, Australian

ABSTRACT

The Madden-Julian Oscillation (MJO) has been demonstrated to play a role in tropical cyclone (TC) activity around the globe in a number of recent studies. While the impact of the MJO on TCs in the Atlantic basin since the mid-1970s has been well documented, a newly-developed 107-year long index for the MJO allows for additional analysis of the impacts of the MJO on Atlantic TC activity. TC activity in the Atlantic increases when MJO-related convection is enhanced over Africa and the Indian Ocean while TC activity in the Atlantic is suppressed when the MJO enhances convection over the West Pacific. This long-term record of the MJO also allows for the analysis of how the MJO's impacts may be modulated by other climate modes, such as the El Niño-Southern Oscillation (ENSO) over interannual timescales (Figure 1) and the Atlantic Multi-decadal Oscillation (AMO) over multidecadal time scales (Figure 2). When climatologically unfavorable conditions such as an El Niño event or a negative AMO phase are present, even TC-favorable MJO conditions are not enough to generate statistically significant increases in TC activity from the long-term average across the Atlantic basin. However, climatologically favorable conditions during a La Niña event or a warm AMO phase act to enhance the modulation of TC activity over the Atlantic basin by the MJO.

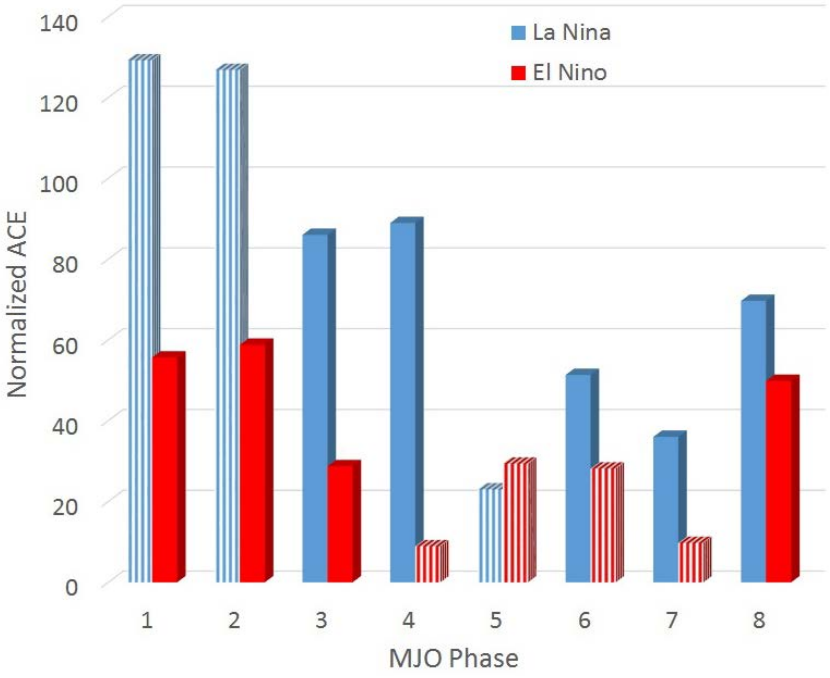

Fig. 1 Normalized ACE generated by each phase of the MJO for La Niña events (blue bars) and El Niño events (red bars). Statistically significant results are highlighted by vertical striping.

Correspondence to: Philip Klotzbach, Department of Atmospheric Science, Colorado State University, Fort Collins, CO; Email: philk@atmos.colostate.edu

This work is currently in press for Journal of Climate. It can be downloaded at: http://journals.ametsoc.org/doi/pdf/10.1175/JCLI-D-14-00509.1.

References

Klotzbach, P. J., and E. C. J. Oliver, 2014: Modulation of Atlantic basin tropical cyclone activity by the Madden-Julian Oscillation (MJO) from 1905-2011. *J. Climate*, in press, doi: 10.1175/JCLI-D-14-00509.1.

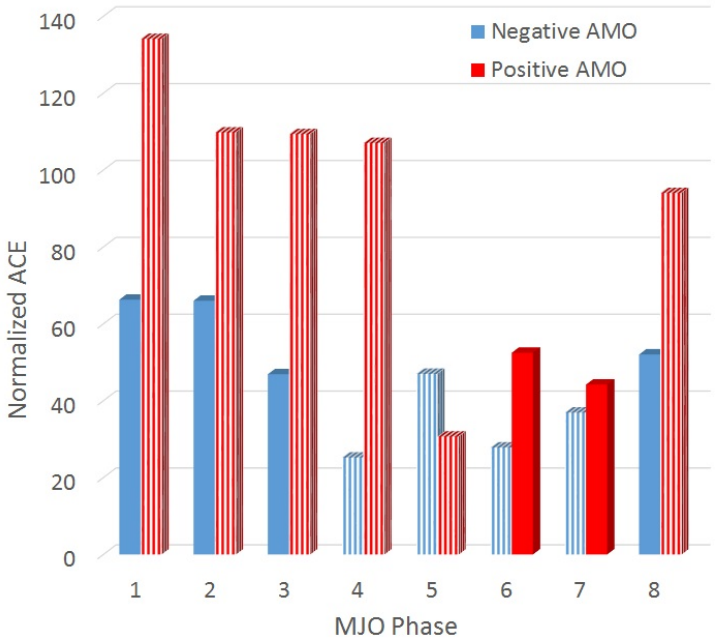

Fig. 2 As in Figure 1 but for positive AMO years (red bars) and negative AMO years (blue bars).

Science and Technology Infusion Climate Bulletin
NOAA's National Weather Service
39th NOAA Annual Climate Diagnostics and Prediction Workshop
St. Louis, MO, 20-23 October 2014

Prediction Skill of North Pacific Variability in NCEP Climate Forecast System Version 2: Impact of ENSO and Beyond

Zeng-Zhen Hu[1], Arun Kumar[1], Bohua Huang[2, 3], Jieshun Zhu[3], and Yuanhong Guan[4]

[1]*Climate Prediction Center, NCEP/NWS/NOAA*

[2] *Department of Atmospheric, Oceanic and Earth Sciences, George Mason University, Fairfax, VA*

[3]*Center for Ocean-Land-Atmosphere Studies, George Mason University, Fairfax, VA*

[4]*School of Mathematics and Statistics, and Center for Data Assimilation Research and Application Nanjing University of Information Science and Technology, Nanjing, China*

ABSTRACT

This work examines the impact of El Niño-Southern Oscillation (ENSO) on prediction skill of North Pacific variability (NPV) in retrospective predictions of the NCEP Climate Forecast System version 2. It is noted that the phase relationship between ENSO and NPV in initial condition (IC) affects the prediction skill of NPV. For the average of lead times of 0-6 months, the prediction skills of sea surface temperature anomalies (SSTA) in NPV (averaged SSTA in (30°-50°N, 150°E-150°W) is defined as the NPV index) increase from 0.42 to 0.63 from the cases of out-of-phase relation between the Niño3.4 and NPV indices in IC to the cases of in-phase relation (Fig. 1). Here, the in-phase (out-of-phase) variations of ENSO and NPV are referred to as SSTA having opposite (same) sign for Niño3.4 and NPV indices. It is suggested that when ENSO and NPV are in-phase in IC, ENSO plays a constructive role in the NPV development and enhances its signals. The physical coherence between North Pacific and the tropical central and eastern Pacific favors the model to consistently predict the anomaly in North Pacific. The situation is opposite when they are out-of-phase in IC. The ENSO may be disruptive to the NPV anomalies and, as a result, the intra-ensemble perturbations become more dominant.

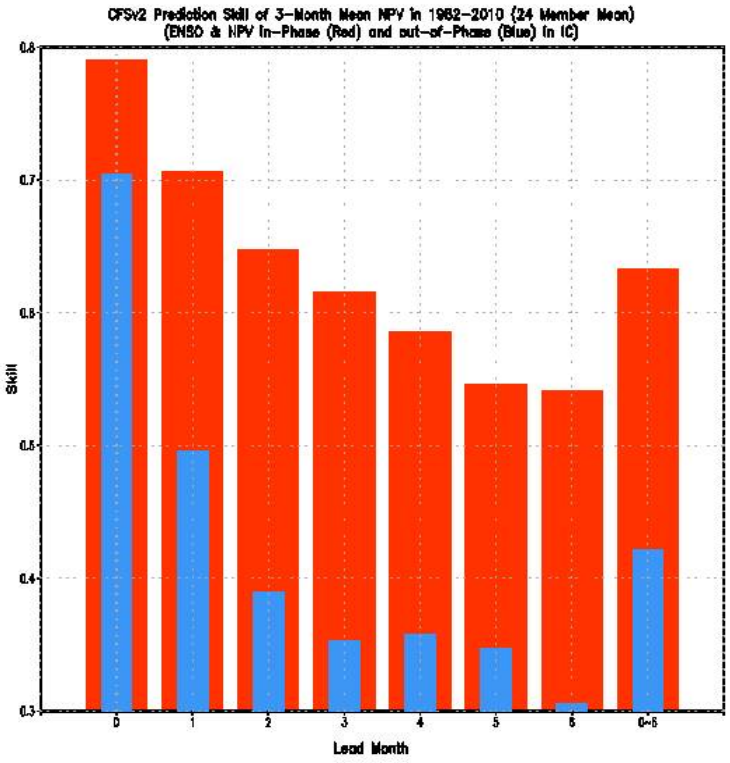

Fig. 1 Dependence of prediction skills of CFSv2 predicted NPV index with IC in January 1982-December 2010 on lead time and phase relationship between Niño3.4 and NPV indices. Red (blue) bars represent the prediction skills of NPV index for in-phase (out-of-phase) variations between Niño3.4 and NPV indices at IC. The most right-hand bar is the average of the skill for 0-6 month lead.

Correspondence to: Zeng-Zhen Hu, Climate Prediction Center, NCEP/NWS/NOAA, 5830 University Research Court, College Park, MD 20740-3818; Email: Zeng-Zhen.Hu@noaa.gov

Nevertheless, when ENSO and NPV are out-of-phase, some pronounced positive NPV events are still predictable (Fig. 2). In these cases, North Pacific is dominated by strong positive SSTA, which may overcome the influence from the tropical Pacific and displays predictability. There are little predictive skills for negative SSTA and small positive SSTA when they are out-of-phase. This asymmetry in the prediction skill may suggest that large positive and negative SSTA in N. Pacific may be associated with different physical processes.

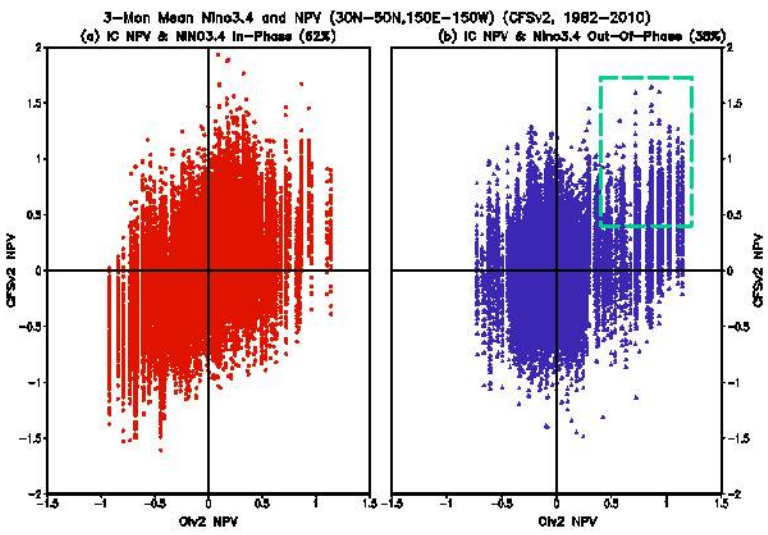

Fig. 2 Scatter of CFSv2 predicted (y-axis) and OIv2 analyzed (x-axis) NPV index for the predictions of 0-6 month lead for all in-phase (a) and out-of-phase (b) variations between Niño3.4 and NPV indices in IC in January 1982-December 2010. The green rectangle box in (b) represents NPV index larger than 0.4°C in both OIv2 and CFSv2.

This work has been published in Journal of Climate in 2014.

References

Hu, Z.-Z., A. Kumar, B. Huang, J. Zhu, and Y. Guan, 2014: Prediction skill of North Pacific variability in NCEP Climate Forecast System Version 2: Impact of ENSO and beyond. *J. Climate*, **27**, 4263-4272. doi: http://dx.doi.org/10.1175/JCLI-D-13-00633.1

5. INTRASEASONAL PREDICTABILITY

Science and Technology Infusion Climate Bulletin
NOAA's National Weather Service
39th NOAA Annual Climate Diagnostics and Prediction Workshop
St. Louis, MO, 20-23 October 2014

Intra-Seasonal Mid- and High-Latitude Circulation Fluctuations Forced by and Coherence with Tropical Heating: Predictability and Prediction

David M. Straus[1], Erik T. Swenson[2], and Cara-Lyn Lappen[3]

[1]*George Mason University, Fairfax, Virginia*
[2]*APEC Climate Center, Busan, South Korea*
[3]*Texas A&M University, College Station, Texas*

ABSTRACT

A three-dimensional evolution of Madden–Julian oscillation (MJO) diabatic heating for October–March from satellite data is constructed: the heating propagates eastward for three cycles, modulated by the likelihood for a given MJO phase to occur on a given calendar day. This heating is added to the temperature tendencies of each member of an ensemble of 48 (1 October–31 March) simulations with the Community Earth System Model.

The leading two most predictable modes of the planetary wave vertically integrated total (added plus model generated) heating capture 81% of the ensemble-mean variance and form an eastward-propagating oscillation with very high signal-to-noise ratio. The two most predictable modes of the extratropical Northern Hemisphere 200-hPa height form an oscillation, as do those of the 300-hPa height tendency due to synoptic vorticity flux convergence, the 200-hPa Rossby wave source, and the envelope transient kinetic energy. The North Atlantic Oscillation (NAO+) occurs 15–25 days after the MJO convection crosses the 90°E meridian (see Fig. 1 left panel), supported by synoptic vorticity flux convergence and a distinct pattern of Rossby wave source.

The daily North Atlantic circulation anomalies are categorized into four circulation regimes with a cluster

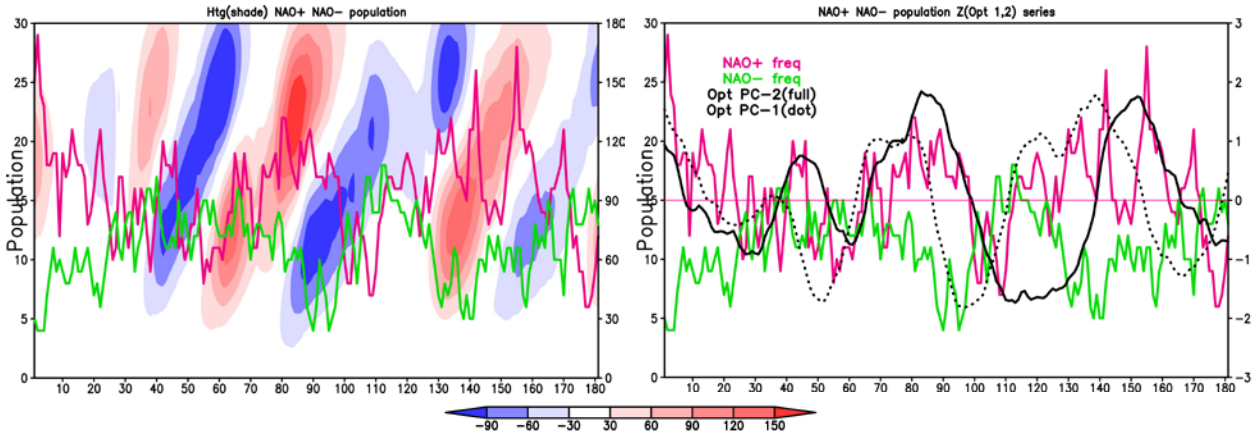

Fig. 1 Number of occurrences of NAO+ regime (red curve) and NAO- regime (green curve) in all ensemble members, as a function of day (see left-hand scale). Shading in left panel is the vertically integrated planetary wave diabatic heating synthesized from the leading two most predictable modes (W m^{-2}, see color bar) as a function of longitude (see right-hand scale). Dotted (solid) curve in the right panel is the ensemble-averaged time series of the first (second) most predictable mode of the extratropical Northern Hemisphere 200 hPa height (see right-hand scale). Time series are normalized to unit variance.

Correspondence to: David M. Straus, George Mason University, MSN 2B3, 4400 University Dr., Fairfax, VA 22030; Email: dstraus@gmu.edu

analysis. The NAO+ and NAO− are equally likely in the control model runs, but the NAO+ is 10% more likely in the model runs with heating, compared to a difference of 14% in reanalyses. The daily occurrence of the NAO+ regime in the heating ensemble shows maxima at times when the leading two optimal modes of height also indicate NAO+ but also shows maxima at other times (see Fig. 1 right panel).

This work has been published in Journal of the Atmospheric Sciences in 2015.

References

Straus D. M., E. Swenson, and C.-L. Lappen, 2015: The MJO cycle forcing of the North Atlantic circulation: Intervention experiments with the Community Earth System Model. *J. Atmos. Sci.*, **72**, 660–681. doi: http://dx.doi.org/10.1175/JAS-D-14-0145.1

Science and Technology Infusion Climate Bulletin
NOAA's National Weather Service
39th NOAA Annual Climate Diagnostics and Prediction Workshop
St. Louis, MO, 20-23 October 2014

Predictability of Eastern Pacific Intrasesonal Variability

J. M. Neena[1], Xianan Jiang[1], Duane Waliser[1, 2], June-Yi Lee[3, 4], and Bin Wang[3]

[1] *Joint Institute for Regional Earth System Science and Engineering, University of California*

[2] *Jet Propulsion Laboratory, California Institute of Technology, California*

[3] *International Pacific Research Center and Department of Meteorology, University of Hawaii*

[4] *Institute of Environmental Studies, Pusan National University, Busan*

ABSTRACT

The Eastern Pacific (EPAC) warm pool is a region of strong intraseasonal variability (ISV) during boreal summer. While the EPAC ISV is known to have large-scale impacts that shape the weather and climate in the region (*e.g.* tropical cyclones and local monsoon), simulating EPAC ISV is still a great challenge for the present day global weather and climate models. In the present study, the predictive skill and predictability of the EPAC ISV are explored in eight coupled model hindcasts from the Intraseasonal Variability Hindcast Experiment (ISVHE). Relative to the prediction skill for the boreal winter Madden-Julian Oscillation (MJO) in the ISVHE (~15-25 days), the skill for the EPAC ISV is considerably lower in most models with an average skill around 10 days. On the other hand, while the MJO exhibits a predictability of 35-45 days, the estimate of predictability for the EPAC ISV gives a 20-30 day range (Figure 1). The prediction skill was found to be higher when the hindcasts were initialized from the convective phase of the EPAC ISV as opposed to the subsidence phase. Higher prediction skill was also found to be associated with active MJO initial conditions over the Western Pacific (Figure 2, evident in 4 out of 8 models), signaling the importance of exploring the dynamic link between the MJO and the EPAC ISV. The results illustrate the possibility and need for improving our dynamical prediction systems to facilitate more accurate and longer-lead predictions of the EPAC ISV and associated weather and short-term climate variability.

This work was published in Journal of Climate in 2014.

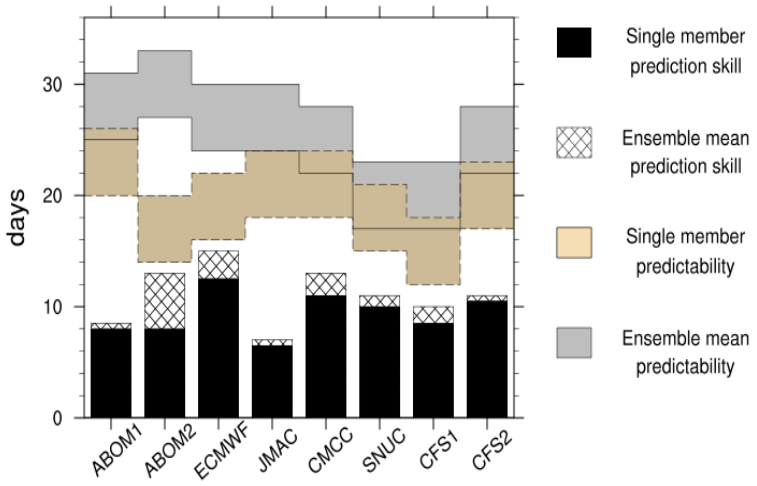

Fig. 1 Signal to noise ratio based estimates of prediction skill and predictability for EPAC ISV PC1 in the eight models (x-axis). Average individual hindcast prediction skill estimates are shown as black bars and ensemble mean prediction skill estimates are shown as hatched bars. A +/-3 day range for single member and ensemble mean estimates of predictability are represented by the tan and grey shaded areas respectively.

References

Neena, J.M., X. Jiang, D. Waliser, J. Lee, and B. Wang, 2014: Eastern Pacific intraseasonal variability: A predictability perspective. *J. Climate*. doi:10.1175/JCLI-D-14-00336.1, in press.

Wheeler, M. C. and H. H. Hendon, 2004: An all-season real-time multivariate MJO index: development of an index for monitoring and prediction. *Mon. Wea. Rev.*, **132**,1917–1932.

Correspondence to: J. M. Neena, Joint Institute for Regional Earth System Science and Engineering, University of California; Email: njmani@jifresse.ucla.edu

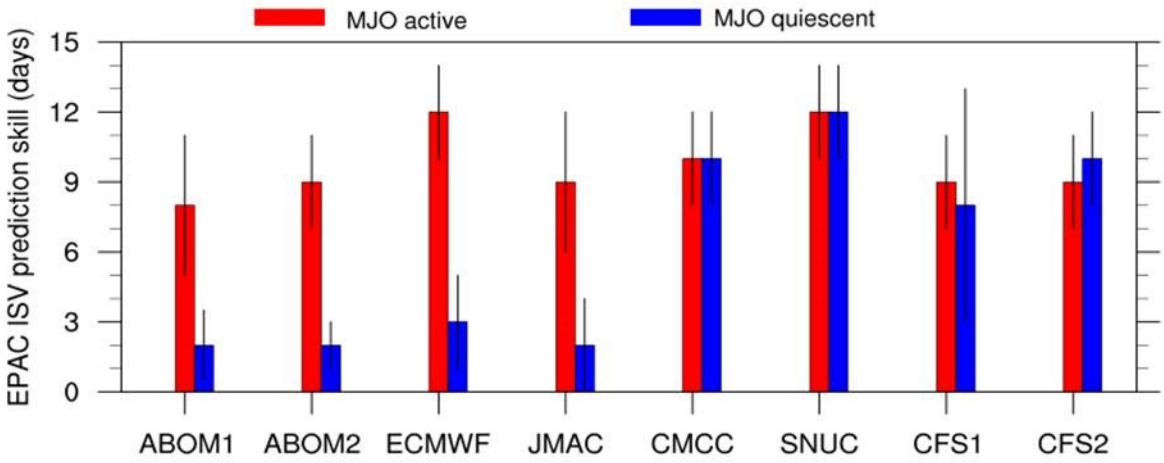

Fig. 2 Average prediction skill for EPAC ISV PC1 in the eight models for hindcasts initiated from active MJO conditions (RMM (Real-time Multivariate MJO indices, Wheeler and Hendon 2004) amplitude > 1.2) (red bars) and quiescent MJO conditions (RMM amplitude <0.8) (blue bars).

6. MONSOON PREDICTABILITY

Science and Technology Infusion Climate Bulletin
NOAA's National Weather Service
39th NOAA Annual Climate Diagnostics and Prediction Workshop
St. Louis, MO, 20-23 October 2014

Variations and Seasonal Prediction of Wet and Dry Season Precipitation over the Maritime Continent: Roles of ENSO and Monsoon Circulation

Tuantuan Zhang[1], Song Yang[1], and Xingwen Jiang[2]

[1]*Department of Atmospheric Sciences, Sun Yat-sen University, Guangzhou, Guangdong, China*
[2]*Institute of Plateau Meteorology, China Meteorological Administration, Chengdu, Sichuan, China*

1. Introduction

The authors analyze the seasonal-interannual variations of precipitation over the Maritime Continent (MC) and their relationships with large-scale climate anomalies. They also investigate the predictability of MC precipitation variations. The hindcast of the National Centers for Environmental Prediction (NCEP) Climate Forecast System version 2 (CFSv2) and several analysis/reanalysis products are used.

2. Results

The seasonal evolution of MC precipitation does not apparently exhibit distinct features for four seasons. Instead, it is clearly characterized by a wet season (from December to March) and a dry season (from July to October) (Figs. 1 and 2). The

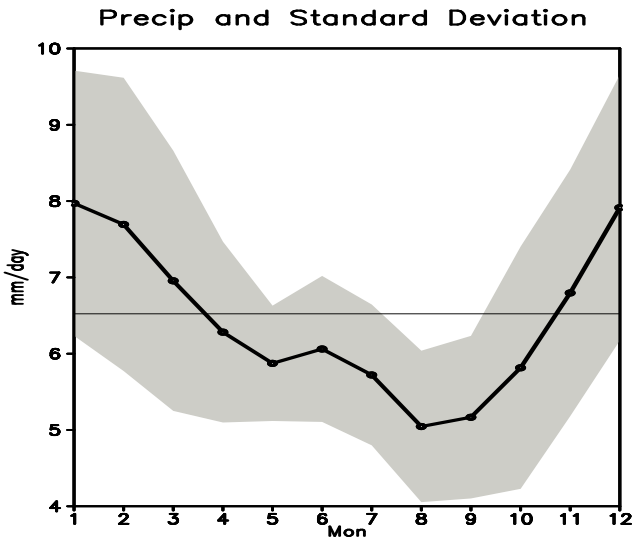

Fig. 1 Observed monthly mean of MC precipitation (mm day-1, black line) and its standard deviations (shaded) from January to December. The MC domain can be seen from Fig. 2. The horizontal line denotes the annual average of MC precipitation. July-October are defined as dry season and December-March as wet season.

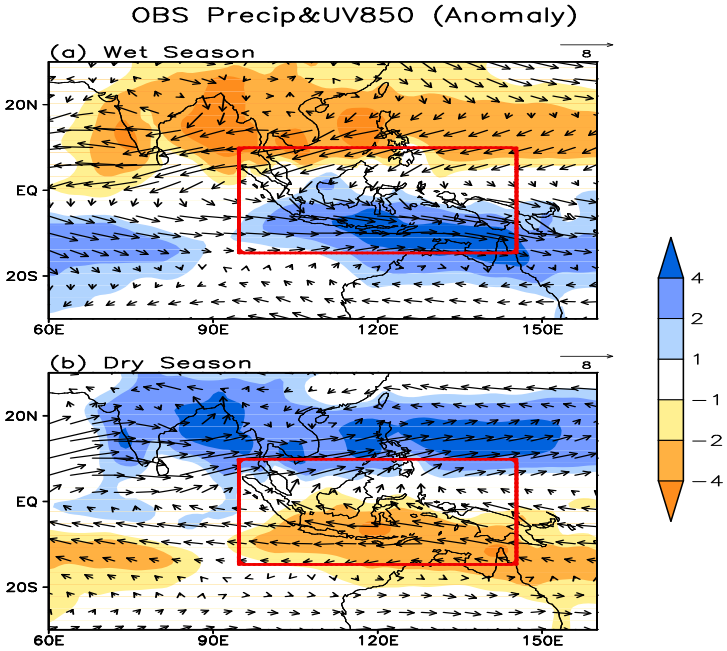

Fig. 2 Anomalies of observed precipitation (mm day-1, shading) and 850-hPa winds (m s-1, vectors) in (a) wet season (December-March) and (b) dry season (July-October). The domain used to define the MC is outlined with red boxes. The figure displays that during wet season rainfall maximizes near 10S and during dry season rainfall band moves to around 15N.

Correspondence to: Song Yang, Department of Atmospheric Sciences, Sun Yat-sen University, Guangzhou, Guangdong, China; Email: yangsong3@mail.sysu.edu.cn

precipitation over MC for both wet and dry seasons is significantly related to El Niño–Southern Oscillation (ENSO) and large-scale Asian-Australian monsoon features. When ENSO signals are removed, the MC precipitation is more strongly related to the climate features over East Asia.

The NCEP CFSv2 shows a high skill in predicting the main features of MC precipitation variations and their relationships with large-scale climate anomalies. It predicts the MC precipitation variation and its related circulation patterns skillfully in advance by several months, especially for the dry season (Fig. 3). The relatively low skill for wet season is contributed mainly from the low prediction skill of the precipitation over Sumatra, Malay, and Borneo (SMB), which is due partly to the unrealistically predicted relationship between the variations of SMB precipitation and ENSO in the wet season (Fig. 4).

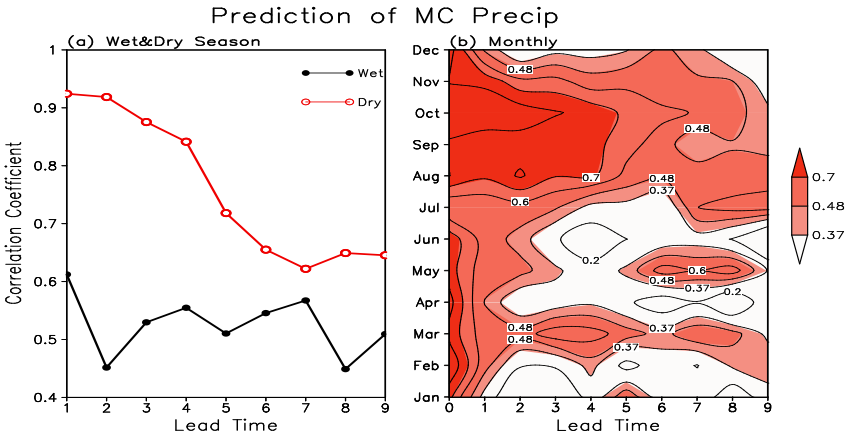

Fig. 3 (a) Coefficients of correlation between the CFS predicted MC precipitation of different leads and observed MC precipitation in wet season (lines with solid circles) and dry season (lines with open circles). (b) Coefficients of correlation between the CFS predicted MC precipitation of different leads and observed MC precipitation for all months. The x-coordinate indicates the corresponding lead months. All values significantly exceed the 95% confidence level in (a), and values significantly exceeding the 95% confidence level are shaded in (b). The figure shows that high skills of MC precipitation prediction are in the dry season and lower skills are in the wet season.

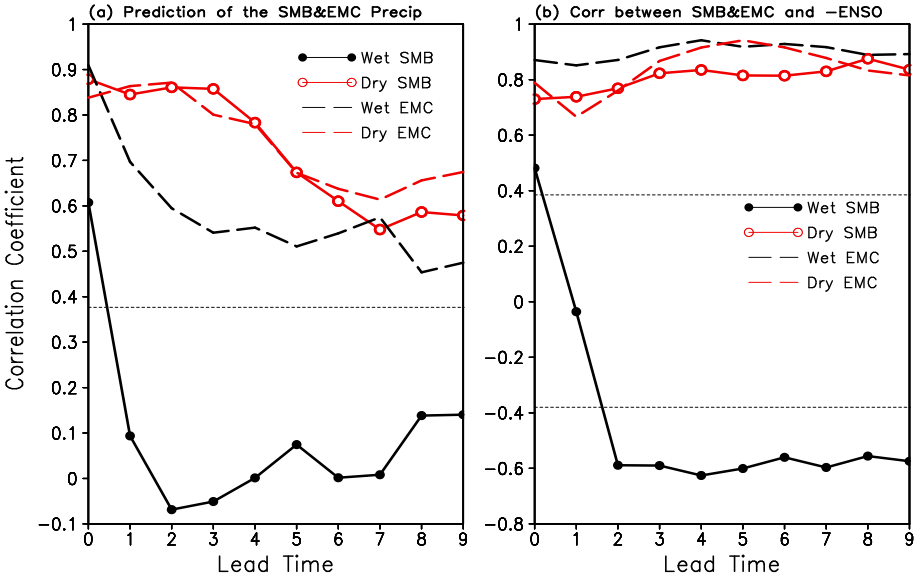

Fig. 4 (a) Coefficients of correlation between the CFS predicted SMB\EMC precipitation of different leads and observed SMB\EMC precipitation in wet season (black solid\dash line) and dry season (red solid\dash line). (b) Coefficients of correlation between the CFS predicted SMB\EMC precipitation and negative Niño-3.4 in wet season and dry season. The x-coordinate indicates the corresponding lead months. Straight dotted lines denote the 95% confidence level.

The figure clearly shows that, for dry season, predictions of precipitation and ENSO-precipitation relationship always have high skills. For wet season, however, high skills can only be found for the predictions of eastern MC precipitation and its relationship with ENSO. No skill can be seen for the predictions of SMB precipitation and its relationship with ENSO.

7. CLIMATE SERVICE DEVELOPMENT AND CHALLENGES

Science and Technology Infusion Climate Bulletin
NOAA's National Weather Service
39th NOAA Annual Climate Diagnostics and Prediction Workshop
St.. Louis, MO, 20-23 October 2014

Evaluation of an Indicator for the Early Warning of Strong Summer Drought over the South Central United States*

D. Nelun Fernando[1], Rong Fu[2], Ruben S. Solis[1], Robert E. Mace[1],
Ying Sun[2], Binyan Yang[2], and Bing Pu[2]

[1]*Water Science & Conservation, Texas Water Development Board, Austin, TX*
[2]*Department of Geological Sciences, The University of Texas at Austin*

1. Introduction

Strong summer droughts over the Southern Great Plains region are often characterized by rapid intensification in the late-spring and early-summer. The decreased rainfall in these drought years are coupled with strong increases in summertime temperature extremes, as for example, was the case with the 2011 drought over Texas and the Great Plains drought in 2012. Dynamic climate models failed to predict these summer droughts. This is largely due to model weaknesses in predicting summer rainfall, underestimating summer rainfall variance, and weaknesses in capturing soil moisture feedbacks. By contrast, climate models are more reliable in capturing the variability in large-scale circulation features and temperature during winter and spring.

Observations show that severe-to-extreme summer drought events over Texas are preceded by dry springs. Over the period 1895-2014, there were 13 severe-to-exceptional droughts (defined as the 12-month Standardized Precipitation Index (SPI, a rainfall based drought index) for August $\leqslant$ -1.2) over Texas. Ninety two percent of these drought events were characterized by anomalously low rainfall in the spring (March through May). Dry springs cause anomalous high pressure systems and anticyclonic (clockwise) flow in the prevailing wind system, which lead to subsidence (sinking motion) in the atmosphere. Such subsidence persists through much of the summer and inhibits rainfall from convective (rising motion) processes. This work explored the potential predictability of strong summer droughts, and the feasibility of using a process-based empirical model to predict summer droughts, over the Southern Great Plains based on such persistent drought-inducing atmospheric circulation patterns and surface dryness in spring.

2. Process-based empirical model for drought early warning

We developed a process-based statistical model to provide an early warning indicator of summer (meteorological) drought based on the anomalous large-scale middle tropospheric (that is, 500 hectopascals level, or approximately 5,500 meters above sea level) circulation, convective inhibition energy (a numerical measure in meteorology indicating the negative energy available in the environment to prevent development of convective weather systems), and land surface moisture conditions in spring (March to May). We used the three aforementioned conditions in spring (March, April, and seasonal mean March through May conditions) as inputs to our statistical model to predict cumulative rainfall deficits or surplus (referred to as the cumulative rainfall anomalies hereinafter) during May-July and the six-month SPI for July.

Comparison of the hindcasts made using the statistical model with the observations shows that the model can predict summer droughts over Texas and the southern Great Plains region in spring with skill levels acceptable to decision makers (~60 percent or higher) — particularly those tasked with drought emergency

* The findings reported here have been published as the Texas Water Development Board Technical Note 15-02 titled 'Early warning of summer drought over Texas and the south central United States: spring conditions as a harbinger of summer drought'. (Full report available at: http://www.twdb.texas.gov/publications/reports/technical_notes/doc/TechnicalNote15-02.pdf)

Correspondence to: D. Nelun Fernando, Water Science & Conservation, Texas Water Development Board, Austin, TX; E-mail: Nelun.Fernando@twdb.texas.gov

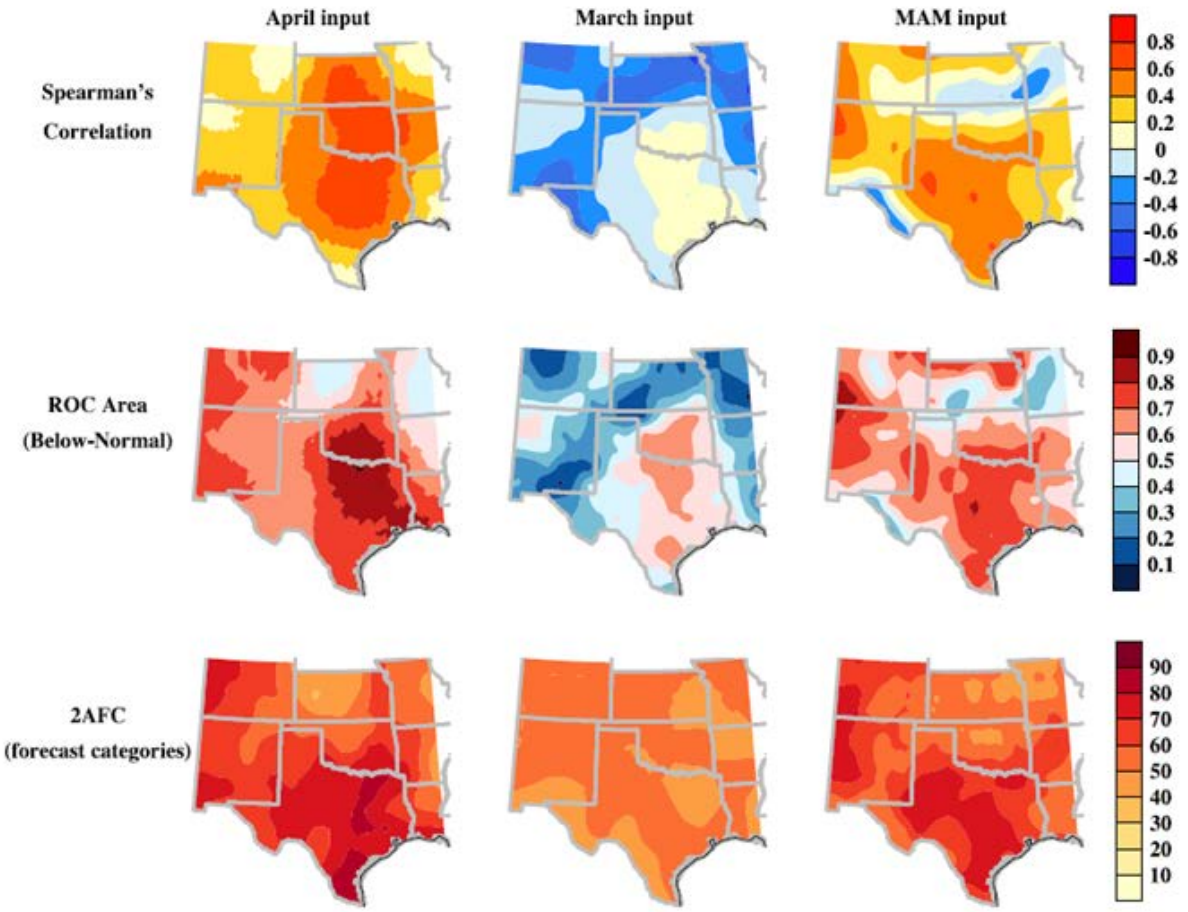

Fig. 1 Skill level as depicted by the Spearman's Correlation (top), Relative Operating Characteristics Area (below-normal) (middle), and two-alternative Forced Choice (forecast categories) (bottom), using April (left), March (center) and March through May seasonal average (right) initial conditions for the predictor fields.

management. The drought indicator shows higher success rates in correctly predicting the occurrence of dry or wet summers than the baseline drought predictability (that is, autocorrelation of rainfall anomalies) and forecasts from dynamical models over south central, central, northern and eastern Texas, western Louisiana, most of Oklahoma and southern Kansas at three to six months lead time. In all realizations of the model, we find that the grid points with the highest skill scores lie within Texas. The best skill is achieved when using April initial conditions (Fig. 1) of the three predictor variables. As a rule of thumb, if there is a high pressure system at 500 hectopascals over the Southern Great Plains, very high values of convective inhibition, and dry land-surface conditions in the region in April, there is a strong probability of an impending intense summer drought over this region.

3. Test prediction for summer 2014 and lead time skill assessment

We made a first forecast for the summer of 2014 using observed April fields. The forecast showed abnormally wet conditions, which better matched observed conditions than the official forecast from the National Oceanic and Atmospheric Administration's Climate Prediction Center for this region (Fig. 2).

We developed a combined dynamic-statistical prediction approach to assess the feasibility of providing an early warning of summer drought at the four- to six-month lead time. This approach uses the ensemble mean dynamic prediction for April conditions, initialized by observed conditions in January, February and March, respectively, as input to the statistical model to predict May through July rainfall anomalies, or the

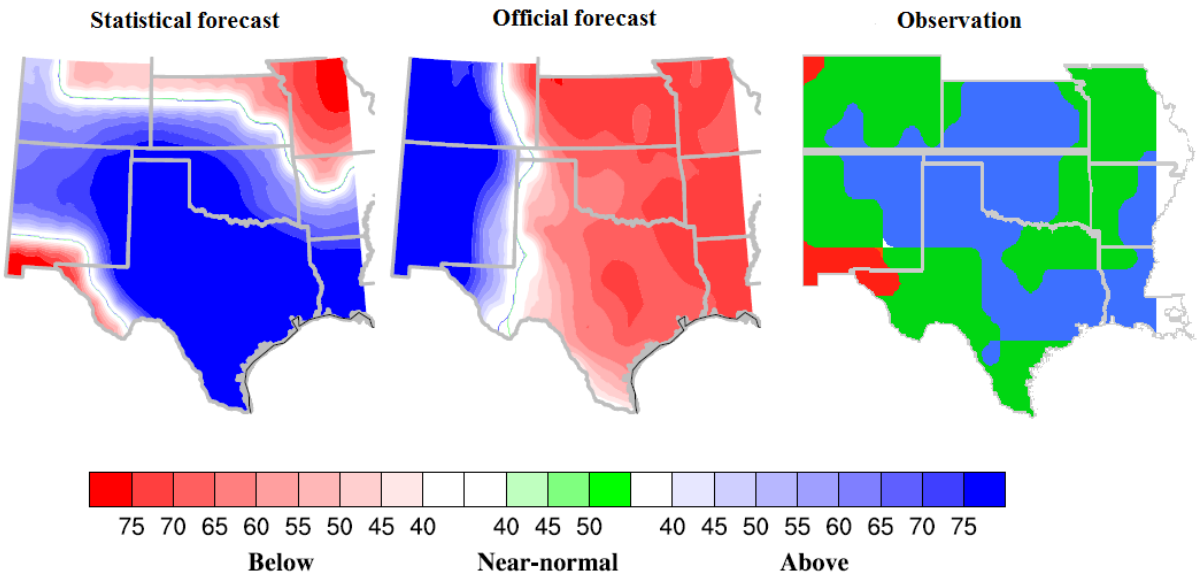

Fig. 2 Statistical prediction (left), official forecast using the National Multimodel Ensemble (middle), and observed (right) precipitation anomalies for the 2014 May through July season.

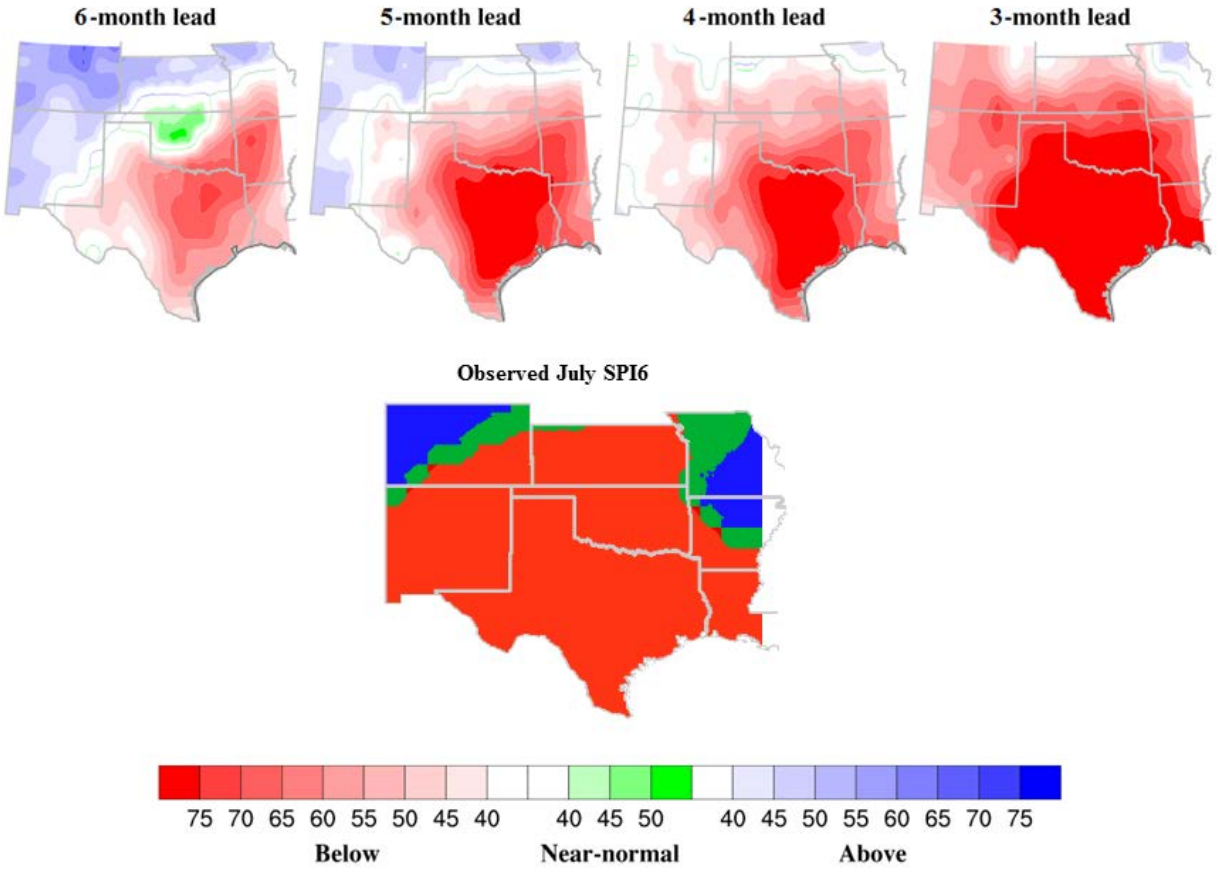

Fig. 3 Six- to three-month lead categorical forecasts of the 6-month Standardized Precipitation Index for July (SPI6) in 2011 (top, from left to right), and observed July SPI6 in 2011 (bottom).

six-month SPI for July, at the 6-month, 5-month and 4-month lead time. The categorical seasonal forecasts (that is, probabilistic estimates of whether a season will be below-, near- or above-normal) from the indicator provide added information on drought susceptibility for up to six-month lead time with the skill levels acceptable to decision makers. Of notable interest is the ability of this combined dynamic and statistical approach to hindcast the 2011 summer drought in January with up to six month lead time (Fig. 3). This implies that the 2011 summer drought over Texas could have been predicted in January 2011.

Given the performance of the drought early warning indicator over Texas, we will explore the possibility for providing summer drought forecasts from January onwards to the Texas Drought Preparedness Council, state emergency management initiatives, and water planners. Such forecasts would ideally be made available to the public through the Texas Water Development Board's drought web page and the Water Data for Texas web site.

Science and Technology Infusion Climate Bulletin
NOAA's National Weather Service
39th NOAA Annual Climate Diagnostics and Prediction Workshop
St. Louis, MO, 20-23 October 2014

Achieving the NOAA Arctic Action Plan: The Missing Permafrost Element

Rachael Jonassen[1], Elchin Jafarov[2], Kevin Schaefer[2], Fiona Horsfall[3], and Marina Timofeyeva[3]

[1]*Department of Engineering Management and Systems Engineering, George Washington University, Washington, DC*

[2]*National Snow and Ice Data Center, Boulder, CO*

[3]*Climate Services Division, NOAA's National Weather Service, Silver Spring, MD*

1. Overview

Permafrost is ground at or below freezing for at least two consecutive years. It occupies about one quarter of the land in the northern hemisphere and 80% of the land in Alaska (see Figure 1a). Permafrost temperature and active layer thickness (ALT) are the two essential climate variables to monitor the status of permafrost (Brown *et al.*, 2008). ALT is the maximum annual depth of thaw and permafrost temperature is the temperature of the permanently frozen soil below the active layer. Observations indicate near surface permafrost has already begun to degrade (Figure 1b). The results of regional modeling of permafrost temperatures in Alaska in high spatial resolution during the 21st century indicate vast permafrost degradation throughout the whole State of Alaska (Jafarov *et al.*, 2012). Observed and projected permafrost degradation imply significant impacts on infrastructure and ecosystems (Oberman, 2008; Callaghan *et al.*, 2011; Schaefer *et al.*, 2014).

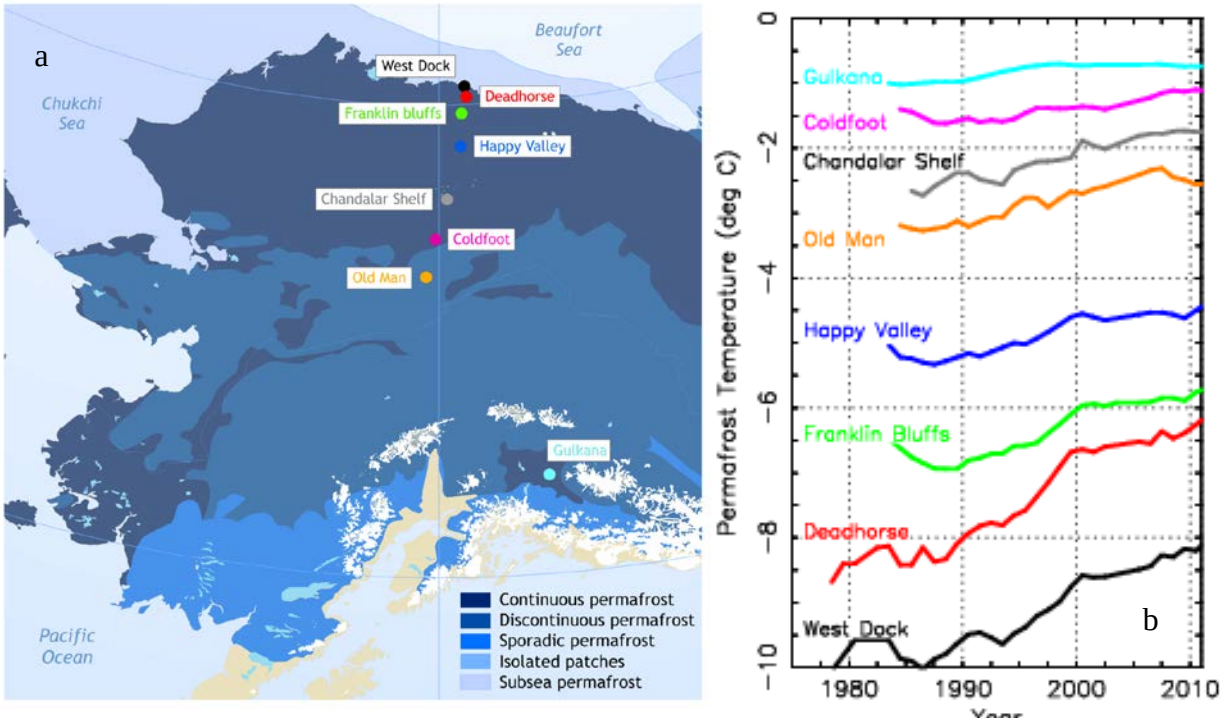

Fig. 1 Time series of annual permafrost temperatures at 20m depth (b) measured from north to south across Alaska (a). Source: http://www.arctic.noaa.gov/report11/permafrost.html

Correspondence to: Rachael Jonassen, Department of Engineering Management and Systems Engineering, George Washington University, Washington, DC; Email: rachaelj@gwu.edu

Among the important Arctic resources threatened by thawing permafrost are vast reserves of oil and gas (O&G) and the associated exploration, production, and transportation infrastructure (Larsen, *et al.*, 2008; Callaghan *et al.*, 2011). The Interagency Working Group on Coordination of Domestic Energy Development and Permitting in Alaska (Clement, *et al.*, 2013) noted that the shorter frozen season for permafrost "presents challenges for land-based development" and details the large number of stakeholders affected by thawing permafrost in Alaska. It calls on the federal government to "strengthen the capacity of science programs to provide focused, ecosystem-based information needed by decision-makers for wise stewardship and development of natural resources."

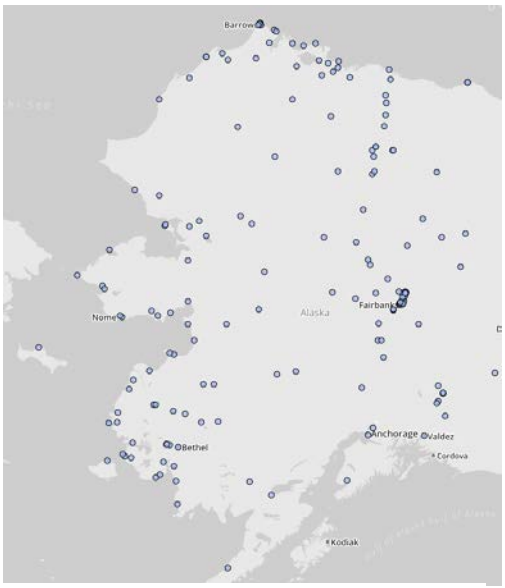

Fig. 2 Locations of existing ground temperature measurements in Alaska.

As NOAA works to implement its 2014 Arctic Action Plan (NOAA, 2014) in response to such critical challenges, services related to permafrost change represent a missing piece of the climate service suite. Although the AAP refers to threats posed to Arctic communities and economies from thawing permafrost and identifies permafrost thawing as evidence of widespread and dramatic change, it fails to propose specific actions to address this challenge while acknowledging the need for additional research and integrated management of resources in general. However, it does list as one of NOAA's six Arctic goals: Strengthen foundational science to understand and detect Arctic climate and ecosystem changes (NOAA, 2014, p. 10*ff*.).

2. Recommendations towards permafrost forecasts

To address this missing element in the AAP, we recommend NOAA link existing seasonal forecasts of temperature and precipitation (Yuan, *et al.*, 2011) with an existing high-resolution model of the thermal state of permafrost (Jafarov *et al.*, 2012) to provide near-term (one year ahead) forecasts of permafrost active layer thickness (ALT). To validate ALT we suggest using current ground temperature measurements available throughout Alaska (Figure 2) in combination with ALT measurement from Circumpolar Active Layer Monitoring Network (CALM) available mainly at the North Slope of Alaska. Given the significant observed and projected damages to O&G and transportation infrastructure, local communities, ecosystems, and the large costs associated with such damage (Callaghan, *et al.*, 2011; Larsen, *et al.*, 2008) we recommend that NOAA integrate existing scientific resources such as the National Climate Predictions and Projections Platform (Rood, 2011) to provide information through research activities and services that will contribute to efforts to reduce permafrost-related loss and damage. This recommendation also addresses a previously identified need within the U.S. National Security Community (Jonassen and Alcorn, 2012).

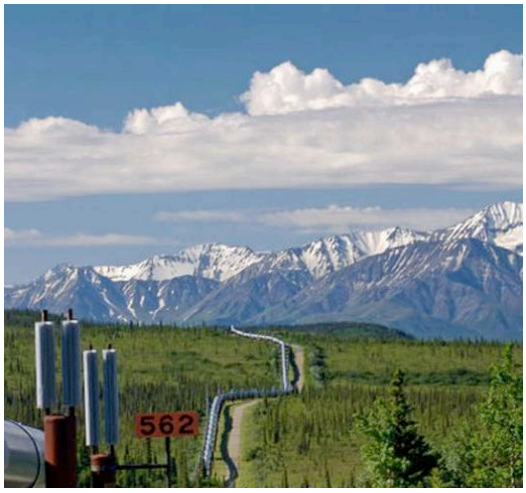

Fig. 3 Thermosiphons protect the trans-Alaska pipeline from permafrost damage. Source: http://www.eoearth.org/article/Permafrost

We distinguish this permafrost forecast service from the available projections of permafrost change (MacCracken, 2001). In particular, the permafrost forecast would be an official NOAA statement [1] of the expected thermal state of

[1] Official operational climate forecasts are specified, defined, and identified in National Weather Service Instruction 10-1001, "Operations and Services, Climate Services, NWSPD 10-10, Climate Outlooks" (October 31, 2011), at http://www.nws.noaa.gov/ directives/sym/pd01010001curr.pdf.

permafrost ALT in Alaska over the coming year on a seasonal basis. It would draw upon seasonal climate forecasts with demonstrated skill (Livezey and Timofeyeva, 2008) for up to a one-year lead. Existing projections are conditional statements of what might happen if certain conditions (particularly greenhouse gas concentration pathways) are realized over long times (decades) in the future (*e.g.* Duchesne, *et al.*, 2008).

A forecast ALT service requires: (1) long-term climate outlooks, (2) detailed understanding of local spatial controls upon soil thermal state such as vegetation and snow cover, soil texture, and ground exposure, (3) high-resolution vertical measurements of the thermal state and characteristics of soils, (4) a permafrost model, (5) integration of climate outlooks and permafrost model, (6) definition of the prognostic permafrost output, and (7) demonstration of forecast skill through pilot studies. Items #2 and #3 are rarely available in Alaska due to the high cost of collecting data and maintaining the relevant databases (Longley, *et al.*, 2001). Thus, pilot efforts at permafrost forecasts should focus on specific sites and infrastructure where the cost of the effort can be justified by the potential returns in avoided loss and damage. O&G production and associated pipelines represents an ideal intersection of commercial and public interests and scientific capabilities for pilot studies. An existing Memorandum of Understanding with three petroleum companies that operate in US Arctic waters (Shell, Conoco-Phillips, and Statoil) provides an example of existing mutually beneficial cooperation (NOAA 2014, p.21).

Examples of the utility of such forecasts begin with the O&G industry where we recommend the first pilot studies would occur. In this case, damage to pipelines is a regular occurrence during normal seasonal variations in ALT and significant engineering effort is required to maintain pipelines and associated infrastructure (Figure 3). Over half of the Trans-Alaska Pipeline System is elevated on vertical support members based on design standards from the period 1950-1970, one of the coldest periods on record (US Arctic Research Commission, 2003). We suggest that, by using ALT forecasts that have demonstrated skill, engineers could identify some months in advance where ALT changes are likely to damage infrastructure. They could focus resources and pre-position equipment so that they could more rapidly respond to pipeline damage and oil spills that might result. If successful, this effort can reduce costs of monitoring and repair as well as ecosystem damage and loss of resources.

3. Future works

Potential applications of ALT forecasts extend beyond the O&G industry. For example, the Inuit Circumpolar Council highlights permafrost degradation as a critical economic issue linked to air transportation, building foundations, and contaminated drinking water (Cochran, 2008). Warming of frozen ground (without thawing) reduces its bearing capacity so that footings and support piles may be destabilized (Williams and Wallace, 1995). Thawing permafrost could add $6 billion in costs for Alaska's public infrastructure, especially transportation infrastructure (Larsen, *et al.*, 2008). NOAA has the opportunity to provide an important new service by offering forecasts of permafrost ALT for Alaska.

References

Brown, J., S. L. Smith, V. E. Romanovsky, H. H. Christiansen, G. Clow, and F.E. Nelson, 2008: Global terrestrial network for permafrost [GTN-P]. *Terrestrial Essential Climate Variables for Assessment, Mitigation and Adaptation*. WMO Global Climate Observing System Report GTOS-52, 24–25.

Callaghan, T.V., M. Johansson, O. Anisimov, H. H. Christiansen, A. Instanes, V. Romanovsky, and S. Smith, 2011: Chapter 5: Changing permafrost and its impacts. *Snow, Water, Ice and Permafrost in the Arctic (SWIPA): Climate Change and the Cryosphere*, Arctic Monitoring and Assessment Programme (AMAP), Oslo, 62 pp.

Clement, J. P., J. L. Bengtson, and B. P. Kelly, 2013: Managing for the future in a rapidly changing Arctic. A report to the President. Interagency Working Group on Coordination of Domestic Energy Development and Permitting in Alaska (D. J. Hayes, Chair), Washington, D.C., 59 pp.

Cochran, 2008, The Arctic: Indicator of Global Change, A Presentation for the International Expert Group Meeting on Indigenous Peoples & Climate Change, April 2-4, 2008, Darwin, Australia. http://www.un.org/esa/socdev/unpfii/documents/EGM_cs08_Cochran.doc.

Duchesne, C., J. F. Wright, and M. Ednie, 2008: High-resolution numerical modeling of climate change impacts on permafrost in the vicinities of Inuvik, Norman Wells, and Fort Simpson, NT, Canada. Proceedings of the Ninth International Conference on Permafrost, 29 June–3 July 2008, Fairbanks, Alaska, USA, D. L. Kane and K. M. Hinkel, Eds., Institute of Northern Engineering, University of Alaska, Fairbanks, 385–390.

Jafarov, E. E., S. S. Marchenko, and V. E. Romanovsky: Numerical modeling of permafrost dynamics in Alaska using a high spatial resolution dataset. *The Cryosphere*, **6**, 613-624. doi:10.5194/tc-6-613-2012.

Jonassen, R. G. and J. M. Alcorn, 2012: Climate: Opportunities for improving engagement between NOAA and the US national security community, LMI, Mclean, VA, ISBN 978-0-9661916-8-4, 52 pp.

Larsen, P. H., S. Goldsmith, O. Smith, M. L. Wilson, K. Strzepek, P. Chinowsky, and B. Saylor, 2008: Estimating future costs for Alaska public infrastructure at risk from climate change, *Global Environmental Change*. doi:10.1016/j.gloenvcha.2008.03.005.

Livezey, R., and M. Timofeyeva, 2008: The first decade of long-lead U.S. seasonal forecasts: Insights from a skill analysis, *Bull. Amer. Meteor. Soc.*, **89**, 843–854.

Longley PA, M. A Goodchild, D. J. Maguire, and D. W. Rhind, 2001: Geographic Information Systems and science chichester, UK: John Wiley, 454 pp.

MacCracken, M., 2001: Prediction versus projection—forecast versus possibility, *WeatherZine*, Edition Number 26, February 2001, Guest Editorial. http://sciencepolicy.colorado.edu/zine/archives/1-29/26/guest.html.

NOAA, 2014: NOAA's Arctic Action Plan – Supporting the national strategy for the Arctic region. U.S. Dep. Commer., Natl. Oceanic Atmos. Admin., Silver Spring, Md. 30 pp.

Oberman, N. G., 2008: Contemporary permafrost degradation of northern European Russia. Proceedings of the 9th International Conference on Permafrost, D. L. Kane and K. M. Hinkel, Eds., June 29-July 3, Fairbanks, Alaska, Institute of Northern Engineering, University of Alaska Fairbanks, vol. 2, 1305-1310.

Rood, R. B., 2011: National climate predictions and projections platform (NCPP), Briefing, http://www.cpc.ncep.noaa.gov/products/ctb/meetings/2011/CFSv3/Rood_NCPP.pdf

Schaefer, K, H. Lantuit, V. E. Romanovsky, E. A. G. Schuur, and R. Witt, 2014: The impact of the permafrost carbon feedback on global climate, *Env. Res. Lett.*, **9**, 085003, 9pp. doi:10.1088/1748-9326/9/8/085003.

US Arctic Research Commission, 2003: Permafrost task force, climate change, permafrost, and impacts on civil infrastructure, Special Report 01-03 (Arlington, VA, 2003).

Williams, P. J. and M. Wallis, 1995: Permafrost and climate change: Geotechnical implications, philosophical transactions, *Physical Sciences and Engineering*, **352**, 347-358.

Yuan, X, E. Wood, L. Luo, and M. Pan, 2011: A first look at Climate Forecast System version 2 (CFSv2) for hydrological seasonal prediction. *Geophys. Res. Lett.*, **38**, L13402, doi:10.1029/2011GL047792.

Science and Technology Infusion Climate Bulletin
NOAA's National Weather Service
39th NOAA Annual Climate Diagnostics and Prediction Workshop
St. Louis, MO, 20-23 October 2014

Science Planning Perspective on Improving Regional Climate Prediction for Services

Jiayu Zhou

S&TI Climate Mission, Office of Science and Technology,
NOAA's National Weather Service

The vision of National Oceanic and Atmospheric Administration (NOAA) is to build a "Weather-Ready and Climate-Smart Nation". It requires our operation services providing the public skillful and reliable prediction products at the local level. To take on the challenge, National Weather Service (NWS) Science and Technology Infusion (S&TI) Climate Mission works for years to identify key scientific issues/problems in climate prediction and service operations and synthesize research and development needs that contribute to the NWS S&T development strategic plan.

1. Background

The forecast skill has a direct bearing on service quality, which the user community concerns the most. Current short-term climate prediction skill is limited, giving less confidence for decision making.

The seamless prediction concept has been accepted by the weather-climate community. Palmer *et al.* (2008) drew an analogy between the prediction system and a chain, and call to focus on the weakest link that determines the strength of a chain. A further thought would be on where the weakest link is located.

This presentation is to address the challenges facing us. First, we look for clues from forecast outliers and unexpected failures that forecasters routinely see, and then have a discussion on how to get the most from current model output (low-hanging fruit) for better serving the user community. Lastly, a summary is given from the science planning perspective on the hope of improving regional climate prediction for services.

2. Puzzles

The unexpected prediction failures/outliers, which puzzled our forecasters in routine operation, could be just the right entrance point to find the key to move forward. Here are some examples.

2.1 Unexpected outcome

Figure 1 from Dr. van den Dool's presentation in 2012 shows that unexpectedly, the foremost weather forecast error is not due to random processes, nor to local factors, but rather to large-scale climate biases. However, by experimentally removing past N-days running-mean forecast errors, the overall levels of forecast skill are only modest. It becomes clearer that the weather and climate model development has to be unified to achieve breakthrough performance.

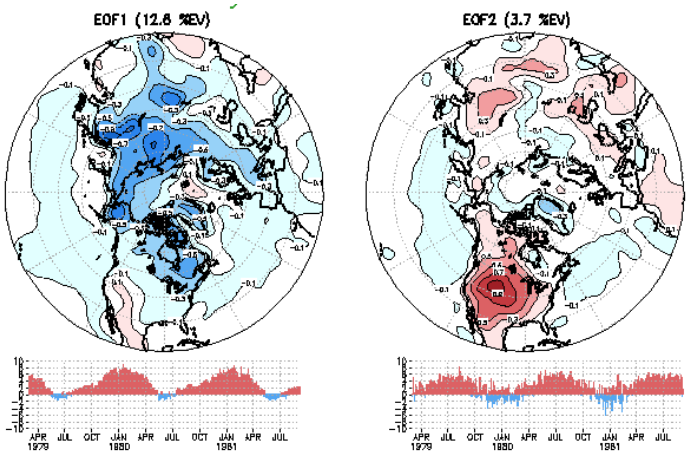

Fig. 1 The leading two EOF modes of 975 hPa temperature 5-day forecast error (1979-12) by NCEP Climate Forecast System (CFS) version 2. (van den Dool 2012)

2.2 Forecast failure

Figure 2 demonstrates a forecast failure, a

Correspondence to: Jiayu Zhou, Office of Science and Technology, NOAA's National Weather Service, 1325 East West Highway, Silver Spring, MD 20910; Email: Jiayu.Zhou@noaa.gov

week-2 forecast running to the opposite of the observation, reported by Mike Halpert in 2006. He looked at the near-range forecast and found that the 6-10 day forecast from 11/26 initial condition can correctly capture the 500 hPa height observed pattern, while that from 11/25 initial condition cannot. There were follow-up discussions between operation and research communities on what had been learned to improve the week-2 forecast, which pointed to key vulnerable spots that need research to focus on, such as upstream regimes of weather system development, Day-1 forecast errors and physical processes and interactions *etc*. This case and the summary of discussion were posted on the Board of Outstanding Open Problem, NWS S&TI Climate Bulletin (http://www.nws.noaa.gov/ost/climate/STIP/ r2o+o2r.htm).

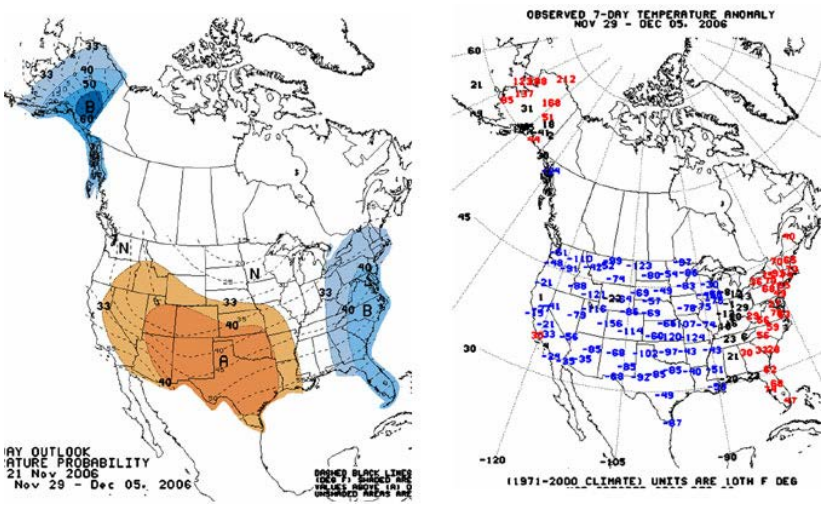

Fig. 2 Left: 8-14 day temperature forecast based on NCEP Global Forecast System (GFS) ensemble made on 11/21 for 11/29-12/5/2006. Right: The observation for verification in the same period. (Mike Halpert 2006)

2.3 Routine prediction outliers

Outliers are extreme deviations from the others seen in routine forecast. Figure 3 was taken from the week 2-4 tendency forecast experiment site maintained by Muthuvel Chelliah. It showed the tendency forecast outliers on 8/16 (week 1P, 6-10 days), 8/20 (Week 2) and 8/26 (week 3). All can be traced back to the initial state around 8/5-6. Here raised an outstanding issue for the data assimilation community to investigate - What is the critical factor to cause the forecast skill dropping off significantly?

2.4 Key predictors

According to our forecasters, seasonal prediction mainly depends on three factors, 1. ENSO, 2. Long-term trend, 3. summertime soil moisture.

For ENSO forecast, it is a long outstanding challenge to predict ENSO phase change. Models are too much like persistence. The events often start too late and then last beyond the time they should. Figure 4 shows the ENSO prediction plume in a recent forecast, from which we can see most models prefer to predict El Niño development. Comparing the performance of GFDL CM2 with that of ESSIC ICM, it is interesting to see that from August to September, when being closer to winter, ENSO development is accelerating predicted by both models but in opposite directions.

For the long-term trend, the warming stagnation has been detected since 1998. Models have difficulties to simulate that. Research speculations are due to underestimation of

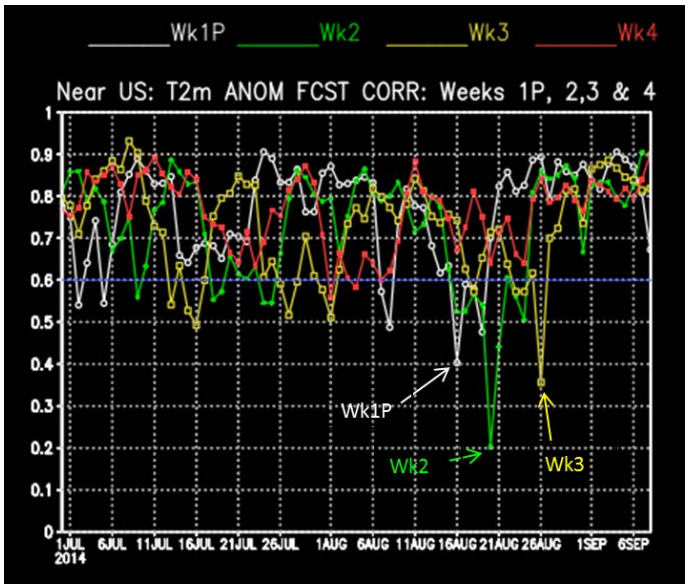

Fig. 3 Anomaly correlation skill of near US 2 meter temperature tendency forecast from late June to early September 2014 for 6-10 days (white), week 2 (green), week 3 (yellow), and week 4 (red). (Chelliah 2014)

internal natural climate variability on decadal and longer time scales, influence of unaccounted external forcing factors, overestimation of the model sensitivity to elevated greenhouse gas concentrations, and roles played by ocean *etc*. These puzzles need to be further explored.

3. Opportunities

Now, CFS v3 development is on the way. Before any model advancement being achieved, how can we get the most from current model outputs to better meet user needs? Following are some emerging opportunities.

3.1 Regional-global model hybrid

Research illustrates down-scaling by a good regional model does provide more useful information for service. But the large scale dynamics could be altered due to the domain constrain. Spectral nudging was used to prevent large unrealistic departures between the GCM driving fields and the RCM fields at the GCM spatial scales.

Instead of doing spectral nudging, Liu and Wang (2014) with Laing took a simpler approach, using CFS to drive CWRF, a climate version of WRF model with optimum multi-physics, and averaging the results of the two models. Preliminary result shows the prediction could not only beat CFS and CWRF individually, but also be comparable with current NMME. (See Figure 5. For illustration purpose, the figure shows each model with a single member.) Since only two models are involved, it is easier to implement in-house and also convenient to upgrade in future.

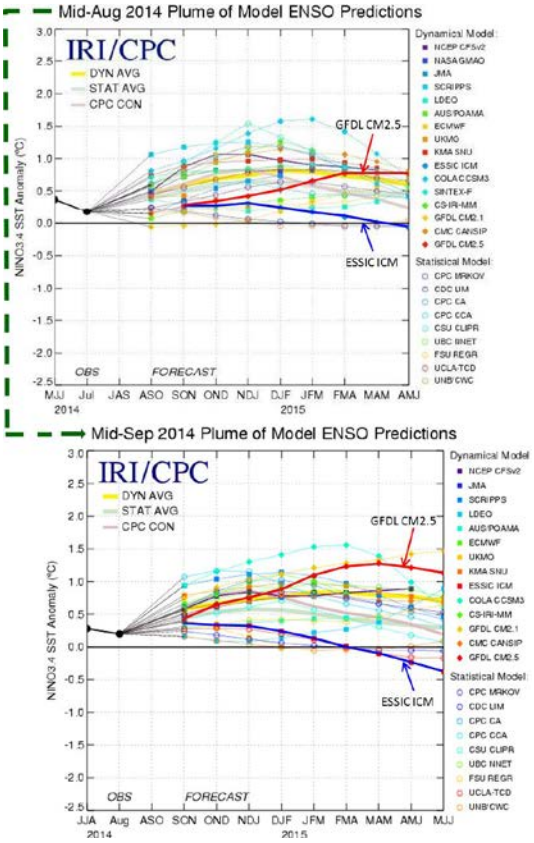

Fig.4 Plume of model ENSO prediction of mid-August (top) and mid-September (bottom).

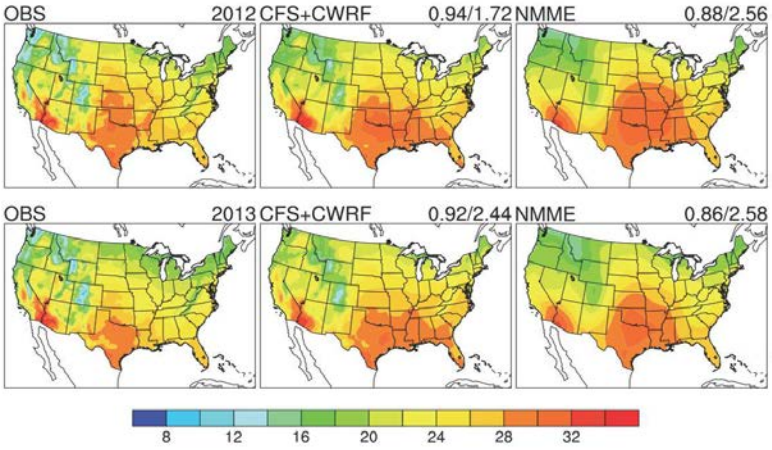

Fig. 5 JJA 2-m temperature (°C) of 2012 (upper) and 2013 (lower). From left to right are GDAS analysis, simulations by CFS and CWRF average and by NMME. The spatial correlation coefficient/RMS error is indicated at the top right corner of each panel for simulations. (Liu, Wang and Liang *et al.* 2014)

3.2 Tendency forecast

Since the tendency correlation between the forecast and the observation is high[1] (Chelliah 2013), this information can be used as forecast supplement to meet particular user needs, such as providing information on when the temperature will cool down during an extraordinary, sustained heat wave event *etc.*

4. Summary

Science planning has to be ahead of the operational development, which requires sensitiveness to research advancement for stepping over existing barriers. Meanwhile, it is also important to communicate the obstacles that block our forecast improvement to research

[1] To be useful for applications, the tendency correlation between forecast and observation has to be well above 0.5 for a single forecast or 0.7 for an ensemble forecast with large members. (Delsole and Cash 2014, personal communication)

community. The NWS S&TI Board of Outstanding Open Problems is set for our research partners to shoot arrows at the targets, thus accelerating our model improvement for better serving the user community. The most challenging issue on effective climate service is to provide users skillful and reliable prediction information at the local level. To move our service beyond obstacles, we need research support and advocate collaboration and mutual development.

Acknowledgements. All materials used in this presentation are credited to their original authors indicated under each figure. Deep appreciation goes to outstanding researches that support NWS science and technology strategic planning and development.

References

Chelliah, M., 2014: Towards filling the gap in NOAA's seamless suite of forecast products; Prospects of "useful" predictions for weeks 3 & 4? *Climate Prediction S&T Digest*, 38th NOAA Annual Climate Diagnostics and Prediction Workshop, College Park, MD, National Oceanic and Atmospheric Administration. 9-12.
[Available online at http://docs.lib.noaa.gov/noaa_documents/NWS/NCEP/CDPW/38th_2014.pdf]

Liu, S., and J.X.L. Wang, 2014: A hybrid approach to improve skills of seasonal climate outlook. *Geophys Res. Lett.*, in revision.

Halpert, M., 2006: A case of week-2 forecast running to the opposite of the observation. *Board of Outstanding Open Problems*, NWS Science and Technology Infusion Climate Bulletin.
http://www.nws.noaa.gov/ost/climate/STIP/r+d/board_op1.htm

Palmer, T.N., F.J. Doblas-Reyes, A. Weisheimer, and M.J. Rodwell, 2008: Toward Seamless Prediction: Calibration of Climate Change Projections Using Seasonal Forecasts. *Bull. Amer. Meteor. Soc.*, **89**, 459–470. DOI: 10.1175/BAMS-89-4-459.

van den Dool, H., 2012: CFS v2 in the context of NMME and IMME. NOAA Climate Test Bed CFS v2 Evaluation Workshop, Riverdale, MD, 30 April 2012.

APPENDIX :

Workshop Photos

Oral Presentations

Poster Presentations

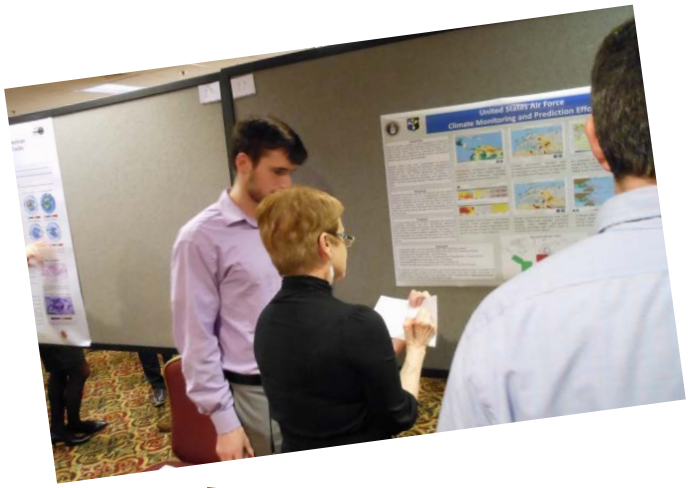

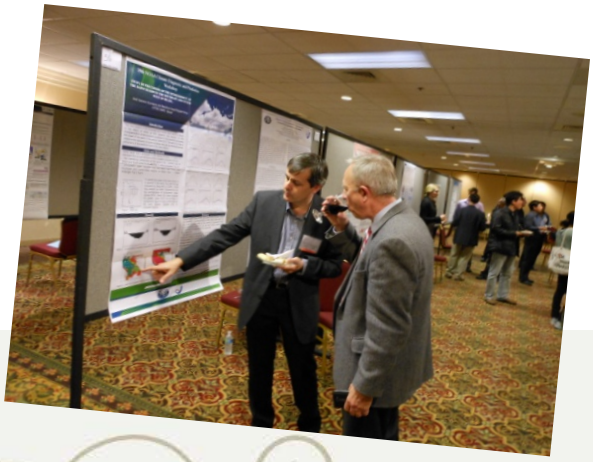

NWS Science and Technology Infusion Climate Bulletin

Featured Special Collections

(http://www.nws.noaa.gov/ost/climate/STIP/Collections.htm)

Climate Prediction Science and Technology Digest

1. 38th Climate Diagnostics and Prediction Workshop
2. 37th Climate Diagnostics and Prediction Workshop
3. 36th Climate Diagnostics and Prediction Workshop
4. 35th Climate Diagnostics and Prediction Workshop
5. 34th Climate Diagnostics and Prediction Workshop
6. 33rd Climate Diagnostics and Prediction Workshop

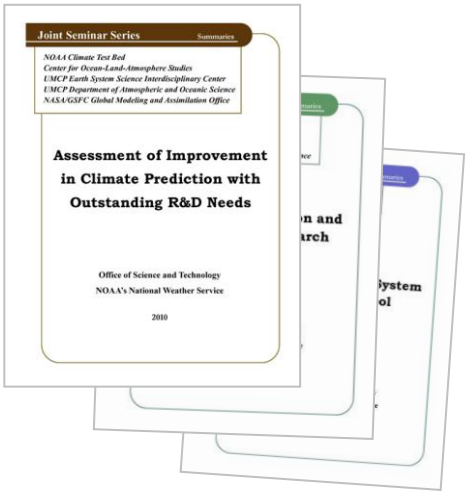

NOAA Climate Test Bed Joint Seminar Series Extended Summaries Collection Volume

1. Unified Modeling, Seamless Prediction and Integrated Services (2010-2011)
2. Assessment of Improvement in Climate Prediction with Outstanding R&D Needs (2009-2010)
3. Research to Operation and Operation to Research (2008-2009)
4. CFS as a Prediction System and Research Tool (2007-2008)

S&T Infusion Lecture Series & Notes

1. Notes about CPC's seasonal prediction
2. Uncertainty and Ensemble Forecast